May 2016

Encapsulation of Cationic Fluorescent Dyes and Photosensitizers into the Nanoscopic Domains of Poly(ethylene Glycol)-b-poly(ε-caprolactone) Micelles

Zhe Cao
University of Wisconsin-Milwaukee

ENCAPSULATION OF CATIONIC FLUORESCENT DYES AND PHOTOSENSITIZERS INTO THE NANOSCOPIC DOMAINS OF POLY(ETHYLENE GLYCOL)-*b*-POLY(ε-CAPROLACTONE) MICELLES

by

Zhe Cao

A Thesis Submitted in

Partial Fulfillment of the

Requirements for the Degree of

Master of Science

in Chemistry

at

The University of Wisconsin-Milwaukee

May 2016

ABSTRACT

ENCAPSULATION OF CATIONIC FLUORESCENT DYES AND PHOTOSENSITIZERS INTO THE NANOSCOPIC DOMAINS OF POLY(ETHYLENE GLYCOL)-*b*-POLY(ε-CAPROLACTONE) MICELLES

by

Zhe Cao

The University of Wisconsin-Milwaukee, 2016
Under the Supervision of Dr. Guilherme L. Indig

This study describes an initial systematic investigation on the molecular determinants associated with the effective encapsulation (or lack thereof) of small cationic molecules into the nanoscopic domains of Poly(ethylene glycol)-*b*-poly(ε-caprolactone) micelles. Out of the seven model dyes investigated here (methylene blue, crystal violet, rhodamine 123, styryl 9M, HITC, DIR and Cardiogreen) only DiR and Cardiogreen were found to partition into the core region of the respective polymeric micelles with a high degree of efficiency. Evidences of weak interactions between styryl 9M and HITC with the corona region of these micelles were also found. No experimental evidences indicating any significant interaction involving methylene

blue, crystal violet and rhodamine 123 with the nanoscopic regions of these micelles were found. The experimental observations described here are in keeping with the expected overall trend of enhanced encapsulation efficiencies associated with more lipophilic guest molecules as compared to those associated with more hydrophilic structural analogs (e.g. HITC vs DiR). Accordingly, the reduced form of crystal violet (i.e. leuco-crystal violet), a neutral and highly hydrophobic molecule, was found to partition into the core region of Poly(ethylene glycol)-*b*-poly(ε-caprolactone) micelles with a high degree of efficiency (comparable to those found for DiR and Cardiogreen), while no micellar interactions involving the respective parent cationic dye crystal violet were found.

TABLE OF CONTENTS

LIST OF FIGURES

1. Introduction

2. Material and Methods

3. Solvent, Concentration and Ionic Strength Effects on the Spectroscopic Properties of Visible and Near-IR Absorbing Dyes

4. Studies on Relative Encapsulation Efficiency of Cationic Dyes into Polymeric Micelles

5. Fluorescence Properties of Visible and Near-IR absorbing dyes

LIST OF TABLES

LIST OF ABBREVIATIONS

λ_{max}	Wavelength of maximum absorption/ fluorescence
$\lambda_{shoulder}$	Wavelength of shoulder absorption/ fluorescence
ACN	Acetonitrile
CG	Cardiogreen
CV	Crystal Violet
CMC	Critical micelle concentration
EPR	Enhanced permeability and retention
LCV	Leuco-Crystal Violet
MB	Methylene Blue
PDT	Photodynamic therapy
PEG-*b*-PCL	Poly(ethylene glycol)-*b*-poly(ε-caprolactone)
Rh-123	Rhodamine-123
S_0	Ground state
S_1	Excited singlet state
SDS	sodium dodecyl sulfonate
TPB	Tetraphenylborate

ACKNOWLEDGEMENTS

To Dr. Indig for giving me the opportunity, guidance, and resources to succeed.

To Dr. Glen Kwon (UW-Madison) and his graduate student Hyunah Cho for polymer samples and directions on how to prepare polymeric micelles.

To my family members, without whom I could have never completed this journey

You have all contributed to this work with your support and patience

1. Introduction

1.1 Polymeric Micelle Structure and Characteristics

Polymeric micelles are nanostructures formed in aqueous environments as a result of noncovalent interactions (hydrophobic effect driven) involving amphiphilic block copolymers. Most typically, di-block and tri-block co-polymers showing both hydrophobic and hydrophilic moieties tend to associate in aqueous media to form spherical, colloidal nanostructures with very low critical micelle concentrations (CMCs). The dimensions of the resulting sphere-like supramolecular assemblies are relatively large, and most typically fall within the 10-100 nm diameter range.

The structure of these supramolecular assemblies can be described as composed by two major distinct nanoscopic domains. The first is represented by a core region in which the most hydrophobic portions of the block copolymers are strongly associate, while the second is represented by the respective more hydrophilic moieties that face the aqueous environment. This last domain is referred to as the corona region of polymeric micelles, and is the region that provides for the solubility of these supramolecular assemblies in aqueous media. A representation of the structure of a typical diblock copolymer micelle is shown in Fig 1.1.1 (Jhaveri and Torchilin, 2014)

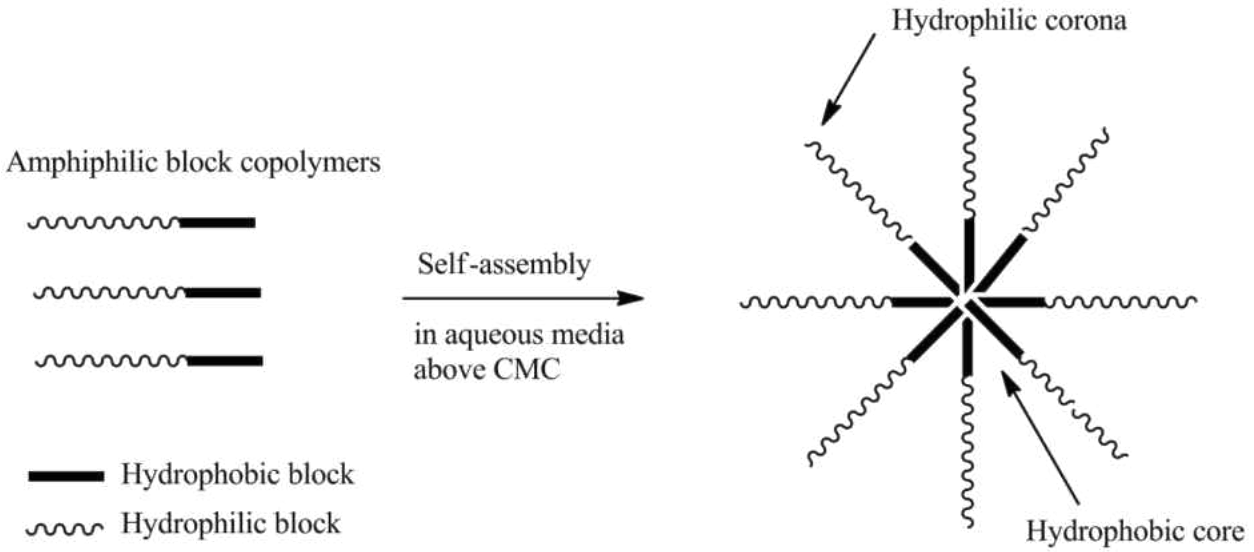

Fig 1.1.1 polymeric micelle formed from self-assembly of an amphiphilic diblock copolymers in aqueous media. (Jhaveri and Torchilin, 2014)

More extensive considerations on the possible structures of polymeric micelles produced by either diblock or triblock co-polymers are presented in Fig. 1.1.2. Depending on the composition of the parent co-polymer, the structure of the final supramolecular assembly can vary quite substantially, providing significant diversity with regard to the possible structures of these assemblies. While the structure of micelles generated by diblock copolymers are more easily predictable, those associate with triblock copolymers are less so. Depending upon whether the triblock copolymer shows two hydrophilic and one hydrophobic regions (Fig. 1.1.2 B), two hydrophobic regions and one hydrophobic region (Fig. 1.1.2 C) or, yet, a cyclic structure (Fig. 1.1.2 D) the respective final structures can show significantly different characteristics.

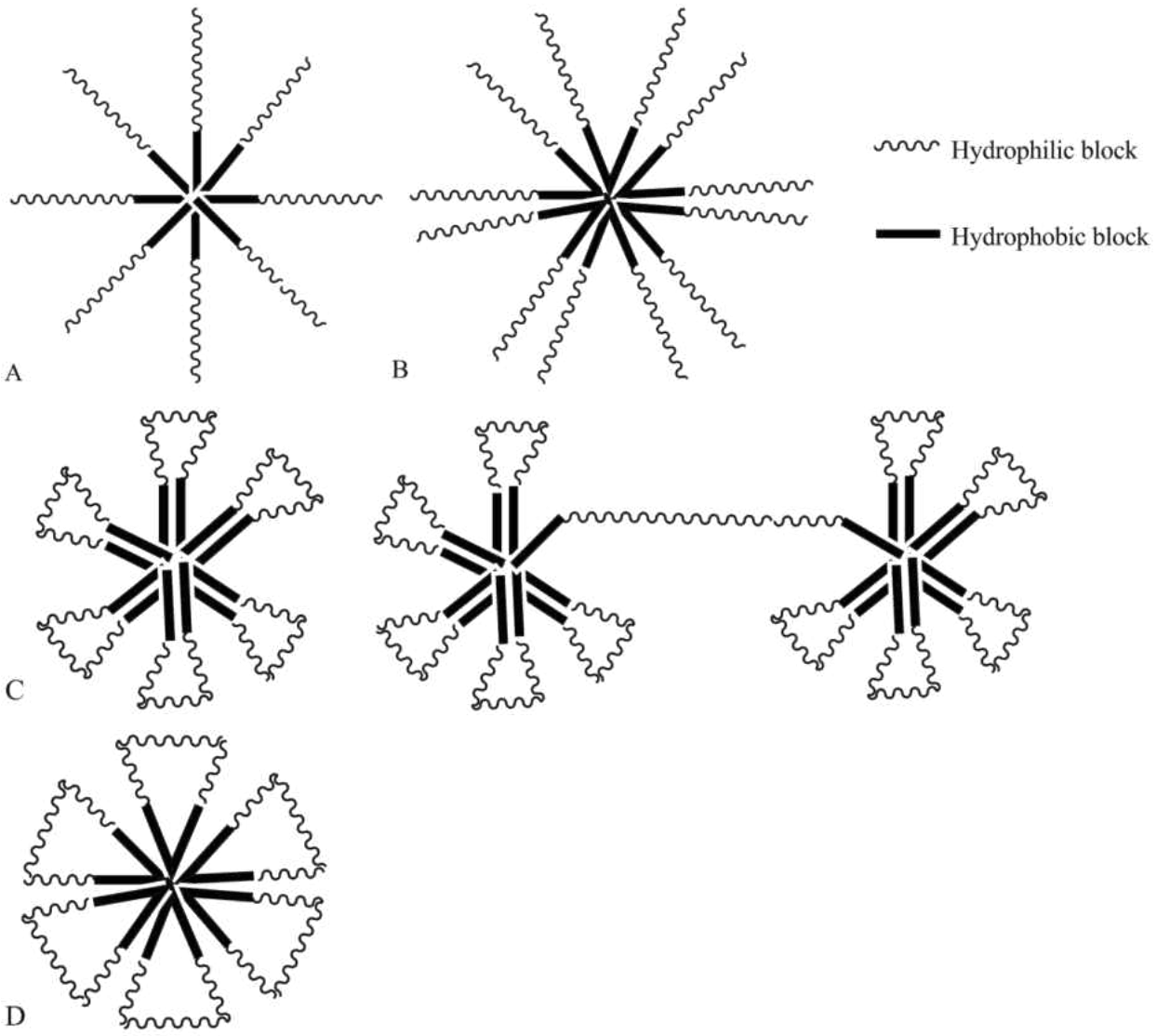

Fig 1.1.2 Polymeric micelles formed by various block polymers. A. diblock copolymers; B. triblock copolymers with two hydrophilic blocks; C. triblock copolymers with two hydrophobic blocks; D. cyclic copolymers. (Gohy, 2005)

The structural diversity of block co-polymer micelles in bound to provide for a variety of distinct technological applications arising from the use these supramolecular entities. However, as far as their application as drug delivery devices is concerned, one of the most immediate characteristic of interest deals with the ratio between the respective core and corona dimensions, or relative volumes. Fig 1.1.3 shows the representation of two "limiting" overall structures of such assemblies. The first represents a case in which the core region of the supramolecular assembly is significantly smaller than the respective corona region. The second represents a case in which the core region is significantly larger than the respective corona. The relative dimensions of these distinct nanoscopic regions play distinct but comparably important roles when these micelles are considered as potential drug delivery devices. While the properties of the core region of these nanoparticles are aimed to provide for maximum loading the drugs of interest, the respective corona region are designed to provide "stealthy" characteristics to these nanoparticles (here the use of PEG as the hydrophilic block represents a common strategy to provide for "stealthy characteristics) . In other words, to enhance blood circulation time before these nanoparticles removed from blood both by the mononuclear phagocytic system (MPS) and by renal clearance (Lu and Park, 2013). The extent to which the core/corona ratio and properties may affect drug delivery efficacy of polymeric micelles represents a subject of current intense scrutiny. The diameter of the core region of the polymeric micelles investigated here show core diameter of approximately 10 nm, and corona diameter of approximately 40 nm, for a total micelle dimension of about 50 nm in diameter (Cho et al., 2012).

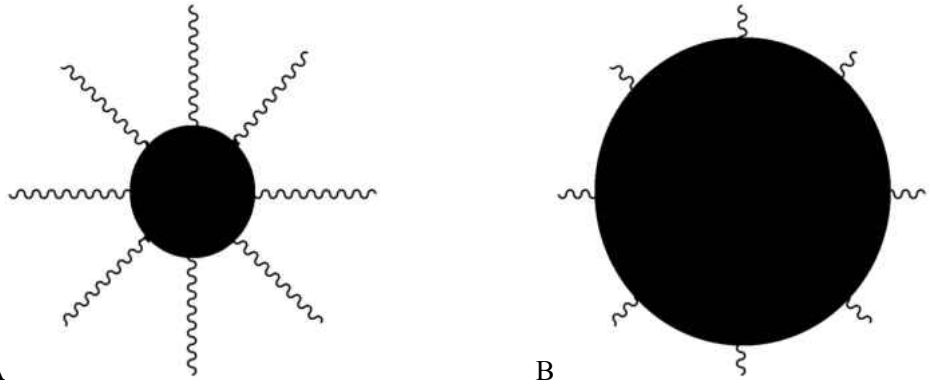

Fig 1.1.3 Two limiting Structures of polymeric micelles formed by block copolymers. A. small core with large corona; B. large core with small corona.

The size of polymeric micelles is large enough to protect them from the renal clearance, whose threshold for nanoparticles is about 5.5 nm (Choi et al., 2007). Accordingly, the prolonged polymeric micelles' circulation and size facilitates their passive accumulate in the areas with leaky vasculature, such as tumor areas (Aliabadi and Lavasanifar, 2006; Kwon and Forrest, 2006). The passive accumulation of polymeric micelles in tumor areas is largely controlled by the so-called Enhanced Permeability and Retention (EPR) effect (Fig 1.1.4; Maeda et al, 2000).

As tumors grow most typically fast, the respective vasculature is commonly defective. That is, this fast growth leads to poor assembling of vascular endothelial cells and, consequently, to leaky vasculatures (i.e. to enhanced Permeation effect, Jain, 1987; Folkman, 1995). In addition,

the fast growing tumor cells tend to compress lymph vessels, forcing them to collapse and leading to the poor lymphatic drainage in tumor areas (i.e. to enhanced Retention effect; Padera et al., 2004). The combination of these two characteristics of solid tumor architecture provides not only for the enhanced uptake of nanoparticles of proper size by those tissues, but also provides for longer retention of those nanoparticle in those desirable targeted areas (Maeda et al., 2000; Iyer et al., 2006).

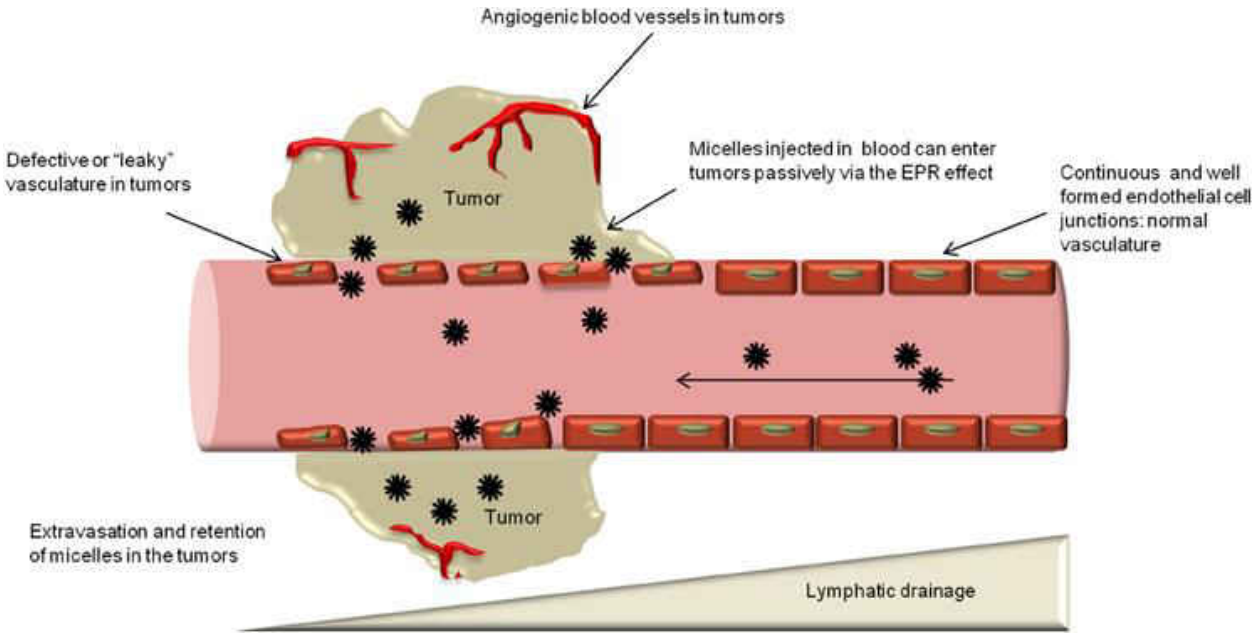

Fig 1.1.4 Enhanced permeability and retention (EPR) effect. (Illustration borrowed from Jhaveri and Torchilin, 2014)

The efficiency of passive accumulation of nanoparticles into tumor areas, as driven by the EPR effect, is highly affected by particle size. The currently dominant set of experimental data strongly suggests that only nanoparticles with diameter of 100 nm or smaller can indeed be

efficiently accumulated in solid tumor areas as a result of the EPR effect. Although no optimum or accurate diameter range has ever been described in the literature, and that may never be found given the endless diversity of tumors, particles with diameters in the 50 nm range have consistently been found to show desirable dimensions for tumor passive localization (Cho et al., 2012).

In addition to their desirable size, another rather convenient characteristic of polymeric micelles as drug delivery devices is represented by their low Critical Micelle Concentrations (CMC). The Critical micelle concentration is the minimum polymer concentration required to form a micelle in aqueous media, a process driven primarily by hydrophobic effects. Polymeric micelles will remain as stable structures in aqueous media when the concentration of the respective block copolymers is kept above CMC (Torchilin, 2007). The CMC of polymeric micelles is most typically found to fall in 10^{-6} to 10^{-7} M range, while those associated with low molecular weight surfactants commonly used as drug delivery vehicles falls within the 10^{-3} to 10^{-4} M range. Due to their low CMC, polymeric micelles can be more desirably used in the preparation as intravenous (IV) formulations. That is, after IV administration, these drug carriers are bound to retain their original structures upon dilutions by blood in the blood stream for significantly longer than the respective vehicles involving low molecular weight surfactants. This fact is bound to lead to longer vehicle circulation times and more effective targeting efficiencies (Adams et al., 2003).

1.1.1. Examples of Polymeric Micelles Use in Drug Delivery.

Low CMC values represent a significant advantage of polymeric micelles as compared to other more traditional formulations. Polymeric micelles can rather efficiently dissolve (i.e. encapsulate) drugs with limited water solubility in their core regions and enhance their bioavailability. Currently, about 40% of marketed drugs and up to 75% compounds under development are poorly soluble in water (Di et al., 2009, 2012; Williams et al., 2013). Compounds with poor aqueous solubility, when accompanied by effective mechanisms of drug excretion and metabolic degradation, tend to show limited therapeutic effects because the build-up of drug concentration to the levels required for the respective therapeutic effects to develop are likewise limited (Torchilin et al., 2003). The use of polymeric micelles as drug delivery vehicles is bound to offset some of the limitations associated with poor water solubility, decrease drug excretion rates, and consequently increase the respective half-life in the targeted organism (Torchilin, 2001). Table 1.1.1 present some of the most successful applications of polymeric micelles in drug formulations currently in use or undergoing intensive pre-clinical evaluations.

Polymeric micelles have also been considered for the delivery of imaging agents to targeted areas both for diagnostics and for intra-operative imaging of tumors. Optical (fluorescence) imaging has been identified so far as the imaging technique of choice for intra-operative guidance of tumor recession. A current human clinical trial employs fluorescein, a fluorescent dye that both absorbs and fluoresces in the visible range of the spectrum as the imaging agent (van Dam G.M. et al., 2011). Although in this last study the imaging agent is not

Micelle Components/Formulation	**Drugs**
Pre-Clinical	
PEG2000-PE	Docetaxel
PEG2000-PE/Vitamin E	Paclitaxel and curcumin
	Paclitaxel and Elacridar
PEG2000-PE/HSPC	Doxorubicin
mPEG-Ad@β-CD-7PLGA/CDDP	CDDP
Stearate grafted dextran	Doxorubicin
mPEG-*b*-poly(D,L-lactide)	Docetaxel
Pluronic P123/F127	Paclitaxel
Clinical	
Genexol®-PM, mPEG-PDLLA (Ph-IV/approved in Korea)	Paclitaxel
NK 105, PEG-p(Asp) (Ph-III)	Paclitaxel
SP1049C, Pluronic L61 and F127 (Ph-III)	Doxorubicin
NK012, PEG-P(Glu)-SN38 (Ph-II)	SN-38
NC-6004, PEG-P(Glu)-cisplatin (Ph-I/II)	cisplatin
NK911, PEG-P(Asp)-DOX (Ph-II)	Doxorubicin
NC-4016, PEG-P(Glu)- DACHPt (Ph-I)	DACHPt

Table 1.1.1 Current applications of polymeric micelles in drug formulations (Jhaveri AM and Torchilin VP, 2014)

delivered to the target tumors by polymeric micelles, but rather as a folate conjugates it exemplifies the current state-of-the-art in this area. Intra-operative fluorescence imaging is always affected by the noise originated from significant light scattering of photons by tissues in the visible region of the spectrum (400-600 nm) (Debbage et al., 2008), significant background due to tissue autofluorescence, and significant light absorption by proteins, heme groups (up to 560 nm), and even water (above 900 nm) (Park et al., 2009). Because all these undesirable events are minimized in the near-IR region of the spectrum (e.g. 700-900 nm), near-IR imaging agents showing proper absorption and fluorescence properties in this region of the spectrum are thought to represent superior characteristics for intra-operative tumor imaging. Indeed, reduced light scattering and reduced tissue "spurious" absorption events provides for the *in vivo* imaging of tumors located at deeper tissue locations as compared to what can be achieved with the use of visible agents. As recently demonstrated, polymeric micelles loaded with near-IR fluorescent probes can be satisfactory utilized for tumor imaging in intra-operative surgical guidance of tumor resection. Cho and co-workers (Cho et al., 2012) have recently demonstrated that the Near-IR fluorescent dye 1,1'-dioctadecyltetramethyl indotricarbocyanine iodide (DiR) encapsulated into PEG-*b*-PCL micelles represent a viable and potentially advantageous alternative for intra-operative tumor imaging as compared to those provided by visible dyes. These authors have also demonstrated that the fluorescence characteristics of dye-loaded polymeric micelles can be easily controlled by formulation. In other words, the fluorescence properties of these supramolecular assemblies can be modulated on basis of micellar loading.

While low micellar loading is associated with highly fluorescent formulations, permitting the tracking of the systemic distribution of these micelles as a function of time, formulations with high micellar loading show low (quenched) fluorescence. These last formulations are associated with lower systemic fluorescence but yet with comparable final tumor specific imaging contrast upon tumor localization and drug (dye) release (Fig 1.1.5). In high micelle-loading formulations fluorescence quenching is at least in part a result of the formation of H-type dye aggregates in the nanoscopic environment(s) of polymeric micelles. This subject will be explored in significant detail in this study.

Although the concept of using polymeric micelles as drug delivery devices is largely based on the EPR effect, a variety of attempts designed to further enhance target selectivity have been more recently described in the literature. These efforts are based on the concept that the targeting of polymeric micelles to specific tissues can be further enhanced by the modification of the surficial corona region of these micelles to include affinity ligands that can selectively bind to specific targeted cells. Abnormal cells like tumor commonly have certain receptors or antigens overexpressed compared to normal cells (Park et al., 2008; Kamaly et al., 2012). Active targeting takes advantages of this feature and achieve more specific and efficient accumulation of polymeric micelles in targeting areas (Nie et al., 2007). A variety of targeting ligands have been investigated for active targeting of polymeric micelles. Some of the widely used ligands are antibodies (Jin et al., 2011; Sawant et al., 2013a), peptides (Gülçür et al., 2013; Miura et al., 2013), proteins (Fonge et al., 2012; Sawant et al., 2013b), aptamers (Xu et al., 2013), sugar

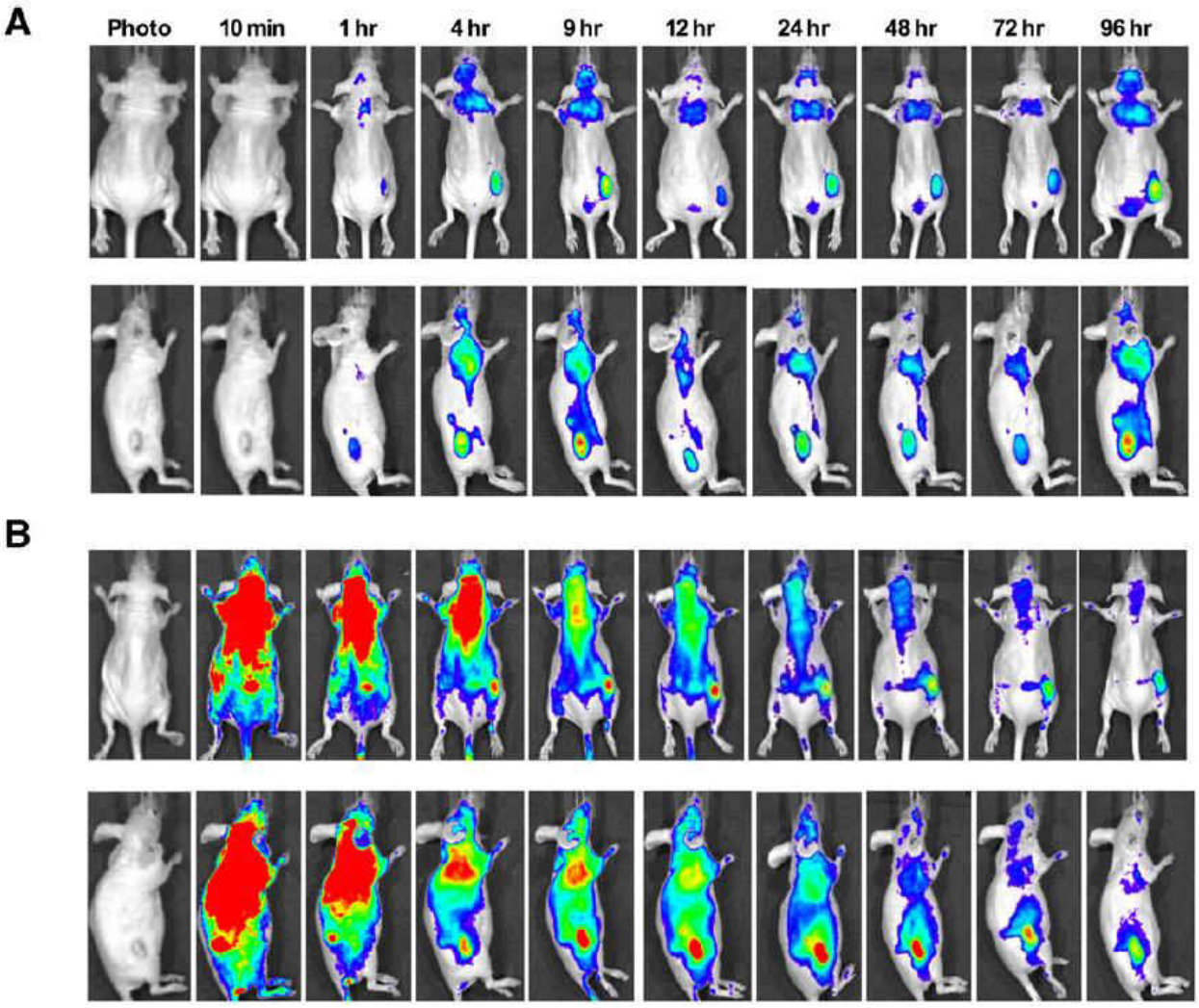

Fig 1.1.5 Real time *in vivo* fluorescence whole-body images of mice with LS180 human colon carcinoma xenografts. Time-dependent images of (A) high loading DiR PEG-*b*-PCL micelles (B) low loading DiR PEG-*b*-PCL micelles (Figure borrowed from Cho et al., 2012)

moieties, (Sun et al., 2011; Yang et al., 2011) and small molecules (e.g. folate) (Qiu et al., 2013; Yang et al., 2013). For example, Cho and co-workers have recently proposed a new neoadjuvant strategy for the treatment and subsequent intra-operative imaging of ovarian cancers (Fig 1.1.6) that includes micelle corona modification with a tumor-specific polypeptide that strongly associates with the phosphatidylserine lipid residues exposed to the extracellular environment during programed cell death (apoptosis). According to this new strategy, the targeted tumors are first challenged with polymeric micelles loaded with chemotherapeutic agents only. In this initial ("debulking") step the polymeric micelles accrue in the targeted tumor area via the passive mechanisms associated with the EPR effect. Then, in a second step, the tumors are challenged with the modified (apoptosis-targeting) polymeric micelles loaded with a Near-IR fluorescent imaging agent prior to surgery. This two-step strategy has shown enhanced efficiency in intra-operative tumor identification and removal in animal model experiments exploring surgical tumor resection under the guidance of optical imaging. (Cho et al., 2014; Schutters et al., 2010)

Polymeric micelles have also been investigated as delivery devises for applications involving a variety of other imaging strategies. For example, Single Photon Emission Computed Tomography (SPECT) imaging monitors the small amounts of gamma-emitting isotopes like technetium99m (^{99m}Tc), indium-111 (^{111}In) and iodine-125 (^{125}I). A recent study investigated ^{111}In-loaded DTPA-PEG-*b*-PCL micelles, which was made by coupling the ^{111}In to the chelating molecules (DTPA) that are conjugated to the polymers, showing increased accumulation in tumor areas. (Lee et al., 2010) Positron emission tomography (PET) imaging visualizes the

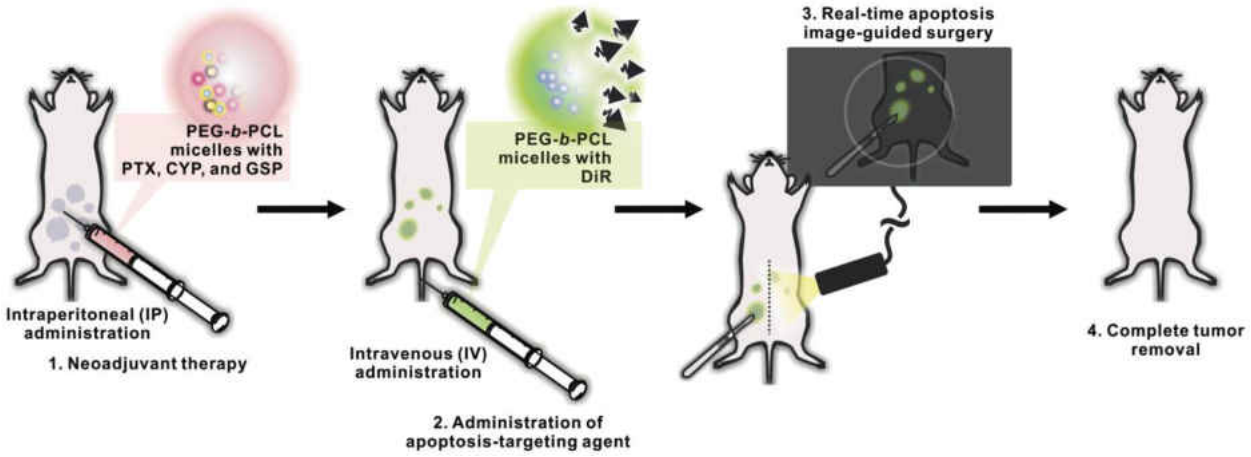

Fig 1.1.6 Schematic illustration of two-step strategy for neoadjuvant therapy, apoptosis-targeted optical imaging and intraoperative surgical guidance. (Illustration borrowed from Cho et al., 2014)

positron-emitting isotopes like fluorine-18 (^{18}F), copper-64 (^{64}Cu) and zirconium-89 (^{89}Zr). Recently, Pressly and co-workers have utilized PMMA-*co*-PMASI-*g*-PEG polymer conjugated with the chelating agent DOTA. When ^{64}Cu was incorporated into this micellar formulation, the respective blood circulation was found to increase. (Pressly et al., 2007; Fukukawa et al., 2008)

Polymeric micelles have also been used in the development of contrast agent formulations for use in magnetic resonance imaging (MRI). Two major methods for developing contrast agents for MRI are the following: (i) incorporation of iron oxide nanoparticles particles into polymeric micelles, and (ii) coupling of paramagnetic metals into the hydrophilic block of polymeric micelles with the assistance of chelating agents. Talelli and co-workers have encapsulated the superparamagnetic iron oxide nanoparticles (SPIONs) into mPEG-*b*-poly[N-(2-hydroxypropyl) methacrylamide dilactate] polymeric micelles, which

contains biodegradable blocks (Talelli et al., 2009); Khemtong and co-workers loaded SPIONs into PEG-*b*-PLA micelles and proposed a method to enhance the respective contrast effects (Khemtong et al., 2009); Lu and co-workers prepared SPIONs incorporated into mPEG-*b*-PCL micelles and described improved contrast between small lesions and normal tissues (Lu et al., 2009). In addition, Fluorine-19 (^{19}F) containing agents have been identified as effective contrast agent for MRI imaging, but many of the new compounds consider for this application show limited aqueous solubility. One of the attempts to overcome this issue is represented by the direct fluorination of block copolymers used to prepare polymeric micelles. The synthesis of block copolymers consisting of a hydrophilic PEG block and a hydrophobic block containing ^{19}F have been described, and their imaging properties evaluated in a series of *in vitro* studies (Du et al., 2008; Torchilin et al., 1999).

1.2 Dye Aggregation and the Molecular Exciton Theory

In vivo optical imaging of tumors assisted by the delivery of fluorescent agents to desirable targeted areas by polymeric micelles represents a subject of current interest. Several distinct experimental techniques can be applied to the characterization of drug/fluorescent dye encapsulation into the nanoscopic domains of polymeric micelles. In this regard, absorption spectroscopy represents a relatively simple and often powerful tool. Changes in extinction coefficients, medium effects on spectroscopic distributions (e.g. as represented by shifts maximum absorption wavelengths) and the identification of spectroscopic fingerprints characteristic of the formation of dye aggregates can all provide reliable proofs of micellar

encapsulation. Besides, the formation of dye aggregates in the nanoscopic domains of polymeric micelles is bound to control the fluorescence properties of the respective formulations. In this section the theory behind the spectroscopic changes associated with dye aggregation is presented.

The interpretation of the spectroscopic shifts associated with the noncovalent formation of molecular aggregates in solution is permitted by the application of the Molecular Exciton Theory. The Molecular Exciton theory is a quasi-vectorial theory that describes the magnitude and direction of spectroscopic shifts observed upon formation of noncovalent molecular aggregates in solution on basis of the relative orientation/geometry of transition dipole moments of the respective molecular constituents within the respective aggregates, along with the respective extinction coefficients and intermolecular distances. The direction of the spectroscopic shift observed upon aggregation is solely controlled by the relative orientation of transition dipole moments within the aggregate. Accordingly, while parallel orientations of the respective transition dipole moments lead to blue (hypsochromic) spectroscopic shifts, head-to-tail (or "brick-work") orientations lead instead to red (bathochromic) spectroscopic shifts. Intermediate transition dipole moment orientations (i.e. oblique orientations) are associated with monomer band splitting, which contributions observed simultaneously both at the blue and red regions of the spectrum. A representation of these distinct transition dipole moment orientations is shown in Fig 1.2.1.

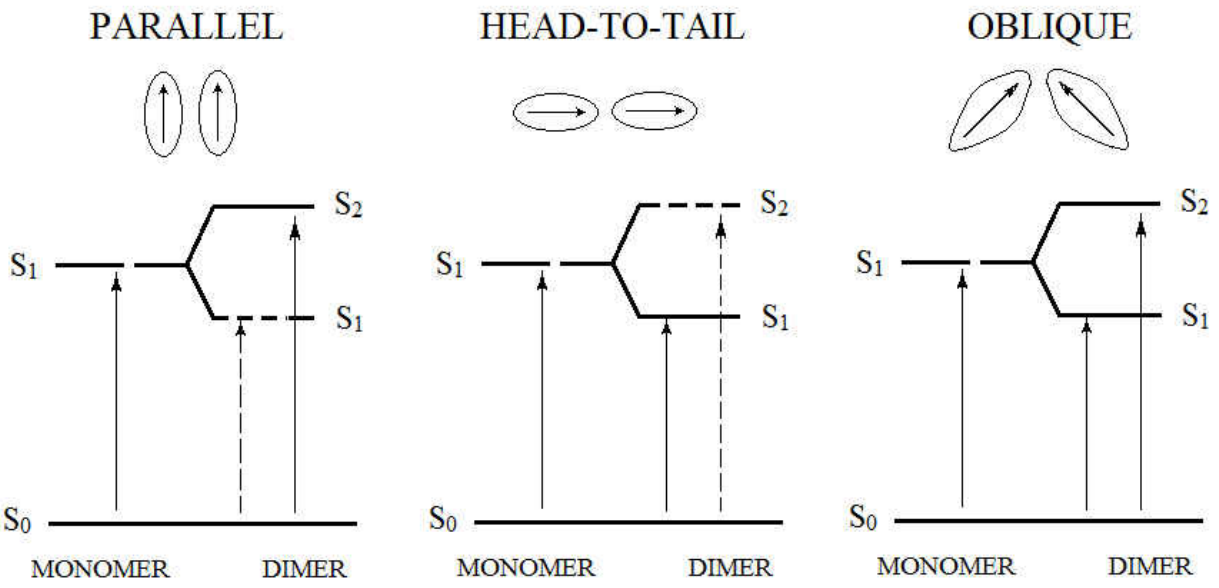

Fig 1.2.1 Diagrams for exciton band structure in molecular dimers with various geometrical arrangements of transition dipoles. (Kasha, 1963)

Noncovalent aggregates showing parallel orientation of the respective transition dipole moments (i.e. batochromic spectroscopic shifts) are referred to as H-type aggregates. Fig 1.2.2 represents in more details the molecular exciton energy diagram for a H-type dye dimer. The characteristic blue shift associated with H-type aggregates is explained by the fact that electronic transitions from the ground state (S_0) to the lower (split) exciton energy level are forbidden (i.e. transition moment = 0; note the quasi-vectorial nature of the theory), while that associated with

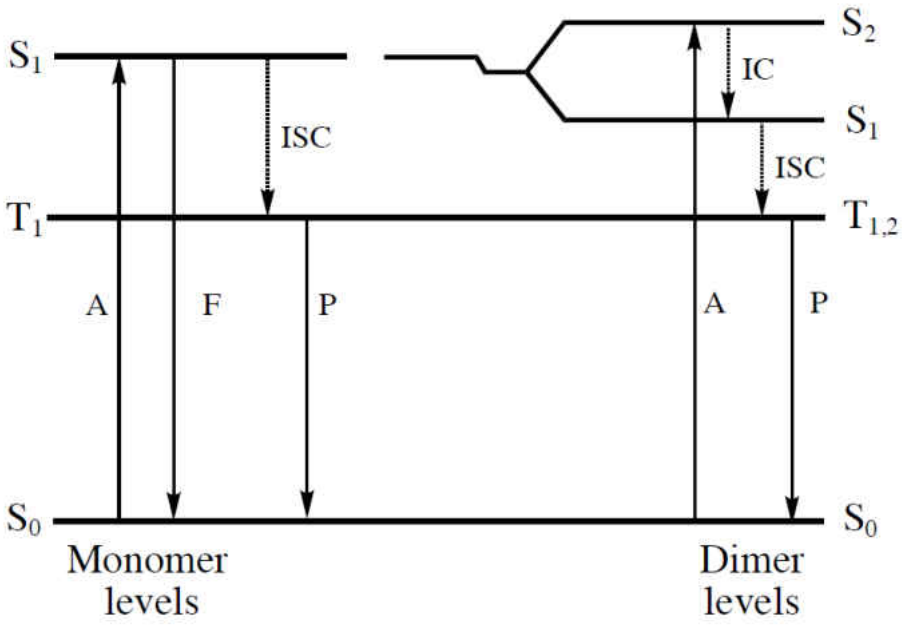

Fig 1.2.2 Excitation pathways without (monomer) and with (dimer) exciton splitting for a H-type dimer. A, absorption; F, fluorescence; ISC, intersystem crossing; P, phosphorescence; IC, internal conversion.

the higher (split) energy exciton energy level are allowed (i.e. transition moment different from zero; for zero-order approximation equal to two times that of the respective monomers; note again the quasi-vectorial nature of the theory). Therefore, upon exciton splitting of the original (monomer) electronic transition a new blue-shifted (H-type) absorption band is observed. In addition, since internal conversion from the upper exciton level to the lower exciton level is very fast, the original excitation energy ends up, nevertheless, at the lower exciton level before total relaxation back to the ground state. Because electronic (i.e. radiative) transitions between the ground and first exciton state are here forbidden, the formation of H-type aggregates leads to a

decrease in fluorescence quantum yield is observed in these aggregates as compared to the respective monomers (Kasha et al., 1965; Kasha, 1947; McRae and Kasha, 1958). Besides, because the mechanism of total relaxation of the lower exciton state back to the ground state is bound to count on higher contributions arising from intersystem crossing (ISC) to the respective triplet state, the photoreactivity of these aggregates can be expected to be typically higher than those associated with the respective monomers (e.g. via intramolecular photoinduced electron transfer mechanisms; McRae and Kasha, 1958)

Analogously, aggregates showing head-to-tail (or "brick-work") orientation of the respective transition dipole moments show forbidden electronic transitions to the higher exciton state and allowed transitions to the lower exciton state (see Fig. 1.2.1), and therefore the bathochromic spectroscopic shifts observed upon the formation of such aggregates (referred to as J-Type aggregates). The oblique orientation of transition dipole moments within the aggregate leads to arrangements in which both exciton levels can be populated by direct electronic excitation (see Fig. 1.2.1). In this last case, the experimentally observed evidence of aggregation is represented by the spectroscopic splitting of the original monomer absorption band, with new contributions observed both at longer and shorter wavelengths of the spectrum as compared to the wavelength of maximum absorption characteristic of the respective monomer.

In this study, the formation (or dissociation) of dye aggregates in solutions has been explored as spectroscopic indicators of effective dye encapsulation into polymeric micelles, or at least as an indication of the occurrence of significant interaction between these two distinct

entities. In this study, other environmental-dependent spectroscopic variables have also been explored for these purposes, and described in the subsequent section.

1.3 Solvatochromic Effects as Indicators of Environmental Characteristics

Solvatochromism refers to the ability of some dyes to change color (i.e. maximum absorption wavelength and spectroscopic distribution) as a result of variations in solvent or otherwise "microenvironment" characteristics. Local polarity/polarizability has been the most intensively studied environmental property as far as solvatochromic effects are concerned. This parameter represents a measure of the ability of solvent to stabilize a solute's charge or dipole. Accordingly, differences is solvent polarity leads to different stabilizations of the ground and respective excited states of susceptible chromophores, which by its turn results in variation of the energy gap between these electronic states, along with shifts in the respective spectra (Reichardt and Welton, 2010). Hypsochromic shifts observed upon increasing results from solvent polarity are termed negative solvatochromism, while bathochromic shifts observed upon decreasing solvent polarity are termed positive solvatochromism (Reichardt and Welton, 2010).

Part of the reasons why solvent "polarity" still represents a predominant parameter in studies dealing with solvatocrhomic effects are based on the fact that solvent polarity effects has been identified as a reliable reporter on the character of the electronic states involved in the respective transitions. That is, solvent polarity effects often provide reliable information on whether an electronic transition shows either n-π or π-π* origins. However, other important solvent/environmental parameters must also be taken into consideration in order to more

rigorously describe the determinants of the observed solvatochromic effects. One of the most comprehensive and inclusive models ever developed to describe solvatochromic effects (currently the dominant model) has been originally proposed by Kamlet and Taft over 40 years ago (Kamlet et al., 1981; Kamlet et al., 1977; Chawla et al., 1981; Kamlet et al, 1979a; Abboud et al., 1977; Kamlet et al., 1979b; Taft et al., 1976; Taft et al., 1979). According to this model, three intrinsic solvent properties are required in order to more precisely describe solvatochromism. Namely, the respective polarity/polarizability (described by the so-called Π^* scale), the ability of the solvent to donate a proton in a solvent-to-solute hydrogen bond interaction (described by the so-called α scale), and the ability of solvent to accept a proton in a solute-to-solvent hydrogen bond interaction (the so called β scale). In this study all Kamlet and Taft solvatochromic parameters have received equal attention.

The study of how and to which extend the solvatochromic properties of any and all imaging agents and photosensitizers of interest to this study might provide information on the efficiency with which these agents are encapsulated into PEG-*b*-PCL polymeric micelle rests on previous observations dealing with the use of solvatochromisns as an reliable experimental tool for use in the characterize of noncovalent interactions between dyes and macromolecules. Fig 1.3.1 shows an example of a highly solvatochromic dye previously used in experimental exercises designed to enquire about the (solvatochromic) properties of macromolecular binding sites (Jones and Indig, 1996).

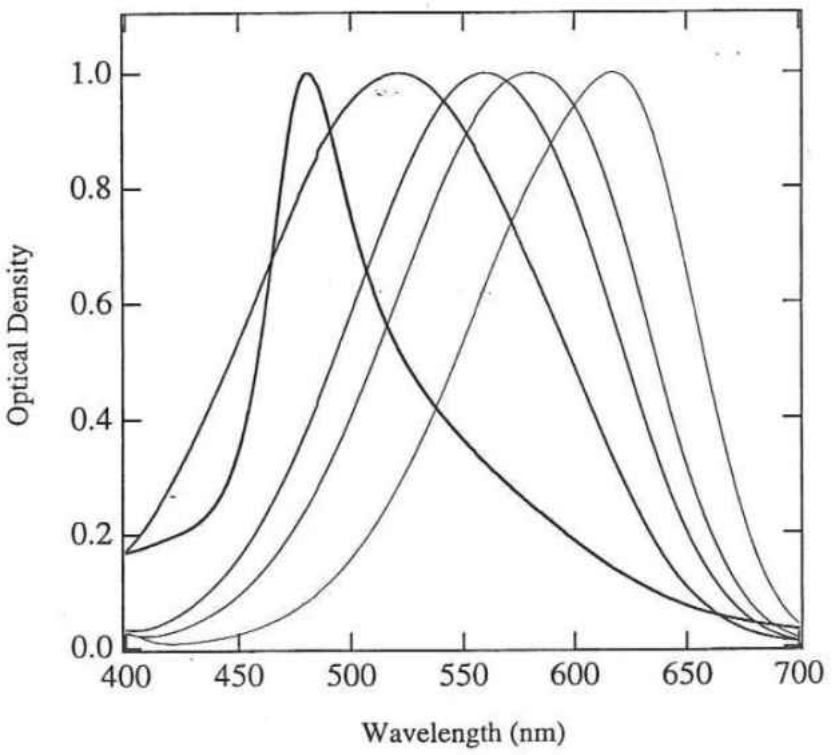

Fig 1.3.1 Absorption spectra of Styryl-7 in various media. From the left to right, at the wavelength on maximum absorption: aqueous PMAA (poly(methacrylic acid); Polymer/Dye ratio = 1.0, pH = 8.0), water, acetone, 1-propanol, and 1,2-dichloroethane. (Jones and Indig, 1996)

2. Material and Methods

2.1 Materials

2.1.1 Chemical Reagents and Disposables

Sodium Chloride (NaCl), Sodium bromide (NaBr), Sodium Iodide (NaI), Sodium Tetraphenylborate (NaTPB), Crystal Violet (CV), Rhodamine 123 (Rh123), Leuco Cystal Violet (LCV), n-Pentanol, 1,1’,3,3,3’,3’-Hexamethylindotricarbocyanine iodide (HITC), Sodium 4-[2-[(1E,3E,5E,7Z)-7-[1,1-dimethyl-3-(4-sulfonatobutyl)benzo[e]indol-2-ylidene]hepta-1,3,5-trienyl]-1,1-di--methylbenzo[e]indol-3-ium-3-yl]butane-1-sulfonate (Cardiogreen) and 2-[[3-[2-[4-(Dimethylamino)phenyl]ethenyl]-5,5-dimethyl-2-cyclohexen-1-ylidene]methyl]-3-methylbenzothiazolium tetrafluoroborate (Styryl 9M) were purchased from Sigma-Aldrich Chemical Co. (St Louis, MO), 1,1'-Dioctadecyl-3,3,3',3'-Tetramethylindotricarbocyanine Iodide (DiR) was obtained from life technologies (Eugene OR), Methylene Blue was purchased from Fluka (Buchs, Switzerland), Quinolinium,6-(dimethylamino)-2-[4-[4-(dimethylamino)phenyl]-1,3-butadienyl]-1-ethyl, perchlorate (LDS751) was obtained from Exciton (Dayton, OH), Methanol, Acetone, Acetonitrile, n-Propanol, i-Propanol were purchased from Fisher Chemical (Pittsburgh, PA), Ethanol was obtained from Decon (King of Prussia, PA), n-Butanol were purchased from Acros Organics (Morris Plains, NJ), and Poly(ethylene glycol)-*b*-poly(ε-caprolactone) (PEG-*b*-PCL) from Polymer Source (Dorval, Quebec, Canada) was kindly supplied by Prof. Glen Kwon (UW-Madison). Unless otherwise stated all chemicals were used as supplied. Water was purified, deionized, and filtered prior to use (Millipore Milli-Q

Direct-Q3 system; resistivity, 18MΩ cm). PD-10 columns obtained from GE Healthcare Life Sciences (Buckinghamshire, UK) were equilibrated with 20 mM aqueous NaCl solutions before use.

2.1.1 Instruments

Measurements of Absorption spectra were carried out at room temperature on a Shimadazu UV-2101 PC spectrophotometer (Kyoto, Japan). Fluorescence experiments were performed at room temperature on a LPS-220 Timemaster Strobomaster fluorometer from Photon Technology International, Inc. (South Brunswick, NJ). All spectroscopic data were treated and analyzed with the assistance of Igor Pro 6, a scientific analysis software application from Wave Metrics Inc. (Portland, OR).

2.2 Methods

2.2.1 Absorption Spectroscopy Studies

Concentrated stock dye solutions were typically prepared by weighting the desirable amounts of each dye of interest, followed by their respective dissolution using analytically accurate volumetric vials. In studies dealing with solvent effects, typically 1.0 mM dye stock solutions were first prepared in methanol, and then subsequently diluted to either 1.0 μM or 5.0 μM final concentrations using the different solvents of interest. Therefore, in these studies the solutions typically contained either 0.1% or 0.5% methanol, respectively. For the case of expensive dyes (e.g. DiR), concentrated solutions were first prepared and then aliquoted for future use. The solvent present in these aliquots were removed by evaporation and the respective

dry samples stored protected from light at 4 ^{0}C.

In experiments designed to explore the TPB-induced precipitation of Methylene Blue, 2.5μM MB solutions in the presence of variable concentrations of TPB concentrations were kept at room temperature for up to three days. During that period, the respective supernatants were removed, mixed with equal volumes of ethanol, and the respective concentrations evaluated on basis of standard MB solutions prepared in 50% water : 50% ethanol. Likewise, the respective precipitates were dissolved in pure ethanol and subsequently quantified.

In studies dealing with environmental (i.e. solvent) effects on the spectroscopic properties of all dyes of interest here, three distinct spectroscopic parameters have been analyzed. Namely, the wavelength of maximum dye absorption (λ_{max}), the wavelength associated with the spectroscopic shoulder ($\lambda_{shoulder}$) typically observed at the left-hand side of the respective absorption envelops (exception made here only to the case of Styryl 9M), and the difference in frequency observed between the respective λ_{max} and $\lambda_{shoulder}$ (i.e. $\Delta\bar{\upsilon}$). Accurate values of $\lambda_{shoulder}$ were obtained from the first derivative of the respective absorption spectra, and identified as the middle point observed between the respective (first derivative) inflection points (Fig. 2.2.1). The difference in frequency between λ_{max} and $\lambda_{shoulder}$ (i.e. $\Delta\bar{\upsilon}$) was calculated using the following equation: $\Delta\bar{\upsilon} = 1/\lambda_{shoulder} - 1/\lambda_{max}$, and represented in cm^{-1} units.

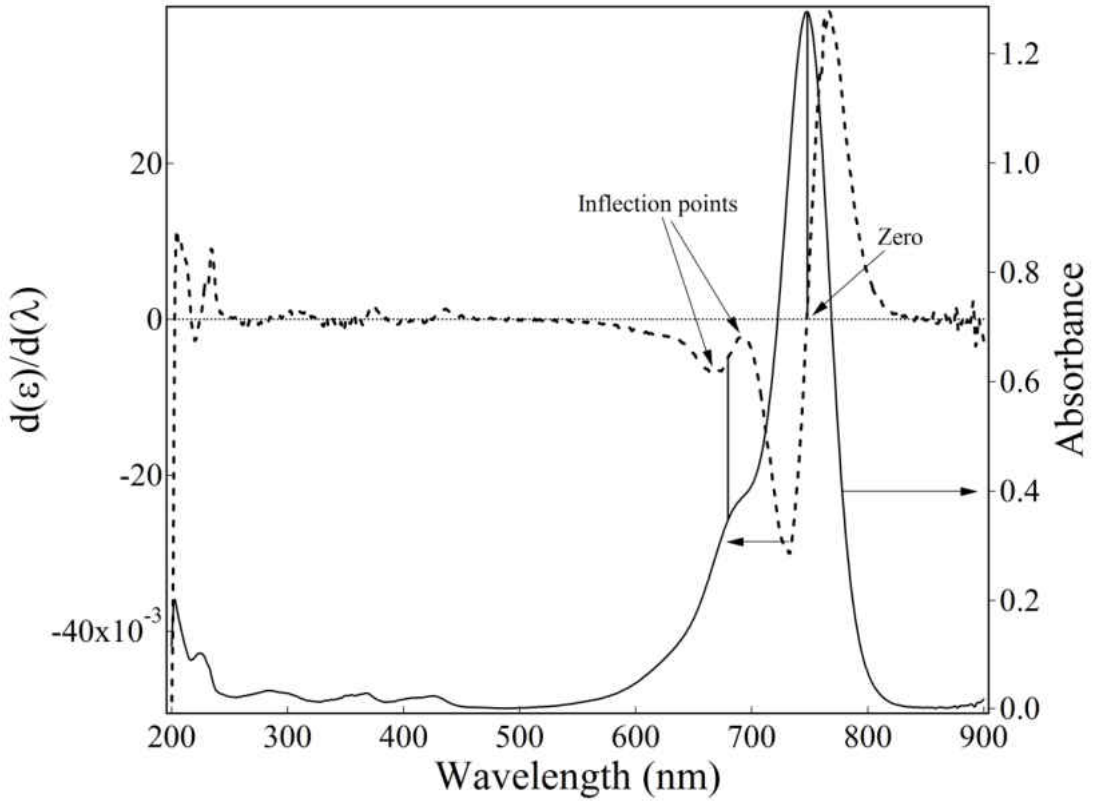

Fig 2.2.1 Absorption spectrum of 5μM DiR in Methanol (solid line) and its differential spectrum (dash line).

2.2.2 Fluorescence Spectroscopy Studies

In order to avoid the experimental artifacts typically associated with inner-filter effects, all fluorescence studies described here were carried out using properly diluted samples. That is, using samples showing absorption values at the wavelength of maximum absorption below 0.05 absorption units (Lakowics 2006; Demas and Crosby 1971; Parker and Rees, 1962). Stock solutions that provided for the accurate measurement of absorption values at the wavelength of excitation were properly diluted immediately before fluorescence analysis, and the respective

experiments always carried out in triplicates.

Relative values of fluorescence quantum yields were measured using of the classical Demas and Crosby equation (equation 2.2.1; Demas and Crosby, 1971), where X and R represent the unknown and reference samples, respectively. In equation 2.2.1 A represents the absorbance values associated with the respective samples at the wavelength of excitation, B the integral area of the respective corrected fluorescence spectra, I the relative intensity of the excitation light source at the respective excitation wavelengths, η the refractive index of the solvent used to prepare the respective solutions and, finally, Φ_X the relative value of fluorescence quantum yield of the unknown sample as compared to that of the reference sample (Φ_R).

$$\Phi_X = \Phi_R (A_R/A_X) (B_R/B_X) (I_R/I_X) (\eta_X/\eta_R)^2 \qquad \text{equation 2.2.1}$$

For two reasons our experimental design has provided for a simplification of equation 2.2.1. First, we have always used the same solvent to prepare the unknown and reference samples (therefore, $(\eta_X/\eta_R)^2 = 1$); Second, we have also always excited both samples at the same wavelength (therefore, $(I_R/I_X) = 1$). Consequently, under the experimental conditions used in this study equation 2.2.1 can be re-writhen in a simplified form as:

$$\Phi_X = \Phi_R (A_R/A_X) (B_R/B_X) \qquad \text{equation 2.2.2}$$

Although apparently rather simple, equation 2.2.2 still requires the use of corrected integral fluorescence data in order to provide for the acquisition of reliable values of fluorescence quantum yields. While measurements of relative values of absorbance at the wavelength of excitation are trivial, those associated with the respective fluorescence integrals

are not. These last values must be properly corrected for the response of the detection system (i.e. monochromator and photomultiplier) as a function of fluorescence emission spectroscopic distribution before any reliable quantum yield data can be obtained. For example, the monochromators found in most fluorometers are biased at or around 500 nm (e.g. ours is biased at 500 nm, with 1200 lines/cm), and also most "visible" photomultipliers are optimized to respond with maximum quantum efficiency near the 500 nm range (including ours). In this study we propose to compare fluorescence quantum yields of dyes that emit at wavelengths significantly longer than those to which our equipment was originally designed to perform at peak efficiency.

In this study we have used one fluorescence spectroscopic standard, namely LDS 751 to correct the response of our detection system for its low response efficiency at wavelengths above c.a. 600 nm. These corrections were performed following a standard protocol described by Lakowicz (2006). That is, the corrected (and published) spectroscopic distributions of LDS 751 were compared to the respective spectroscopic distributions obtained with the use of our own equipment. Then, the respective normalized spectra were rated with respect to each other to generate correction curves optimized to the respective spectroscopic ranges. The multiplication of our raw experimental fluorescence data by these correction curves finally provided for the characterization of the respective "corrected" fluorescence spectra and fluorescence distribution integrals.

2.2.3 Polymeric Micelle Formulations

Poly(ethylene glycol)-*b*-poly(ε-caprolactone) (PEG-*b*-PCL) were prepared using the standard solvent-evaporation method (Cho et al., 2012, 2014). Here, these micelles were typically prepared as follows: 1.6 mL of acetone solutions of PEG-*b*-PCL solutions of desired starting concentrations were diluted to a final volume of 2 ml either with pure acetone, for the preparation of empty micelles, or with dye solutions of proper concentrations, also prepared in acetone, for the respective micelle-dye formulations. These solutions were subjected to magnetic stirring and subsequently quickly mixed with and an equal volume (2 ml) of 18 MΩ cm Milli-Q water. The final water-acetone mixtures were then kept in open vials at 60^0C for 3 hours to provide or the removal of acetone. The final aqueous solutions were finally carefully diluted to 10 ml using volumetric vials in order to minimize potential variations in final micelle concentration between samples as a result of differences in water evaporation. The only exception to the standard protocol described above deals with the case of Cardiogreen formulations. Because this dye is mostly insoluble in acetone, the respective formulations were prepared via addition of aqueous solutions of CG (instead of pure water) to acetone solutions containing only the polymer (instead of polymer-dye acetone solutions).

Relative efficiencies of dye encapsulation into PEG-*b*-PCL polymeric micelles were characterized using constant and high (74:100) dye:polymer molar ratio conditions. Only studies involving DiR have included a systematic evaluation on how and to which extent dye:polymer ratios may affect the final spectroscopic properties of the respective formulations. The distinct

dye:polymer ratios used in the DiR studies are summarized in table 2.2.1

DiR : Polymer	
Weight Ratio	**Molar Ratio**
1:20	74:100
1:40	37:100
1:100	18:100
1:200	9:100
1:400	4:100
1:800	2:100

Table 2.2.1 DiR to polymer ratios used in studies dealing with the question of how, and to which extent, dye loading may affect the final spectroscopic properties of the respective formulations.

2.2.4 Characterization of encapsulation of cationic dyes into polymeric micelles.

In this study we have explored three distinct ways to characterize the encapsulation of cationic dyes into PEG-*b*-PCL micelles. First, by considering potential changes in the wavelength of maximum dye absorption in water as compared to those observed in the respective micelle formulations. Second, by evaluating differences in total dye absorption (i.e. in molar extinction coefficients) in water as compared to those observed in the respective micelle formulations. Third, by evaluating the stability of any dye-micelle interaction as represented by the ability of dye-micelle formulation to retain the dye into the respective nanoscopic micellar domain(s) after being subjected to a size-exclusion chromatographic column. Experiments dealing with size-exclusion chromatography were performed as follows. PD-10 size-exclusion columns were first equilibrated with 20mM aqueous NaCl solutions and then tested with empty micelles for validation of proper performance. To evaluate encapsulation efficiency, 2mL of original, freshly prepared micelle-dye mixtures (see section 2.2.3) were then applied to the size-exclusion column, the respective elution fractions collected in 2 ml volume increments and subsequently analyzed via visible spectroscopy. For further evaluation of relative micelle encapsulation efficiencies, samples of micelles coming out of the first column with significant color (i.g significant dye loading/association) were subjected to a second column, and the remaining loadings compared again on basis of final visible absorption spectra associated with the respective eluted samples.

3. Solvent, concentration and ionic strength effects on the spectroscopic properties of visible and Near-IR absorbing dyes

This study describes an initial systematic investigation on the molecular determinants associated with the effective encapsulation (or lack thereof) of small cationic molecules into the nanoscopic domains of polymeric micelles (core and corona, respectively). Here we have investigated seven model cationic dyes with previously demonstrated use, or at least presumed potential use, both in imaging and photodynamic therapy of tumors. Polymeric micelles provide for the preparation of desirable drug formulations designed for the targeted delivery of hydrophobic drugs to high-value sites. Tumor sites are of particular interest in this area, given the fact that the typical dimensions of polymeric micelles are in keeping with those required for selective tumor accumulation via the Enhanced Permeability and Retention Effect (Choi et al., 2007; Aliabadi and Lavasanifar, 2006; Kwon and Forrest, 2006; Kataoka et al., 1993; Maeda et al., 2000).

The demonstration of encapsulation of drugs into polymeric micelles, along with the respective evaluation of the respective encapsulation efficiencies, require the evaluation of the extent to which one or more of the physical-chemical properties characteristic of the free drug is affected by the encapsulation event. In this study we focus on the encapsulation of both visible and near-IR absorbing drugs (imaging agents and photosensitizers) into PEG-*b*-PCL polymeric micelles.

In this chapter we explore how, and to which extent, concentration and environmental properties affect the absorption characteristics of these agents in solution. While changes in the absorption spectra of these dyes in polymeric micelle formulations (compared to their respective characteristics in water) can provide strong evidences for nanoscopic encapsulation, in this study the characterization of the spectroscopic fingerprints associated with dye aggregation in the polymeric environment(s) is also of particular interest. Micellar dye aggregation may permit the development of non-systemic fluorescent formulations; that is, formulations designed to show low systemic fluorescence but yet high target (tumor) fluorescence, what would, at least in principle, increase intraoperative contrast and facilitate the radical surgical removal of tumors. Here solvent and ionic strength effects on the spectroscopic properties of our dyes of interest (Figure 3.1) are explored, and the respective solvatochromic properties and aggregation tendencies evaluated and discussed.

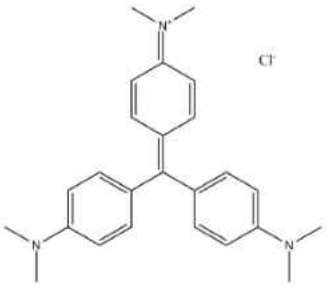

Crystal Violet

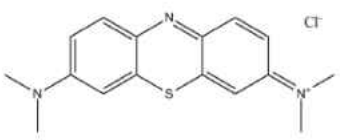

Methylene Blue

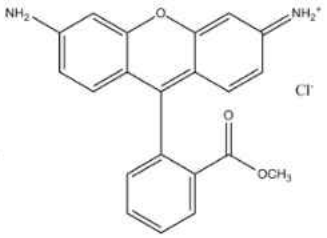

Rhodamine 123

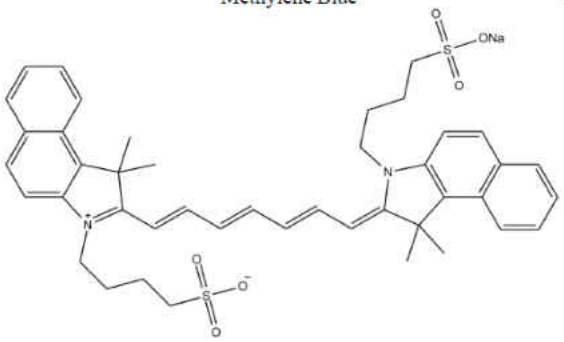

Cardiogreen

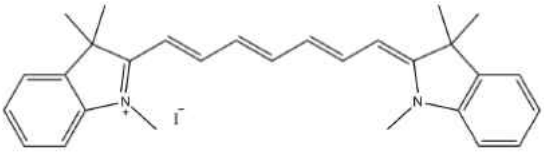

HITC

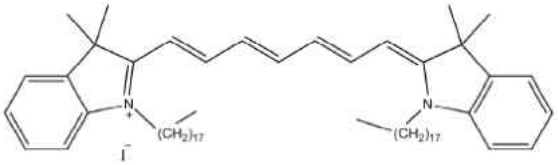

DiR

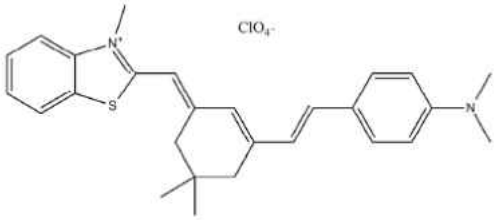

Styryl 9M

Fig 3.1 Structures of dyes involved in this study.

3.1 Crystal Violet and Leuco-Crystal Violet

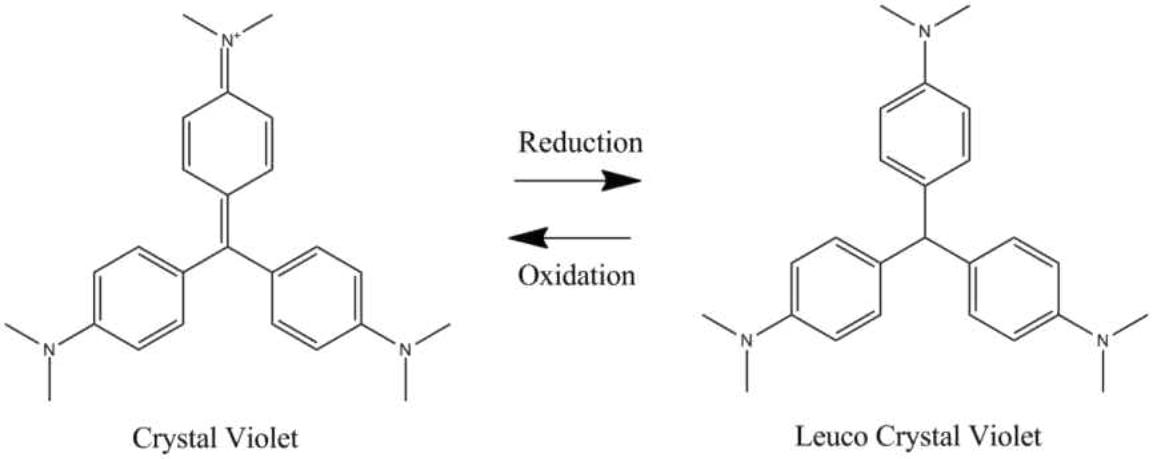

Scheme 3.1.1 Crystal Violet and Leuco Crystal Violet

Crystal violet (CV) is a triarylmethane dye that has been used for more than a century in a large variety of medical and other technological applications. These would include its use as a topical antiseptic agent with desirable antibacterial and antifungal properties, as an anti-trypanosomal drug for the treatment of tropical diseases (e.g. Chagas disease) (Ramirez et al., 1995; Moraes-Souza and Bordin, 1996), as a color agent in industry, including dyeing silk, wool and cotton; using in foods, drugs and cosmetics as colorants (Lewis and Indig, 2000). In addition, crystal violet has been more recently considered as a potentially useful photosensitizer for the selective destruction of tumor cells in photodynamic therapy (Baptista and Indig, 1997, 1998; Bartlett and Indig 1999; Indig et al., 2000). Accordingly, Crystal violet has been found to accumulate spontaneously in the mitochondria of tumor cells in significantly higher concentrations than those observed for typical normal cells, what brings the possibility of

selective destruction of the former cells with just moderate phototoxicity simultaneously impinged upon to the surrounding normal cells.

Crystal violet shows significant tendencies to aggregate in aqueous media, a phenomenon that has significant impacts on both the fluorescence quantum yield and photosensitization efficiency of this dye (Bartlett and Indig, 1999). Figure 3.1.1 show the effect of CV concentration in its respective absorption spectra in aqueous media. Upon increasing CV concentration in water, the absorption originally observed as a shoulder at the left-hand side of the absorption band envelope increases, and this increase is an indication of the formation of H-Type aggregates of CV in that solvent. The magnitude of CV aggregation in water can therefore be qualitatively evaluated through the comparison of how the ration between the absorbance observed at the wavelength of maximum dye absorption, to that observed at the respective blue-shifted shoulder evolves as a function of dye concentration. According to the molecular exciton theory, H-type aggregations consist of non-covalently bound molecules in which the respective transition dipole moments are oriented in parallel to each other (Kasha et al, 1965). H-type aggregates show lower fluorescence quantum yields as compared to the respective dye monomer, and also a higher tendency to engage in intermolecular photoinduced electron transfer events as compared to the respective free dye (monomer).

The formation of dye aggregates in solution is thought to be at least in part driven by hydrophobic interactions. Accordingly, an increase in ionic strength (i.e. salt concentration) can be expected to increase the formation of dye aggregates in solution. The data shown in Figure

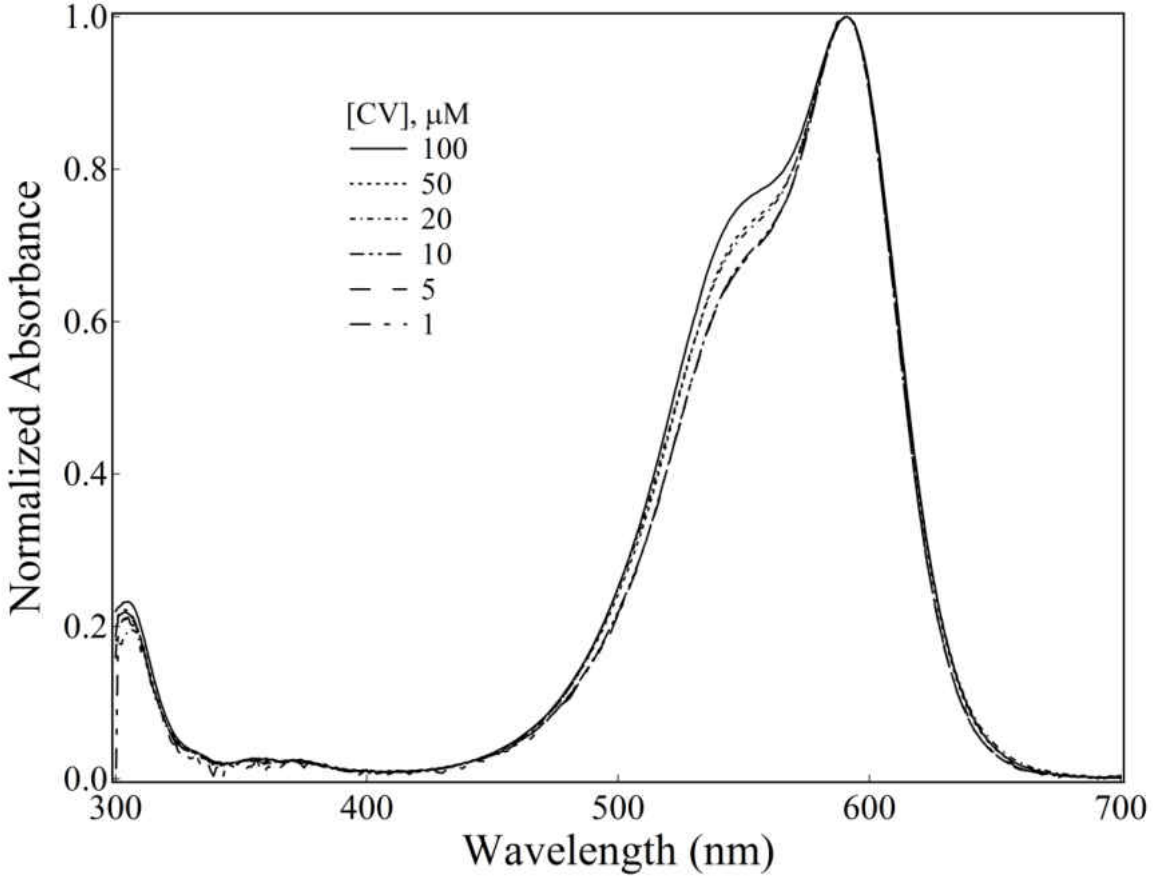

Fig 3.1.1 Effect of concentration on the absorption spectra of Crystal Violet in water.

3.1.2 supports this inference. Upon increasing salt concentration even in very diluted CV aqueous solutions (e.g. 5 μM), the formation of aggregates can be easily characterized. The data presented in Fig. 3.1.2 indicates that a major driving force behind the formation of H-type CV aggregates in aqueous media can indeed be safely attributed to ionic strength. In other words, the observed effects associated with three distinct sodium halide salts (NaCl, NaBr, and NaI) are largely comparable, and this observation suggests that, at least when considering this salt series, the formation of ion-pairs (instead of dye aggregates) as a significant concomitant event behind the experimentally observed spectroscopic changes is unlikely. Just modest variations in aggregation tendencies have been observed upon going from NaCl to NaBr to NaI (Figs 3.1.3 and 3.1.4). Note worth to quote here is also the fact that at very high salt concentrations (e.g. 4M and 5M) CV trimmers and potentially higher aggregates are apparently also formed in aqueous media, as indicated by the observed further shoulder absorption shift into the blue (hypsochromic) region of the spectrum (Fig. 3.1.2).

Because the primary objective of this study can be summarized as an initial attempt to develop new strategies to more effectively load polymeric micelles with imaging agents and photosensitizers, here we have also explored how, and to which extent, the formation of ion pairs (e.g. electrically neutral entities) in solution might represent a new avenue for the loading of otherwise more hydrophilic drugs into either the core or corona domains of these micelles. Figure 3.1.5 shows the effect of the concentration of tetraphenylborate (a soft anion) on the absorption spectrum of a diluted CV solution (2.5 μM) in water. Tetraphenylborate has been

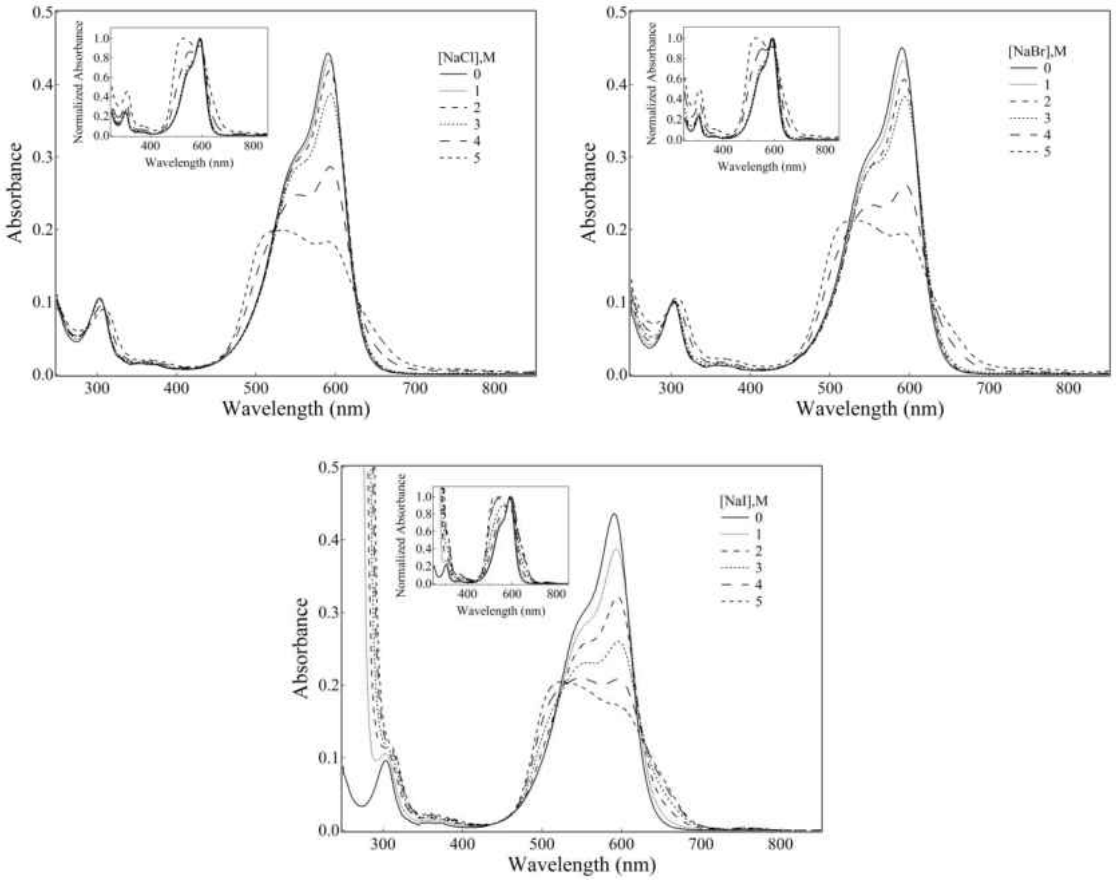

Fig 3.1.2 Salt effects on the absorption spectra of Crystal Violet in aqueous solution. Clockwise, from top left panel: sodium chloride, sodium bromide and sodium iodide. Insets: respective normalized spectra. [CV] = 5 μM

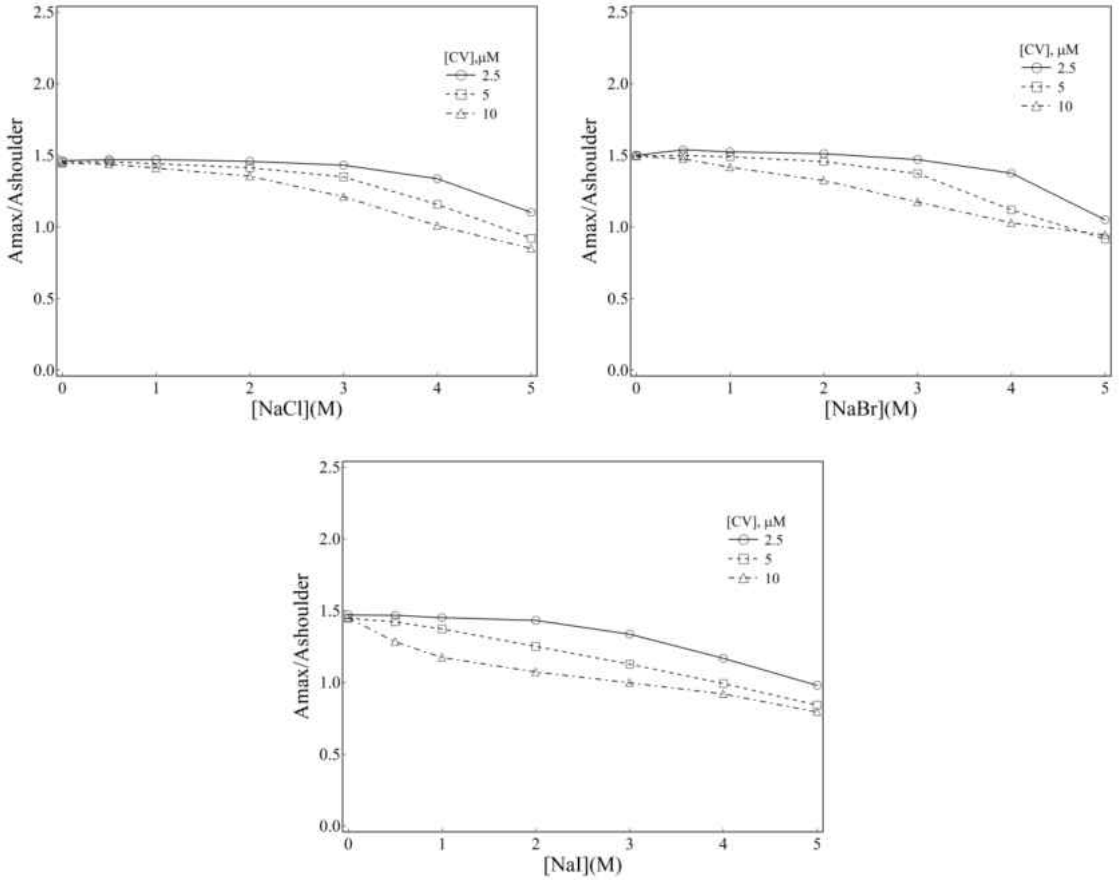

Fig 3.1.3 Effect of dye and salt concentration on the ratio between the absorbance at the wavelength of maximum visible Crystal Violet absorption to that of the shoulder observed at the left-hand side of the respective absorption spectrum in aqueous media. Clockwise, from top left panel: sodium chloride, sodium bromide, sodium iodide.

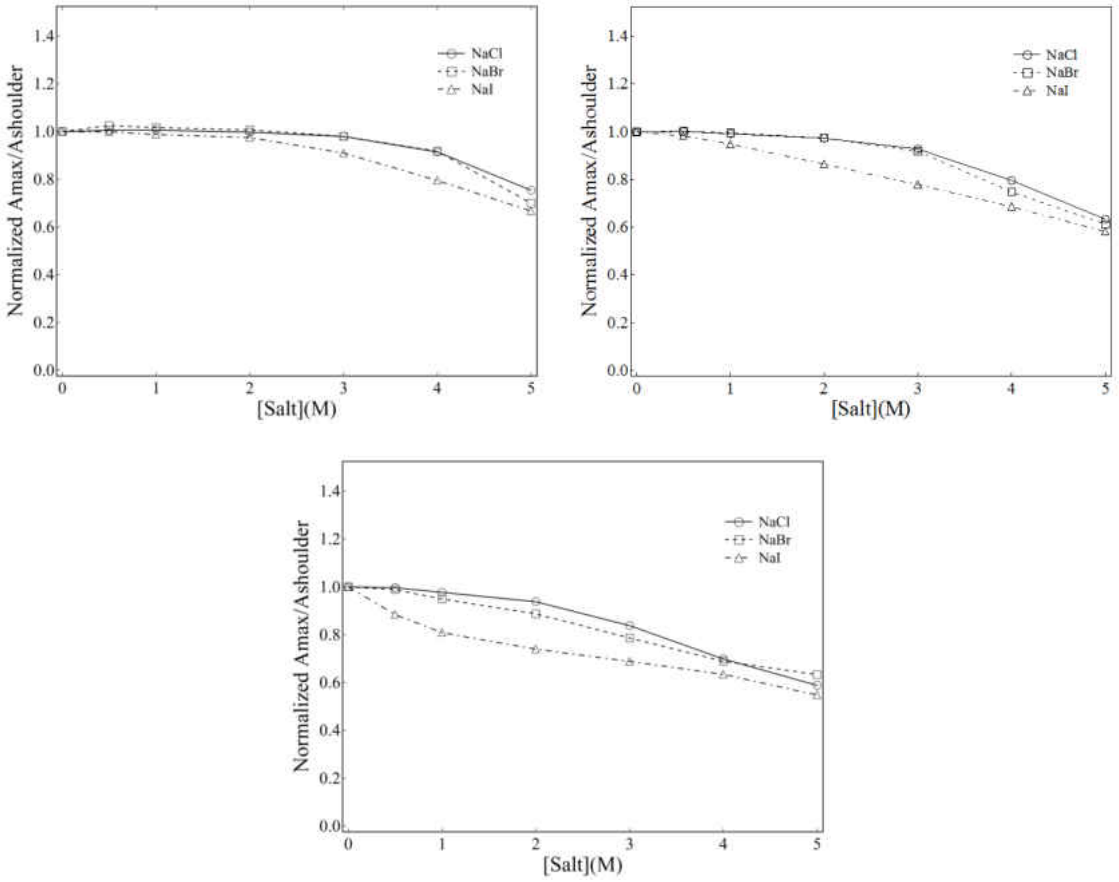

Fig 3.1.4 Salt effects on the ratio between the absorbance at the wavelength of maximum visible Crystal Violet absorption to that of the shoulder observed at the left-hand side of the respective absorption spectrum (aqueous media). Clockwise, from top left panel: ([CV], μM), 2.5, 5 and 10.

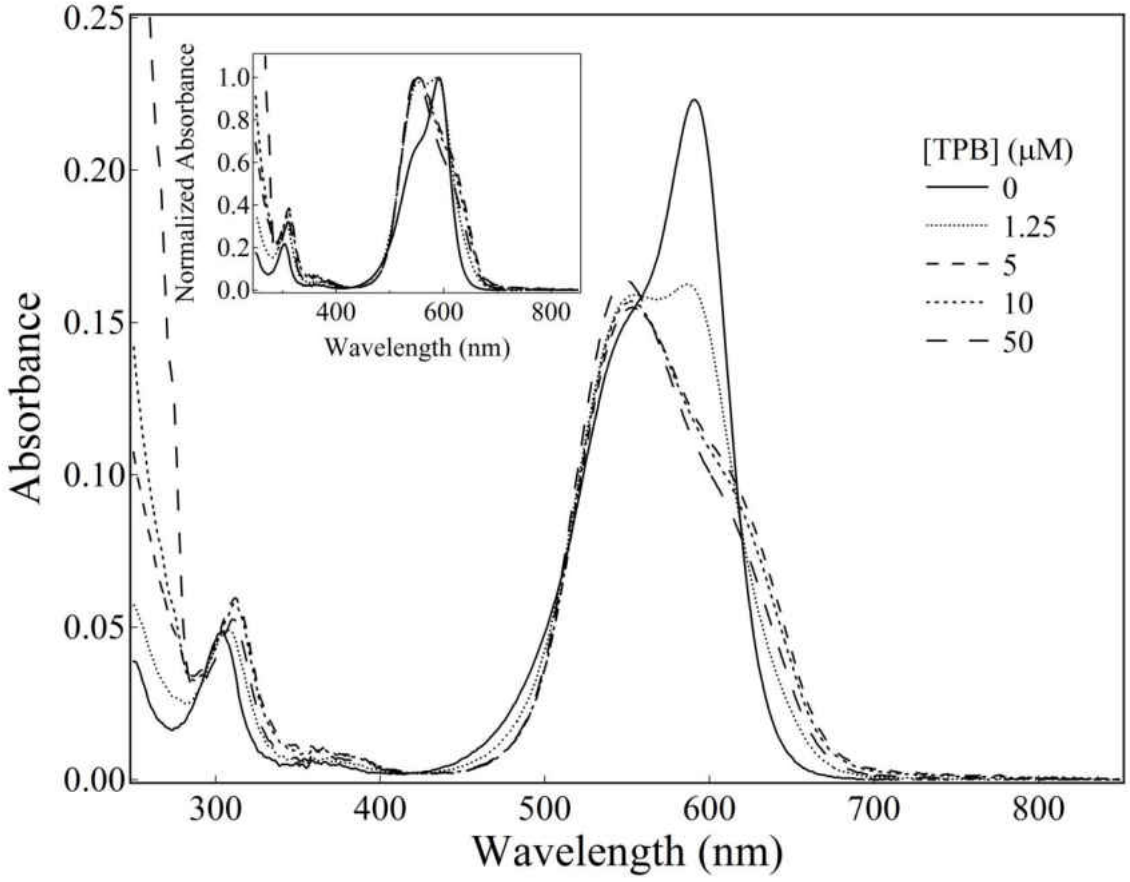

Fig 3.1.5 Effect of sodium tetraphenylborate (TPB) concentration on the absorption spectra of Crystal Violet in aqueous media.

[CV] = 2.5 μM.

previously used by others in studies dealing with the formation of cationic dye ion-pairs in solution (Yoon and Kim, 1985; Moon et al, 1988; Oh et al, 1988; Takada et al, 1983). The observed CV spectroscopic shift observed when in the presence of just 5 μM tetraphenylborate is somehow comparable to that observed when in the presence of about 5M sodium halides (i.e. a seven orders of magnitude difference in terms of concentration effects). The observed CV spectroscopic shifts when in the presence of tetrahydroborate cannot be explained in terms of ionic strength. In this case the observed spectroscopic shifts can be better explained on basis of the formation of ion pairs in solution. Interestingly, the observed spectroscopic shifts observed in the presence of low concentrations of the soft tetraphenylborate ion are not significantly different from those observed when in the presence of high sodium halide concentrations, what suggests that soft ion-pairing may, somehow, facilitate the aggregation of CV in aqueous media.

A potential difficulty associated with this specific approach in terms of micelle loading arises from the fact that CV-tetraphenylborate ion-pairs tend to precipitate in aqueous media. Although ion-pairs may facilitate the loading of polymeric micelles with otherwise hydrophilic drugs, the extent to which this could in fact be accomplished will require further investigation. In this initial exploratory study we have not had the opportunity to explore this hypothesis any further.

As an additional exploratory concept dealing with the development of polymeric micelle formulations designed for the selective delivery of more hydrophilic drugs to targeted tissues, here we have also explored the possibility that neutral (reduced) derivatives of desirable cationic

hydrophilic imaging/photosensitizer agents might provide for the desirable outcome. The reduced form of CV, leuco-CV (Fig. 3.1.6) is far more lipophilic than the parent dye cation, and can be oxidized back to the therapeutically active parent cationic dye via reaction with oxygen active species or endogenous enzymes such as peroxidases (Mottola et al., 1970; Cohn et al., 2005, 2006). In chapter 5 we show that, indeed, the loading of Leuco-CV into polymeric micelles is far more efficient than that observed for the case of CV.

CV has very poor solvatochromic properties. Its wavelength of maximum absorption varies only about 1 nm in going from solvents such as water to 1-butanol (Lewis and Indig, 2000; see subsequent sections in this chapter for dye comparisons). For this reason, here, the "quantitative" evaluation of polymeric CV loading needs to rely on evidences provided by differences in total absorption values obtained for purified micelles as compared to original micelle formulation mixtures (see Chapter 5 for details).

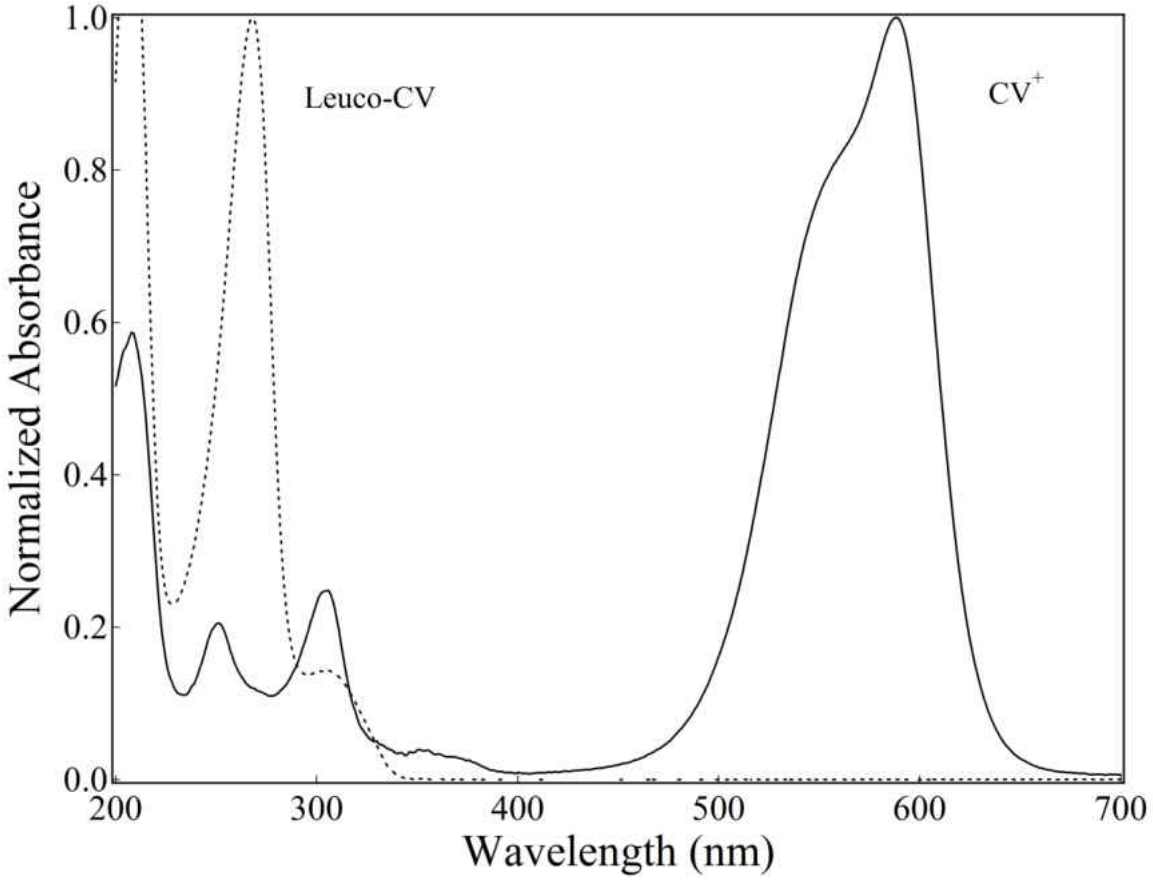

Fig 3.1.6 Absorption spectra of Crystal Violet (solid line) and Leuco-Crystal Violet (dash line) in Acetonitrile.

3.2. Methylene Blue

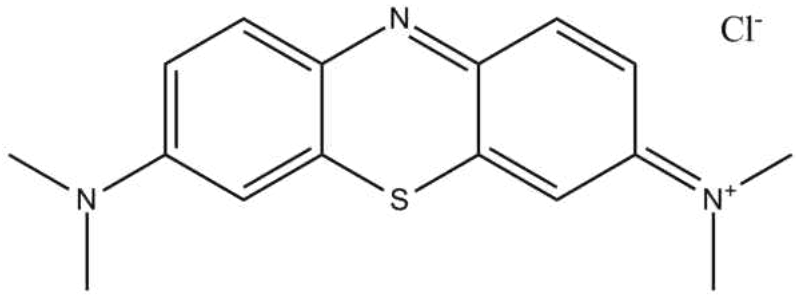

Methylene Blue

Scheme 3.2.1 Structure of Methylene Blue

Methylene Blue (MB) is a widely used thiazine compound. It is commonly utilized as a redox indicator in analytical chemistry and industry due to the color change upon forming Leuco-Methylene Blue (Dilgin and Nisli, 2005). Methylene blue turns colorless with the presence of active enzyme in living eukaryotic cells, while remains blue in dead cells. Thus, it can be also utilized for marking active cells in biological research (Kaprelyants et al., 1993; Kell et al., 1998). In industry, it is widely used for the manufacture of color pens and polygraphic inks (Hideaki, US Patent 2011). For medical application, MB can be used as an antimalarial agent (Guttmann and Ehrlich, 1891; Schirmer et al., 2003). In addition, methylene blue has also been used as a photosensitizer in photodynamic therapy. It is a good generator of singlet oxygen, and show high phototoxic effects toward both bacteria and eukaryotic cells (Wainwright, 2009; Mellish et al., 2002; Tardivo, et al., 2005; Rice et al., 2000; Wainwright et al., 1997).

Although Methylene Blue (MB) shows n-octanol/water partition coefficient comparable, but yet slightly lower than that of CV (1.08 and 2.21, respectively, da Silva et al., 2014; Kandela

et al., 2002); that is, slightly higher hydrophilic properties as compared to CV, its tendencies to aggregate in aqueous media are significantly higher as compared to those observed for the former dye. Presumably the more planar structure of MB, as compared to CV (often referred to as a three-blade propeller) is implicated in this experimental observation.

Figure 3.2.1 shows concentration effects on MB aggregation in aqueous media. Again in this case, aggregation is revealed by an increase in absorption at the region of the spectroscopic shoulder observed at the left-hand side of the respective absorption envelop, as compared to that observed at the wavelength of maximum dye absorption. Here, again, the observed hypsochromic spectral shift is an indication of the formation of H-type dye aggregates in solution, which leads to a decrease in the respective quantum yield of fluorescence along with a higher efficiency of intra-molecular photoinduced electron transfer reactions (Kasha et al., 1965; Kasha, 1947; McRae and Kasha, 1958; Severino et al., 2003).

Even for this more hydrophilic dye, ionic strength appears to represent a major driving force before dye aggregation in aqueous media (Fig. 3.2.2). Accordingly, upon increasing the concentration of sodium halide salts in otherwise diluted (5 μM) MB solutions, the representative ratio of wavelength of maximum dye absorption to that of the respective absorption observed at the left-hand side shoulder of the absorption envelop decreases (Figs 3.2.3 and 3.2.4).

The effect of the soft ion tetraphenylborate concentration on the absorption spectra of diluted MB solutions (e.g. 2.5 M; Fig. 3.2.5) also shows a parallel to those previously observed

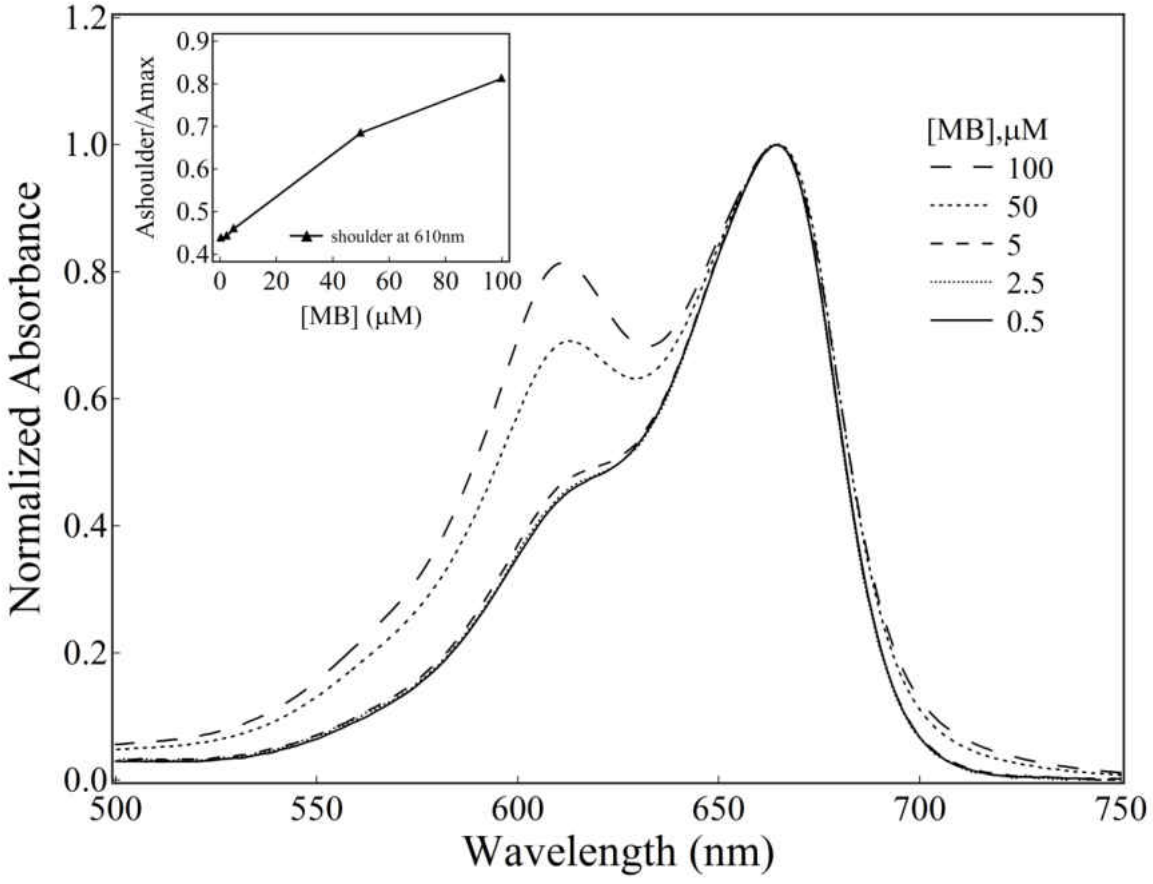

Fig 3.2.1 Effect of concentration on the absorption spectrum of Methylene Blue in water. From top to bottom, at the shoulder observed at the left-hand side of the visible absorption envelope ([MB], μM): 100, 50, 5, 2.5, 0.5.

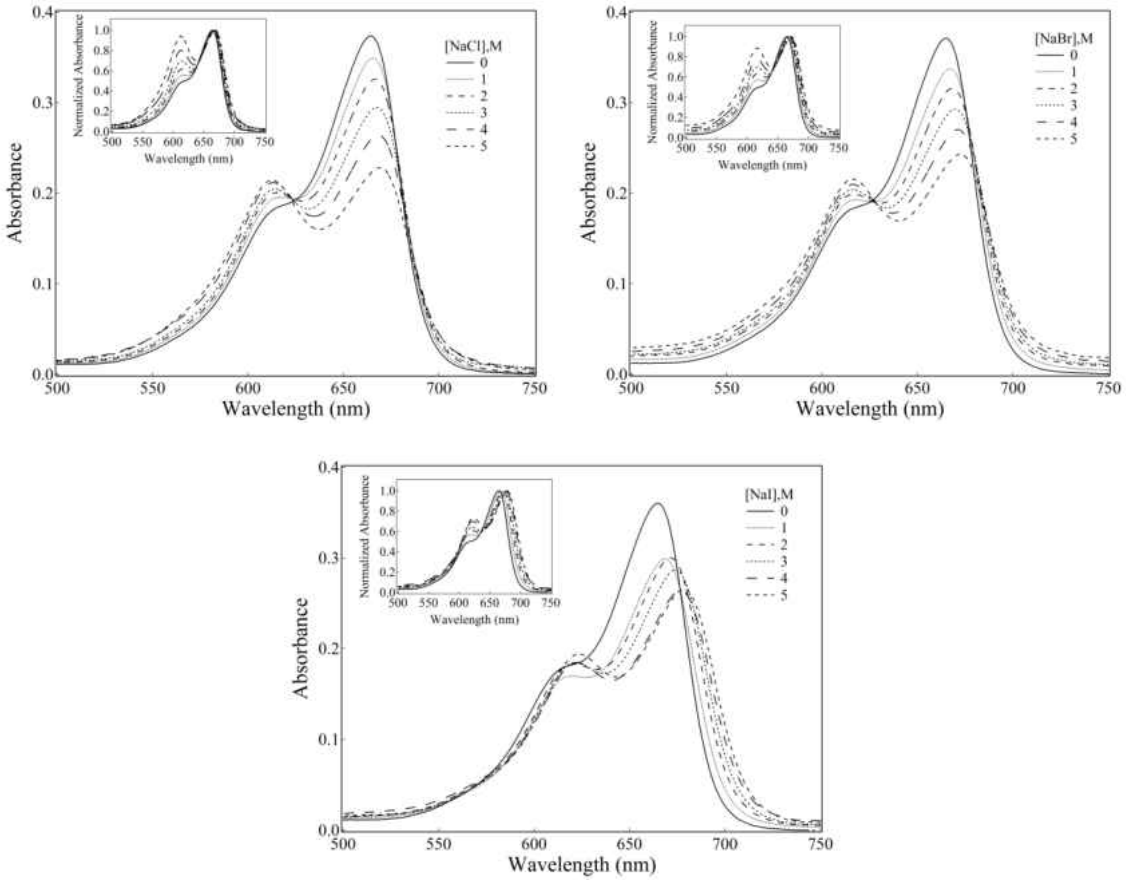

Fig 3.2.2 Salt effects on the absorption spectra of Methylene Blue in water. Clockwise, from top left: sodium chloride, sodium bromide and sodium iodide. Insets: respective spectra normalized at the wavelength of maximum dye absorption in pure water. [MB] = 5 μM.

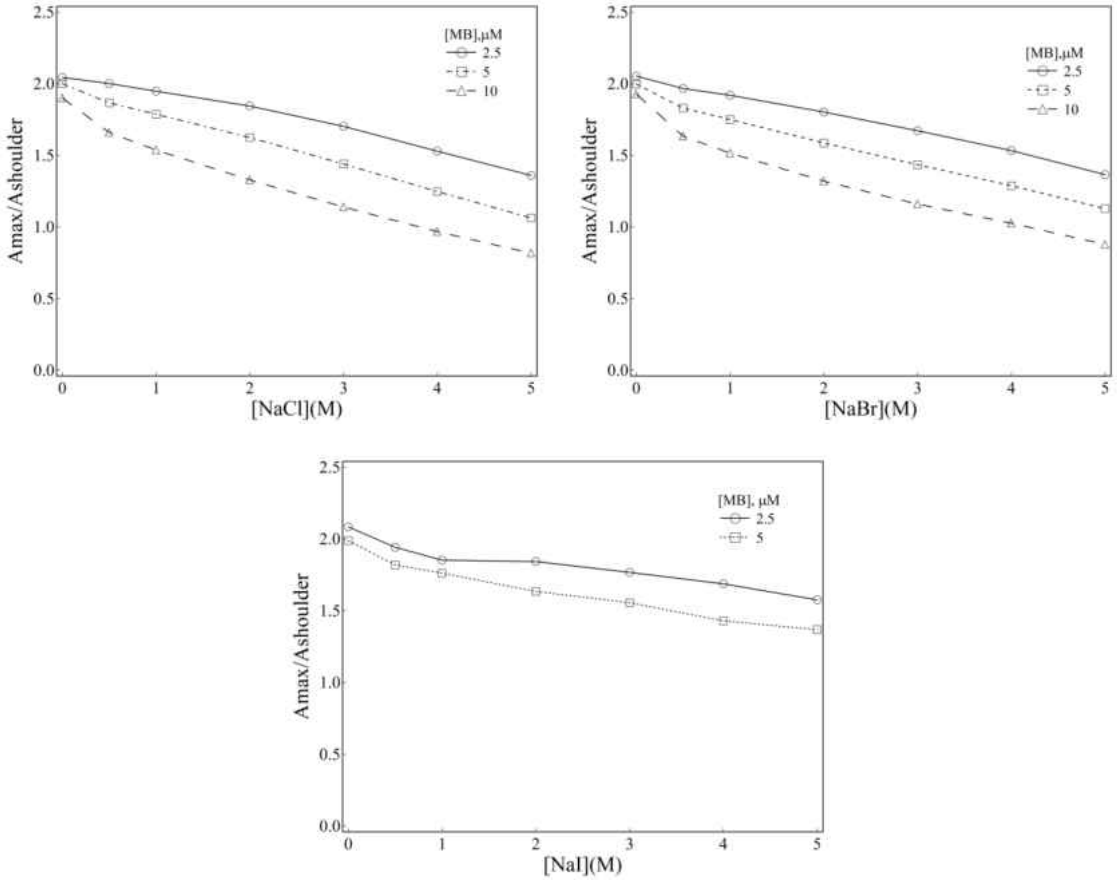

Fig 3.2.3 Effect of dye and salt concentration on the ratio between the absorbance at the wavelength of maximum visible Methylene Blue absorption to that of the shoulder observed at the left-hand side of the respective absorption spectrum in aqueous media. Clockwise, from top left panel: sodium chloride, sodium bromide, sodium iodide. In NaI only 2.5μM and 5.0μM dye solutions were studied because methylene blue tends to precipitate in aqueous NaI at higher concentration (e.g. [MB] = 10μM)

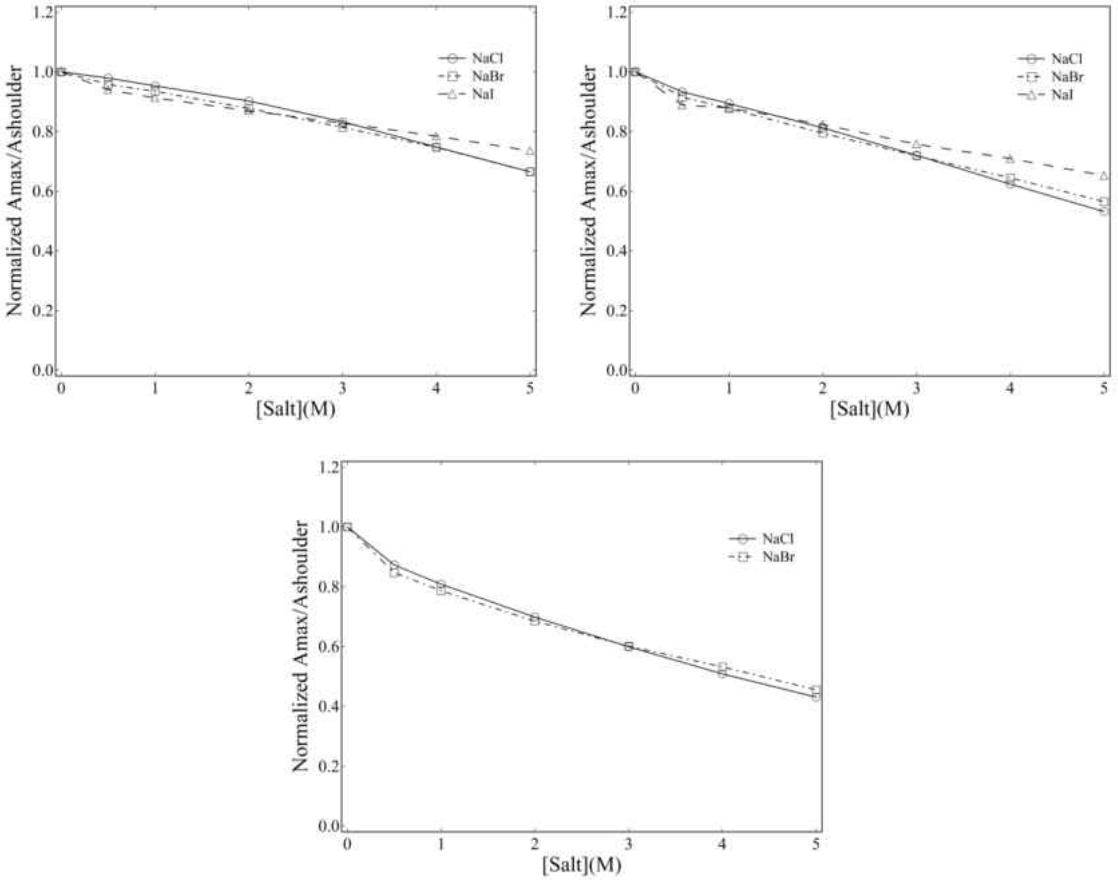

Fig 3.2.4 Salt effects on the ratio between the absorbance at the wavelength of maximum visible Methylene Blue absorption to that of the shoulder observed at the left-hand side of the respective absorption spectrum (aqueous media). Clockwise, from top left panel: ([MB], μM), 2.5, 5 and 10. In NaI only 2.5μM and 5.0μM dye solutions were studied because methylene blue tends to precipitate in aqueous NaI at higher concentration (e.g. [MB] = 10μM)

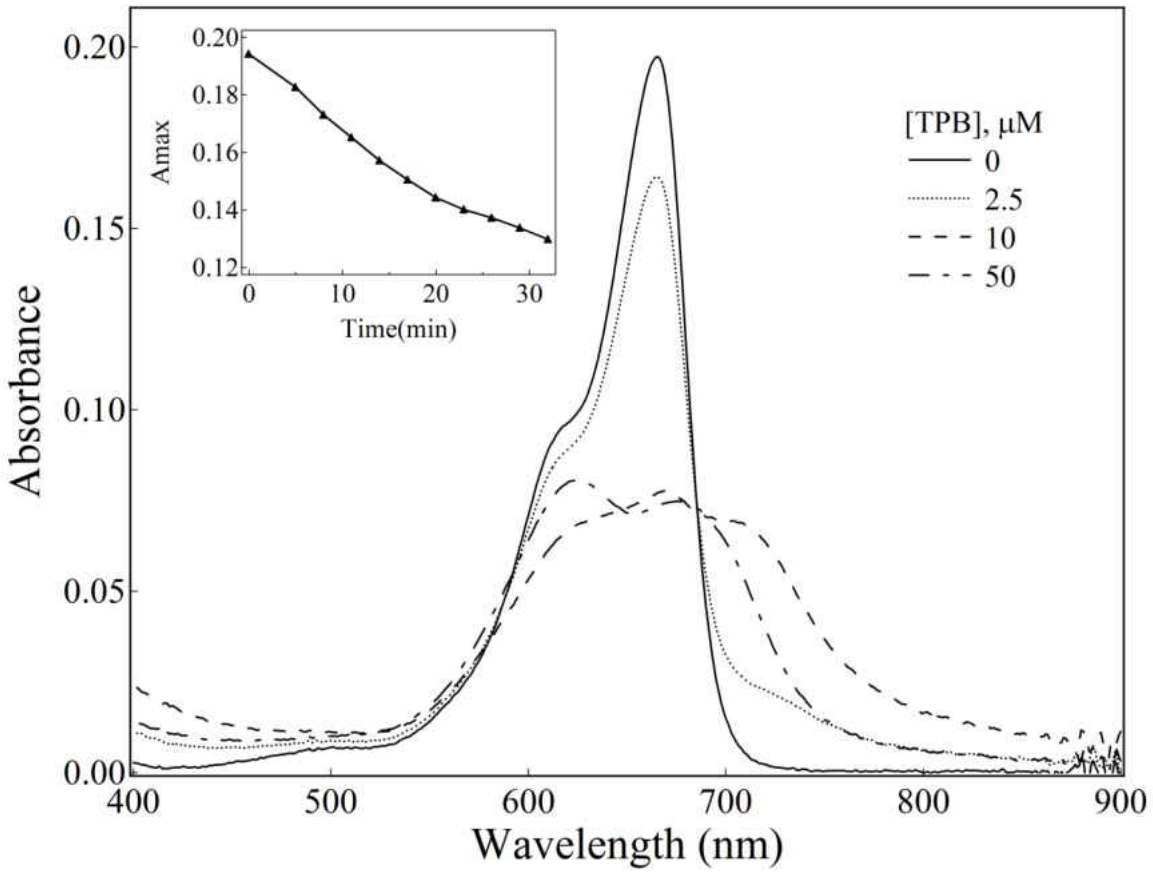

Fig 3.2.5 Effect of sodium tetraphenylborate (TPB) on the absorption spectra of Methylene Blue in aqueous media. Spectra recorded immediately after sample preparation. Inset: Decrease in absorption at λmax as a function of time when in the presence of 2.5 μM TPB. [MB] = 2.5 μM.

for the case of CV. That is, also in this case, the major spectroscopic changes observed upon increasing tetraphenylborate concentration cannot be explained on basis of ionic strength. However, differently from what was observed for the case of CV, the spectroscopic changes observed for MB at low tetraphenylborate concentrations are significantly different from those observed upon increasing sodium halide concentrations to their respective saturation levels (e.g ~ 5M). That is, in the tetraphenylborate case, upon increasing counter ion concentration to just about four-fold (e.g. 10 μM) of that of MB. A significant spectral contribution is observed also at the right-hand side of the respective absorption envelop. This red-shifted (bathochromic) contribution, when combined to the persistent and concomitant contribution observed at region of the original spectroscopic shoulder may, at least in principle, arise from counter-ion facilitate formation of dye aggregates in which the transition dipole moment orientation of the respective monomers keep an oblique orientation with respect to each other. The appearance of a bathochromically shifted absorption band alone would suggest the formation of dye aggregates in which the transition dipole moments of the respective dye monomers are oriented in line (head-to-tail) with respect to each other (J-type aggregates), while the splitting of the band is in keeping with what could be expected for the formation of aggregates in which the transition dipole moments display oblique orientation. Such inference would need to be further investigated though. Mixtures of H-Type and J-type aggregates, or even peculiar properties of the respective MB-tetraphenylborate ion-pairs not previously describe might also explain the observed spectroscopic shifts.

Nevertheless, the effect of tetraphnylborate is significantly more complex for the case of MB as compared to CV. The spectroscopic changes observed for the MB case vary over time, and for high concentrations of tetraphenylborate (e.g. 12 mM) an unidentified reaction is observed, as indicated by changes in solution color from blue to yellow-brown. Interestingly, the MB-tetraphenylborate species formed in aqueous media tends to precipitate when the Dye:conter-ion molar ratio is around 2, but then tends to become more aqueous soluble again as the concentration of the counter ion further increases (Fig. 3.2.6). Whether these solubility effects could facilitate polymeric micelle loading will require further investigation.

The solvatochromic properties of MB have been previously described, and are poor. The wavelength of maximum absorption of MB varies only by 8 nm in going from water to n-butanol as solvent (Gilani et al., 2013). Therefore, in analogy to the CV case, the encapsula -tion of MB into polymeric micelles may be rather difficult to characterize on basis of the spectroscopic changes associated with the effects of the surrounding environment alone on the absorption properties of this dye.

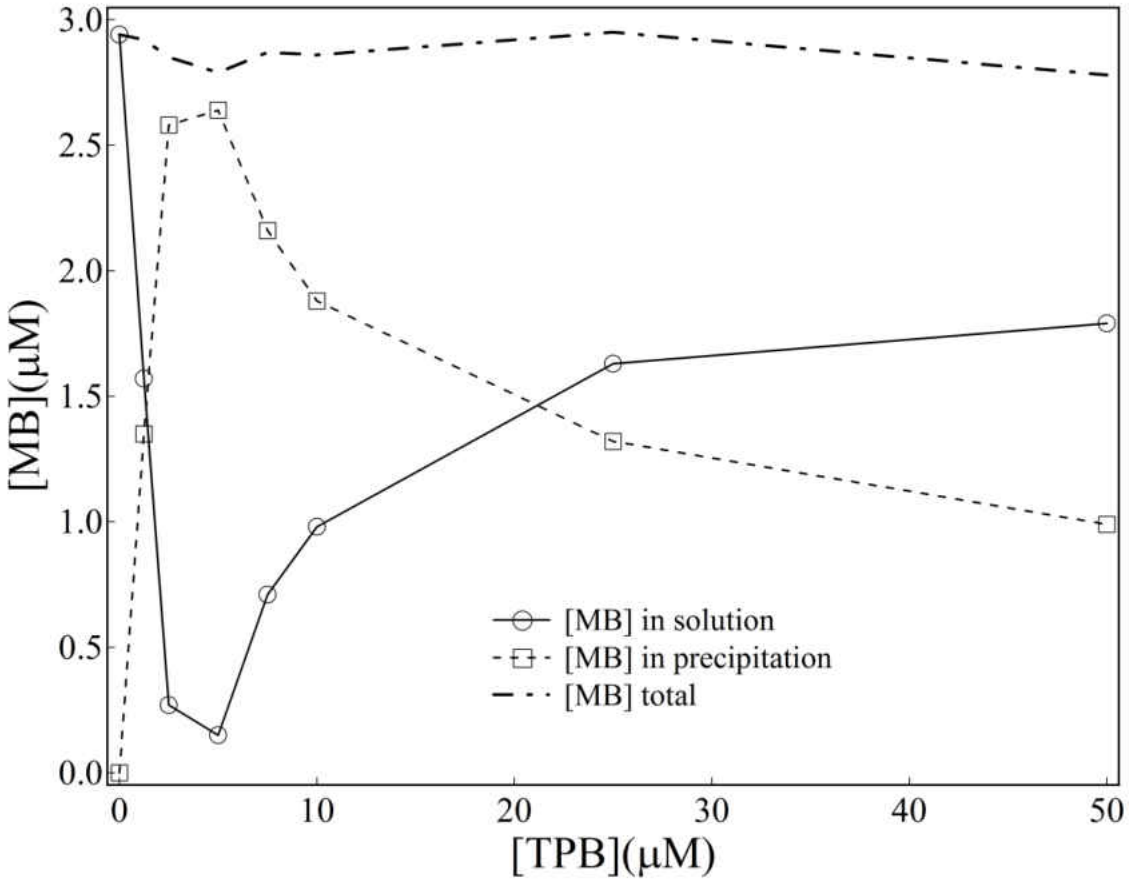

Fig 3.2.6 Amount of methylene blue in solution (solid line) and precipitated (dash line) as a function of TPB concentration. The upper line represents the measured total MB in the system (solution + precipitate). Measurements performed 64 hours after solution preparation. Initial [MB] in solution: 3.0 μM.

3.3 Rhodamine 123

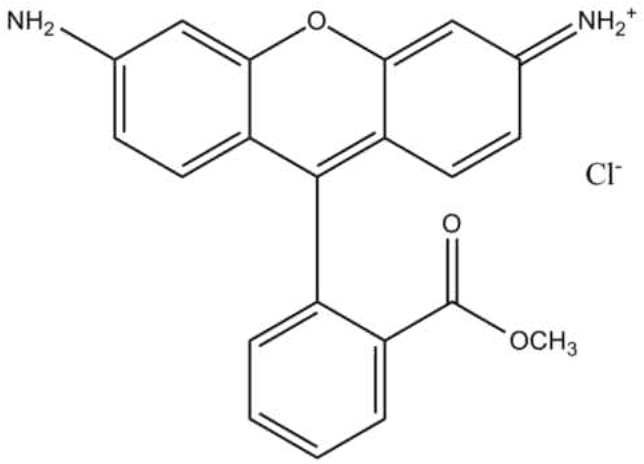

Rhodamine 123

Scheme 3.3.1 Structure of Rhodamine 123

Rhodamine-123 shows high fluorescence quantum yields in a variety of environments, with typically values of Φ_f around 0.8. (Kubin and Fletcher, 1983). Rh-123 is known to accumulate in energized mitochondria with a high degree of selectivity, and for this reason it has been used as a mitochondria-specific probe in fluorescence microscopy. Because the mitochondrial accumulation and retention of Rh-123 is driven primarily by inner mitochondrial membrane potentials, this dye has been extensively used in studies dealing with the measurement of such trans-membrane potentials, and also in studies dealing with the tracking of the depolarization in these membranes as a result of cellular insults (Johnson et al, 1980; Johnson et al., 1981; Chen, 1988; Belostotsky et al., 2011). In addition, Chen and co-workers have demonstrated that the inner-mitochondria trans-membrane potential is typically 60 mV higher in tumor cells as compared to normal cells, and this difference in trans-membrane potential

provides, in principle, for a 10-fold higher accumulation of Rh-123 in tumor cells as compared to normal cells. Accordingly, Rh-123 and analogs have been investigated as potential drugs for chemo and photodynamic therapy of tumors *via* mitochondrial targeting (Chen, 1988; Chen, 1989; Davis et al., 1985; Kandela et al., 2002, 2003; Lewis and Indig, 2002).

Rhodamine-123 is a dye that shows poor tendencies to aggregate. Its tendencies to aggregate are at best negligible in the concentration range investigated here. Fig.3.3.1 shows that upon increasing Rh-123 concentration in water from 2 μM to 100 μM no unambiguous changes on the ratio between the absorption values observed at the wavelength of maximum absorption to those observed at the respective left-handed spectroscopic shoulder can be characterized. The minor fluctuations observed in this absorption ratio would, at best, indicate just negligible aggregation tendencies. In addition, the respective Beer's law plot (inset of Fig. 3.3.1) is quite linear, indicating that no significant dye-dye interactions can be expected to take place in the concentration range investigated. Likewise, no measurable aggregation has been observed for this dye in aqueous media upon increasing ionic strength up to that represented by 4.5 M sodium chloride solutions (Fig. 3.3.2).

On the other hand, Rh-123 is sensitive to the presence of tetraphenylborate in solution. Even in diluted Rh-123 solutions (e.g. 2.5 μM), the presence of tetraphenylborate in concentration as low as 25 μM already leads to quite significant spectroscopic changes (Fig 3.3.3). Here, the appearance of a red-shifted absorption band suggests that ion-pairing may facilitate the formation of J-type dye aggregates of Rh-123 in water. Less structured

spectroscopic changes were observed in the blue region of the spectrum. The observed monotonous and sharp increase in optical density in the UV-visible region of the spectrum upon increasing tetraphenylborate concentration suggests that such contribution may arise from light scattering rather than absorption. That is, such blue contributions may arise from the formation of particulates (precipitates) in solution. The demonstration of such inference will require further investigation though.

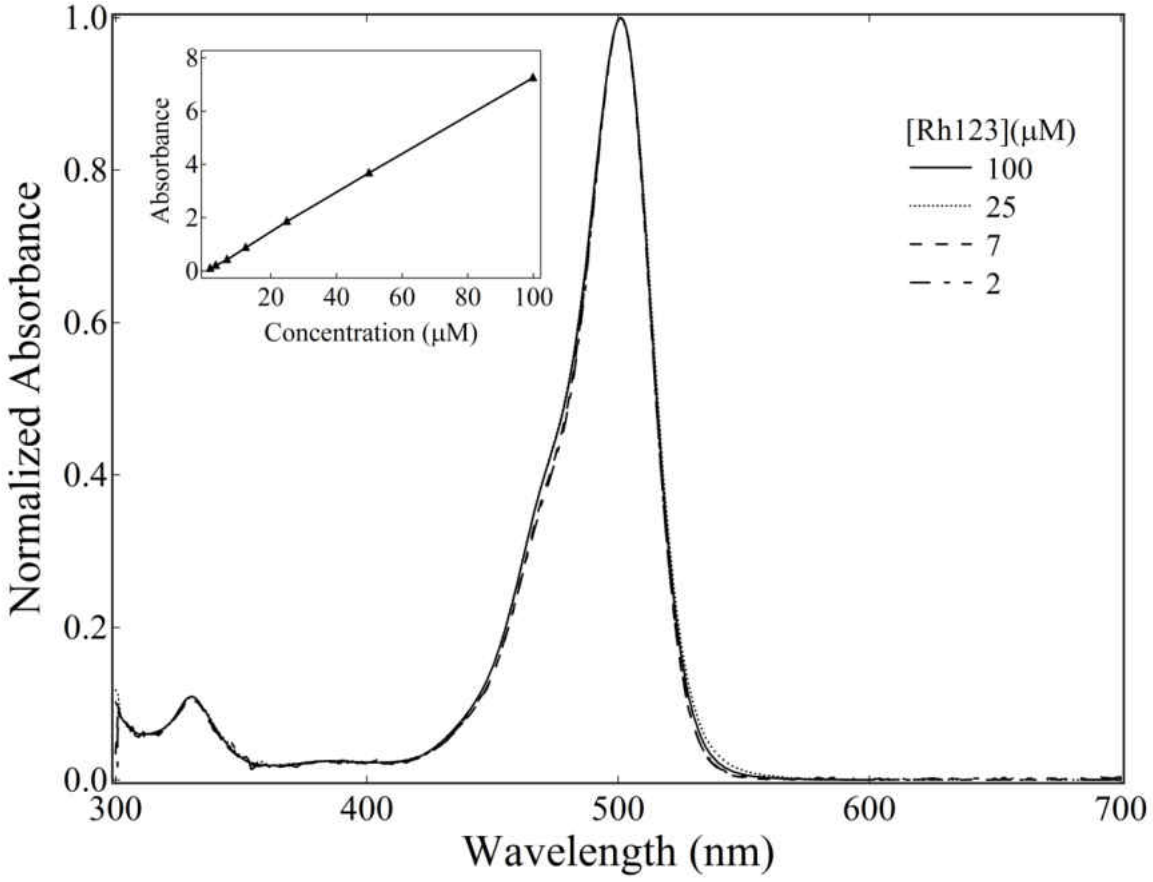

Fig 3.3.1 Effect of concentration on the absorption spectrum of Rhodamine-123 in water. Inset: Absorption at λmax as a function of dye concentration.

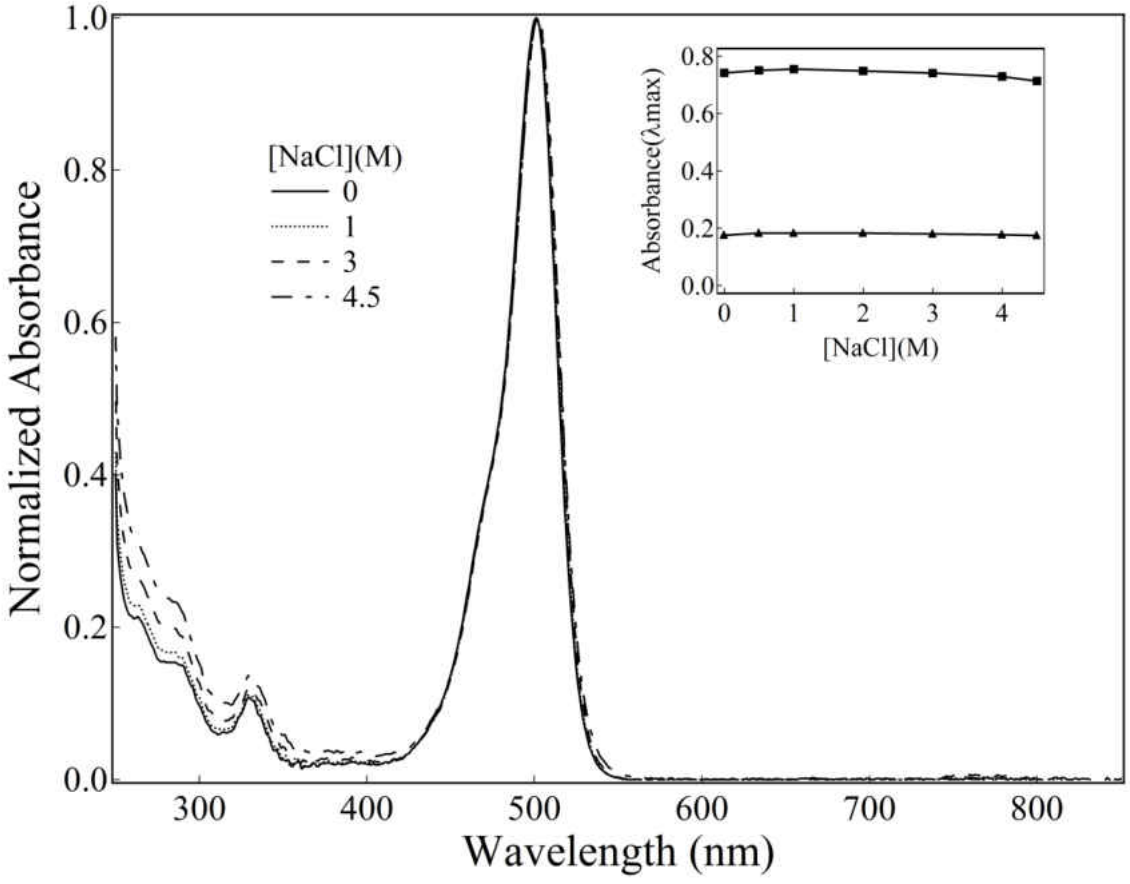

Fig 3.3.2 Effect of sodium chloride on the absorption spectra of 2.5μM Rhodamine-123 in water. Inset: Absorbance at λ_{max} as a function of NaCl concentration, top line: [Rh123] = 10μM, bottom line: [Rh123] = 2.5μM.

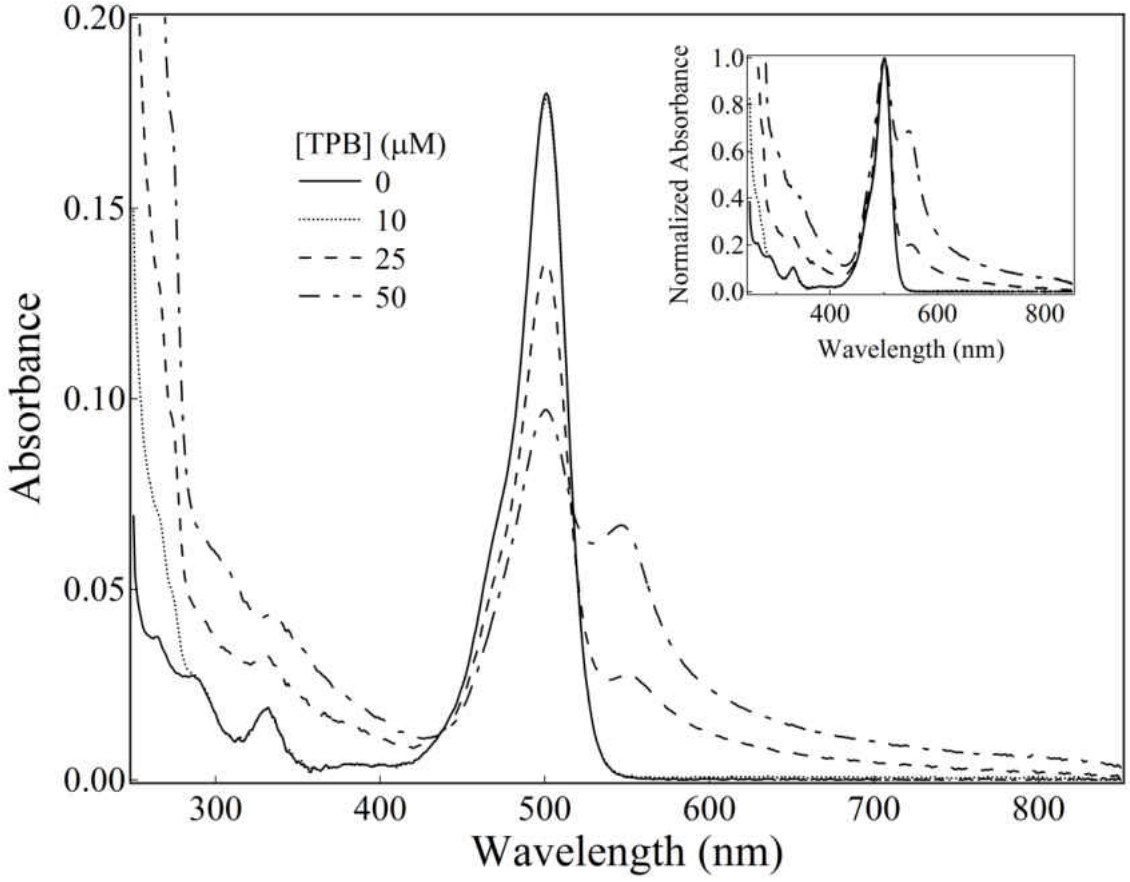

Fig 3.3.3 Effect of sodium tetraphenylborate (TPB) on the absorption spectra of 2.5μM Rhodamine-123 in water. Inset: Respective normalized spectra.

3.4 Styryl 9M

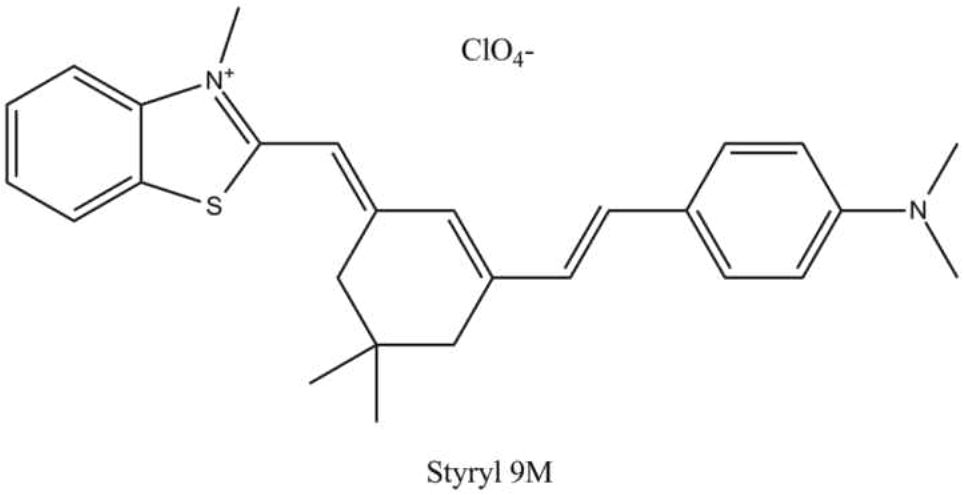

Styryl 9M

Scheme 3.4.1 Structure of Styryl 9M

Styryl dyes are often used as fluorescent imaging agents in neurobiology due to their enhanced fluorescence quantum yields upon binding to plasma membranes (Wu et al., 2009; Amaral et al., 2011). Styryl 9M and other styryl dyes have more recently been employed not only in single-photon steady-state imaging techniques, but also in two-photon time-resolved near-IR imaging of tumor cells. Styryl 9M has been found to show potential as a visible imaging agent that can be effectively excited both at the visible and near-IR ranges of the spectrum (Starkey et al., 2012). In addition, one of the most common characteristics of styryl dyes of particular interest to this study is represented by their solvatochromic properties. That is, their spectroscopic sensitivity toward the properties of the surrounding environments in which they are located (e.g. polarity/polarizability; Jones and Indig, 1996). The study of the remaining dyes described in this chapter will focus primarily on the respective tendencies to aggregate in pure

water, and also on their respective solvatochromic properties (i.e. solvent effects).

Styryl 9M shows reduced solubility in water, and for this reason the upper concentration used to explore its aggregation tendencies was limited by solution saturation (~ 22 μM). Figure 3.4.1 shows normalized absorption spectra of 3 μM to 22 μM aqueous styryl 9M solutions. In this concentration range no indication of dye aggregation has been observed.

Styryl 9M was found to show significant solvatochromism though, with its respective wavelength of maximum absorption varying from 511 nm in water to 602 nm in n-pentanol (Table 3.4.1). Figure 3.4.2 shows the absorption spectra of 10 μM styryl 9M solutions prepared in nine different solvents. Although more abrupt changes were observed both in the wavelength of maximum dye absorption and respective extinction coefficient in going from water to organic solvents, within the organic series only small solvent effects were observed in the respective extinction coefficients, while the changes observed in wavelength of maximum absorption were

Solvent	Π*	α	β	λ_{max}(nm)
Water	1.09	1.17	0.18	511
Acetonitrile	0.75	0.19	0.31	564
Acetone	0.72	0.08	0.48	571
Methanol	0.6	0.93	0.62	574
Ethanol	0.54	0.83	0.77	585
n-Propanol	0.52	0.78	0.9	592
i-Propanol	0.48	0.76	0.95	590
n-Butanol	0.47	0.79	0.88	601
n-Pentanol	0.4	0.84	0.86	602

Table 3.4.1 Solvent effects on λ_{max} for 10μM solutions of Styryl 9M

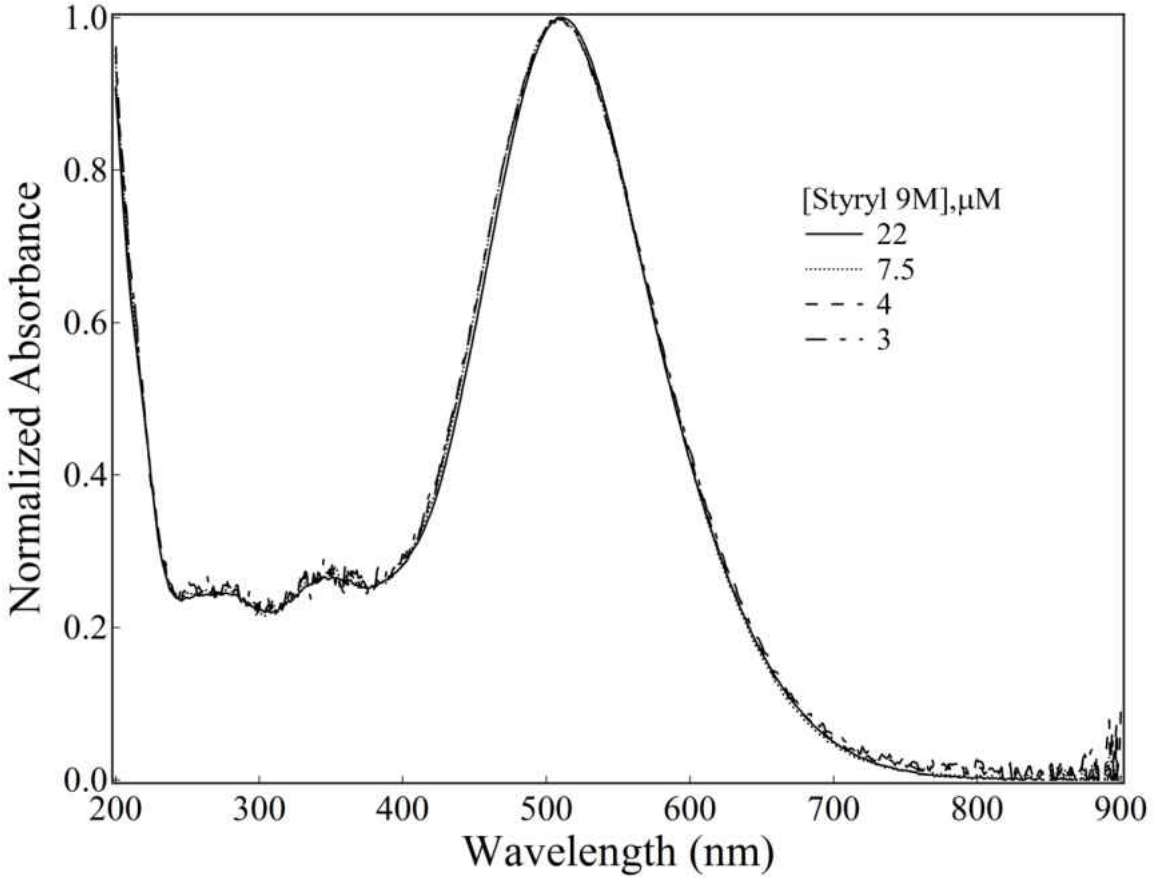

Fig 3.4.1 Absorption spectra of various concentrated Styryl 9M in water.

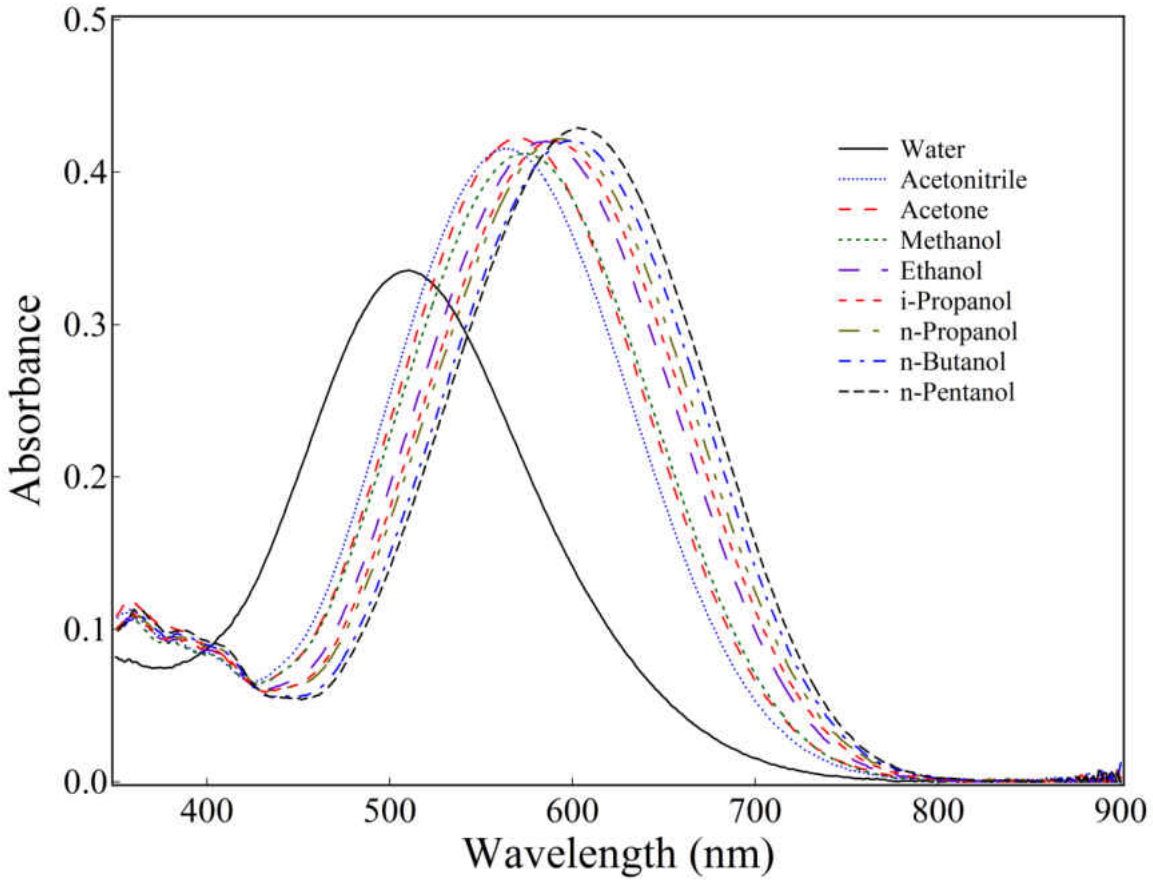

Fig 3.4.2 Absorption spectra of Styryl 9M in different solvents. From left to right, at A = 0.2: water, acetonitrile, acetone, methanol, ethanol, i-propanol, n-propanol, n-butanol and n-pentanol. [Dye] = 10 μM.

found to show a close to linear relationship with solvent polarity/polarizability (Π* scale; Figure 3.4.3). Here the overall observation was a continuous shift of the absorption envelop toward the red region of the spectrum upon decreasing solvent polarizability. This finding indicates that the S_0 -> S_1 transition energies decrease upon decreasing solvent polarizability.

Plots of the other two Kamlet-Taft solvent solvatochromic parameters (α and β) as a function of styryl-9 wavelength of maximum absorption are also shown in Fig. 3.4.3. The dependence of λ_{max} on β (a measure of the solvent hydrogen-bond acceptor basicity) was also found to be close to linear. However, the α values (a measure of the solvent hydrogen-bond acidity) associated with the solvents used in this study were found to be clustered in the two extremes of the range investigated, what make it more difficult to draw inferences on how and to which extent solvent hydrogen-bond acidity affects the spectroscopic properties of styryl 9M. Still, in this last case, an apparent trend of increase in λ_{max} upon increasing α was observed. We have found no evidence for styryl 9M aggregation in any of the organic solvents studied here, at least when in concentrations up to 10 μM (see Appendix A).

The significant environmental effects (i.e. solvent effects) on the absorption spectra of this dye are bound to facilitate the characterization of its localization in the nanoscopic environments (core and/or corona) of the polymeric micelles of interest here.

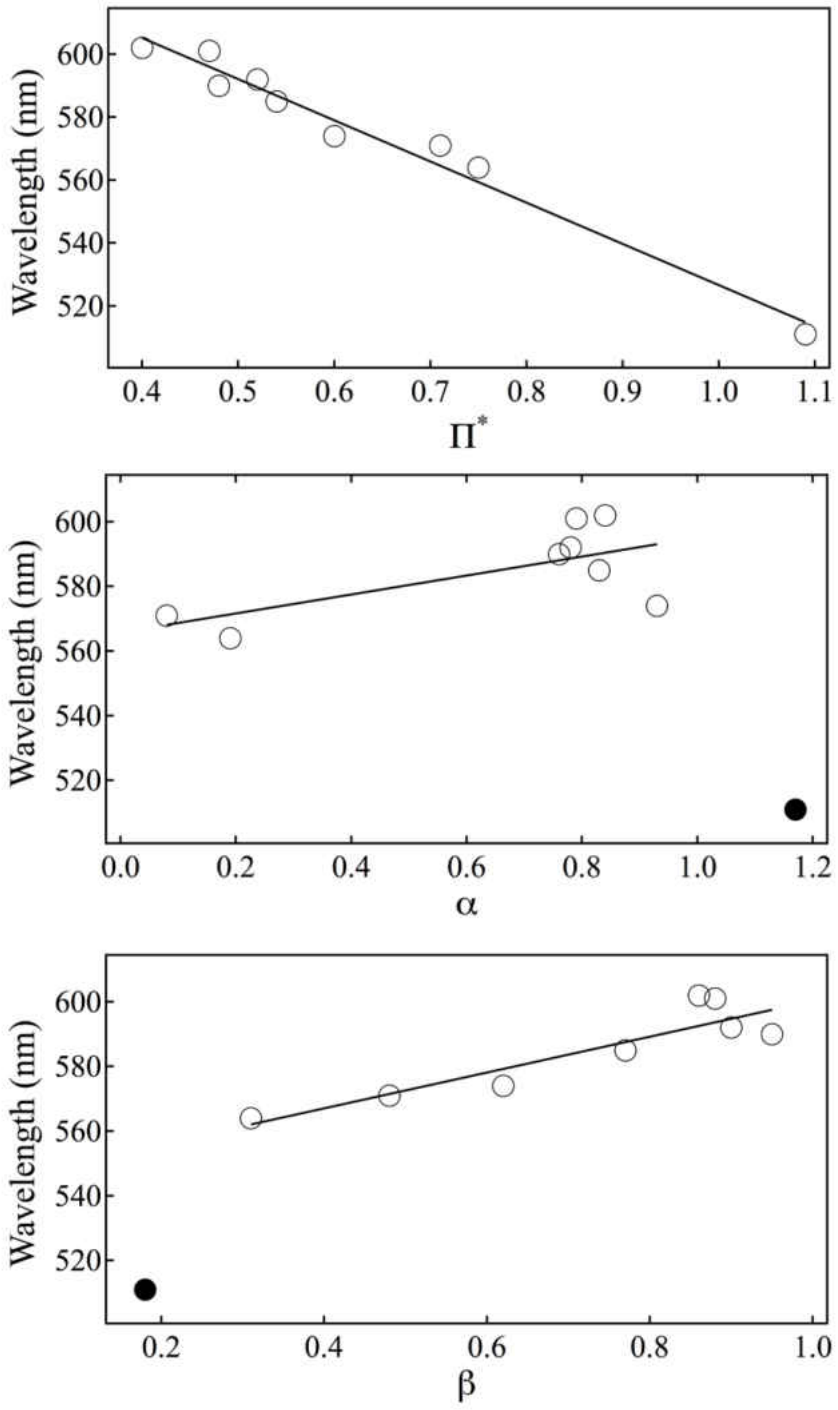

Fig 3.4.3 Solvatochromic effects on the wavelength of maximum Styryl 9M absorption. See table 3.4.1 for respective solvents.

Solid dots represent water.

3.5 HITC

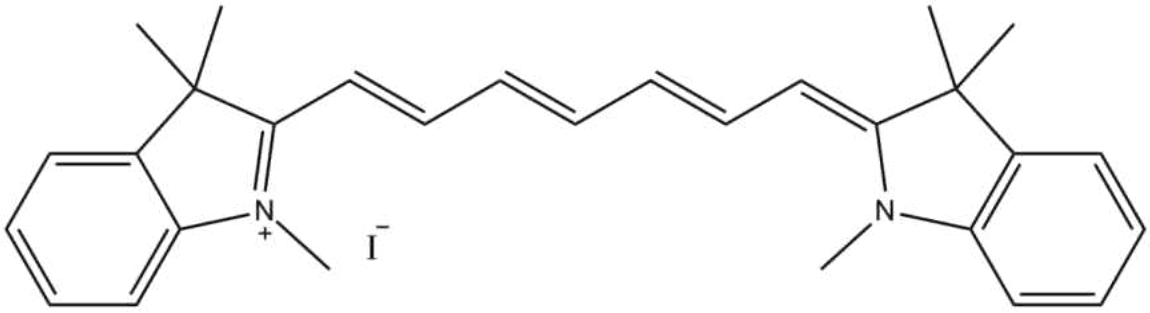

1,1',3,3,3',3'-Hexamethylindotricarbocyanine iodide (HITC)

Scheme 3.5.1 Structure of HITC

Cationic polymethine dyes are widely used as fluorescence tags in biology and biochemistry. For example, Cy3 and Cy5 are routinely used for the fluorescence labeling of dideoxynucleoside triphosphate terminators in mutation detection (Fortina et al., 2000). Polymethine dyes also show photosensitization properties that may be considered as of potential use in cancer phototherapy (Istomin et al., 2006; Delaey et al., 2000). HITC, is a polymethine dye that shows easily measurable fluorescence in the near-IR range of the spectrum (Drexhage, 1976). In this study we have investigated whether and to which extent HITC can be incorporated into polymeric micelles. The chromophoric group of HITC is identical to that of DiR, but HITC is significantly less lipophilic as compared to DiR.

HITC was found to show modest tendencies to aggregate in aqueous media. Figure 3.5.1 shows the effect of concentration on the absorption spectra of this dye in water. Again in this case, aggregation is revealed by an increase in absorption at the region of the spectroscopic

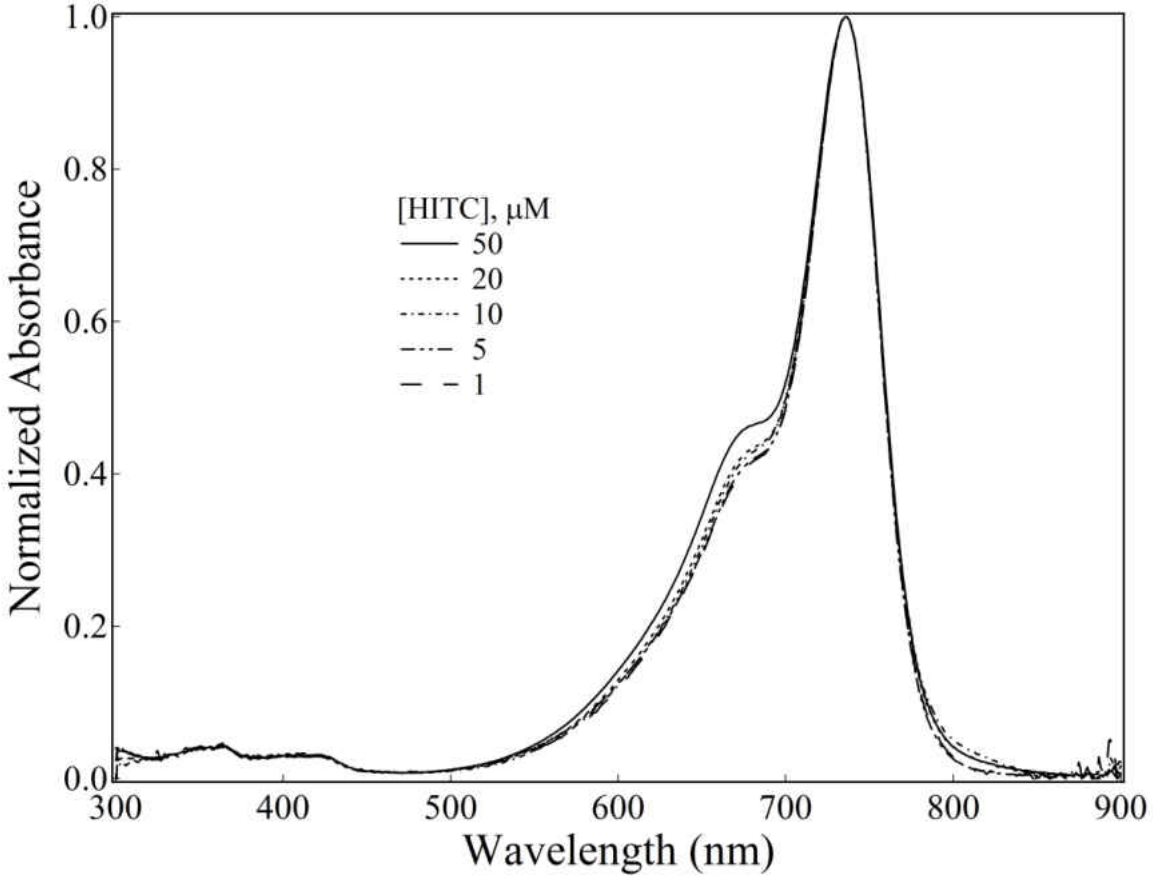

Fig 3.5.1 Effect of concentration on the absorption spectrum of HITC in water.

shoulder observed at the left-hand side of the respective absorption envelop, as compared to that observed at the wavelength of maximum dye absorption. Here, again, the observed hypsochromic spectral shift is an indication of the formation of H-type dye aggregates in solution, which leads to a decrease in the respective quantum yield of fluorescence along with an increase in efficiency of intra-molecular photoinduced electron transfer reactions.

The solvatochromic properties of HITC were found to be significantly less pronounced than those observed for the case of Styryl 9M (see section 3.4), and more in keeping with those previously described for CV and MB (compare sections 3.1and 3.2). For HITC, the wavelength of maximum dye absorption was found to vary from 736 nm in water to 748 nm in n-pentanol (Table 3.5.1). Fig 3.5.2 shows the absorption spectra of 5 μM styryl 9M solutions prepared in nine different solvents. Although again more abrupt changes were observed in the respective extinction coefficient at λ_{max} in going from water to organic solvents, within the organic series only relatively modest solvent effects were observed in the respective extinction coefficients.

In this case we have explored how, and to which extent, the Kamlet-Taft solvent solvatochromic parameters (Π*, α and β) affect the wavelength of maximum dye absorption, the wavelength of absorption observed at the respective spectroscopic shoulder, and also the difference in frequency ($\Delta\bar{\upsilon}$) observed between the wavelengths of maximum and shoulder absorptions (Fig 3.5.3). This exercise has been carried out with the objective of finding the most prominent spectroscopic changes associated with environmental effects. That is, the spectro-

Solvent	Π*	α	β	λ_{max}(nm)	$\lambda_{shoulder}$(nm)	$\Delta\bar{\upsilon}$(cm^{-1})
Water	1.09	1.17	0.18	736	671	1358.7
Acetonitrile	0.75	0.19	0.31	741	674	1341.5
Acetone	0.72	0.08	0.48	742	674	1359.7
Methanol	0.6	0.93	0.62	740	673	1345.3
Ethanol	0.54	0.83	0.77	743	676	1333.9
n-Propanol	0.52	0.78	0.9	745	678	1326.4
i-Propanol	0.48	0.76	0.95	744	677	1330.2
n-Butanol	0.47	0.79	0.88	747	679	1340.6
n-Pentanol	0.4	0.84	0.86	748	681	1315.3

Table 3.5.1 Solvent effects on λ_{max}, $\lambda_{shoulder}$ and $\Delta\bar{\upsilon}$ of 5μM HITC solutions

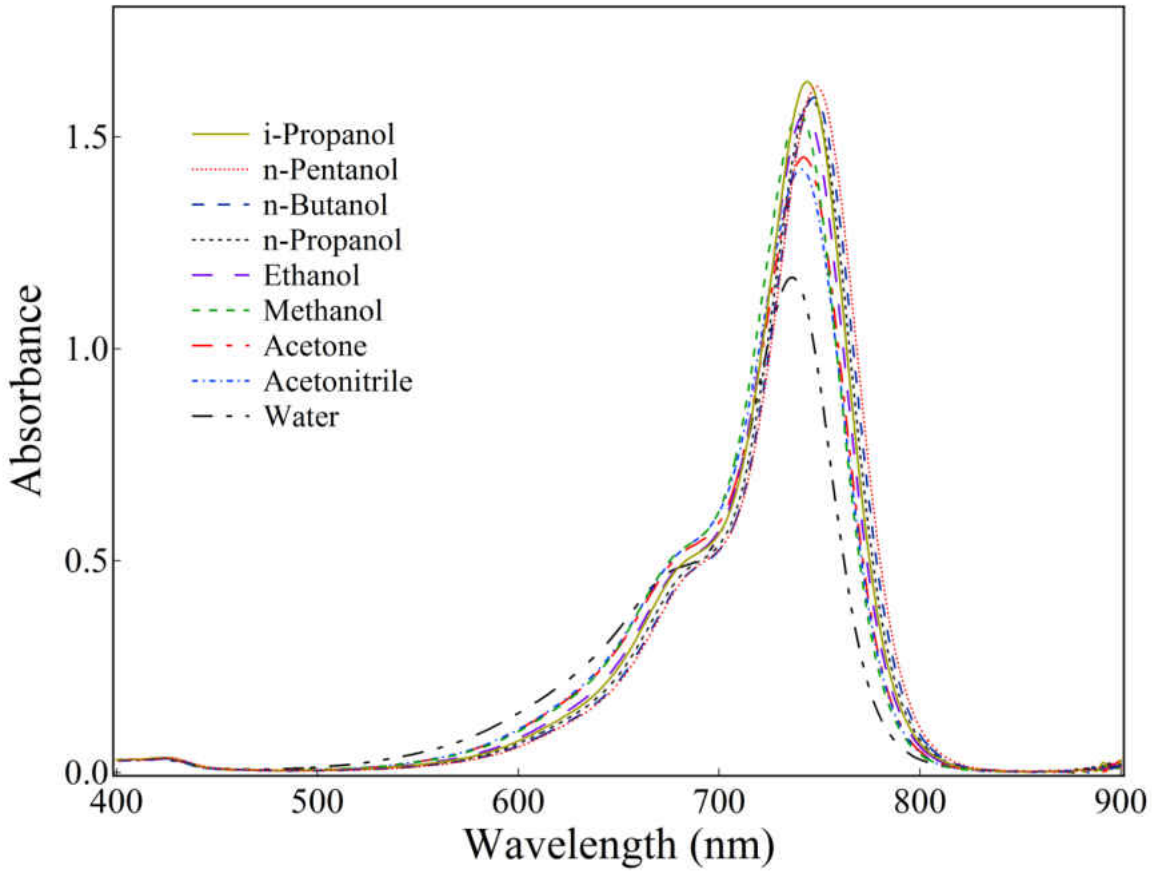

Fig 3.5.2 Absorption spectra HITC in different solvents. [HITC] = 5μM.

scopic changes that most effectively could provide for the characterization of HITC interaction with the nanoscopic environments of polymeric micelles. However what we have found was that, regardless of the parameter considered, environmental effects on the spectroscopic characteristics of HITC are just too modest to be considered as useful tools for such characterization. For this dye, changes in total sample (dye) absorption observed for the original formulation, as compared to those associated with the respective purified micelles, should provide more direct information on encapsulation efficiency

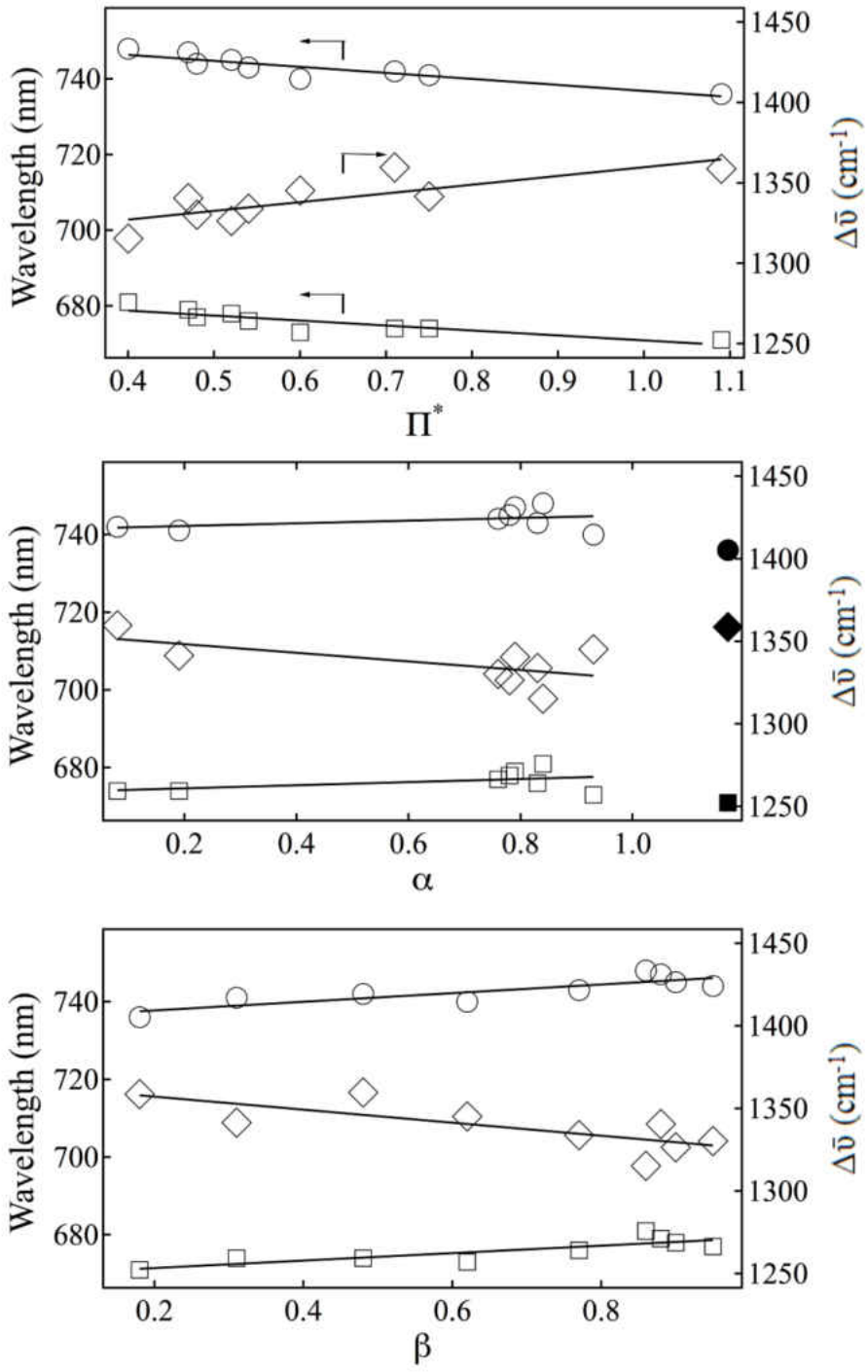

Fig 3.5.3 Solvatochromic effects on λ_{max}, $\lambda_{shoulder}$ and $\Delta\bar{\upsilon}$ for HITC. Empty circles, $\lambda_{max;}$ empty diamond, $\Delta\bar{\upsilon}$; solid square, $\lambda_{shoulder}$.

Solid dots, squares and diamonds represent water

3.6 DiR

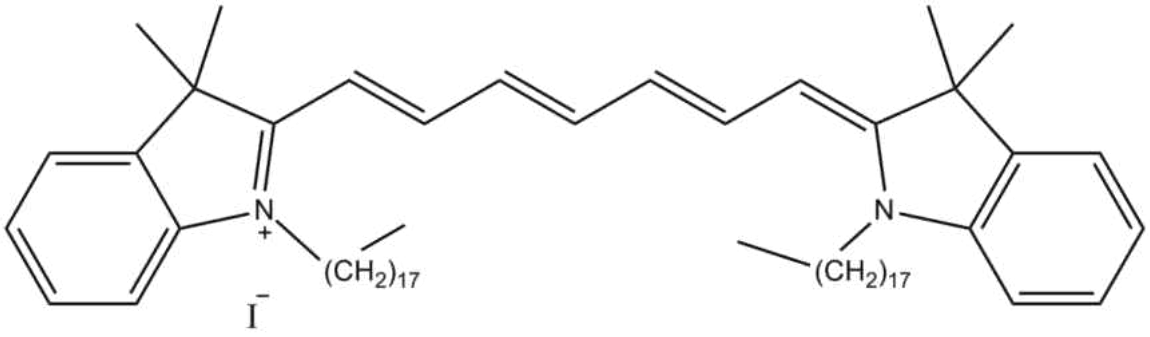

1,1'-dioctadecyltetramethyl indotricarbocyanine iodide (DiR)

Scheme 3.6.1 Structure of DiR

DiR is a lipophilic carbocyanine dye that shows high extinction coefficient(s) and desirable fluorescence quantum yield in the near-IR region of the spectrum. It has been used as a fluorescent probe in a variety of imaging applications, including the staining of cell membranes and liposomes (Trotter et al., 1989; Kalchenko et al., 2006; Shim et al., 2012). Lipid nanoparticles loaded with DiR have shown desirable staining properties in studies involving both *in vitro* and *in vivo* imaging of live cells (Texier et al., 2009). DiR has also been previously encapsulated into polymeric micelles for *in vivo* imaging of tumors (Cho and Kwon, 2011; Cho et al., 2012, 2014).

DiR is structurally analogous to HITC. The only difference between these two dyes is represented by the size of the alkyl groups linked to the respective quaternary ammonium moieties. While octadecyl substituents are present in DiR, the respective substituents in HITC are methyl groups, and this difference makes DiR significantly more hydrophobic then HITC.

Indeed, while the tendencies of HITC to aggregate in water are modest (see section 3.5), those associated with DiR are, on the other hand, remarkable. DiR was found to be the dye showing the highest aggregation tendencies amongst all dyes considered in this study. Here DiR was always found to be mostly presented in its aggregated state when in aqueous media, even when in concentrations as low as 0.05 μM (Fig. 3.6.1). Upon increasing DiR concentration first to 5 μM, and then to saturation, the further spectroscopic shifts observed toward the blue (bathochromic) region of the spectrum (Fig. 3.6.1) indicates the formation of molecular assemblies with aggregation numbers higher than two (i.e. trimmers and possibly higher aggregates).

The comparison between the aggregation tendencies of HITC and DiR in water can be rationalized in terms of the distinct contributions associated with the hydrophobic effect when acting upon these two distinct but yet structurally related dyes. At least for the case of DiR the hydrophobic effect can be expected to represent the major driving force behind dye aggregation.

We have also observed that when in the presence of the anionic detergent sodium dodecyl sulfonate (SDS), such aggregates start to dissociate even when exposed to SDS concentrations far below the respective critical micellar concentration (CMC), and tend to display the spectroscopic fingerprint expected for the respective dye monomer as the SDS concentration approaches the respective CMC (Fig. 3.6.2). This observation suggests that the DiR aggregates start to dissociate initially as a result of ion pairing with SDS molecules, and the respective molecules are eventually entirely diluted to the respective dye monomers as the SDS concentra-

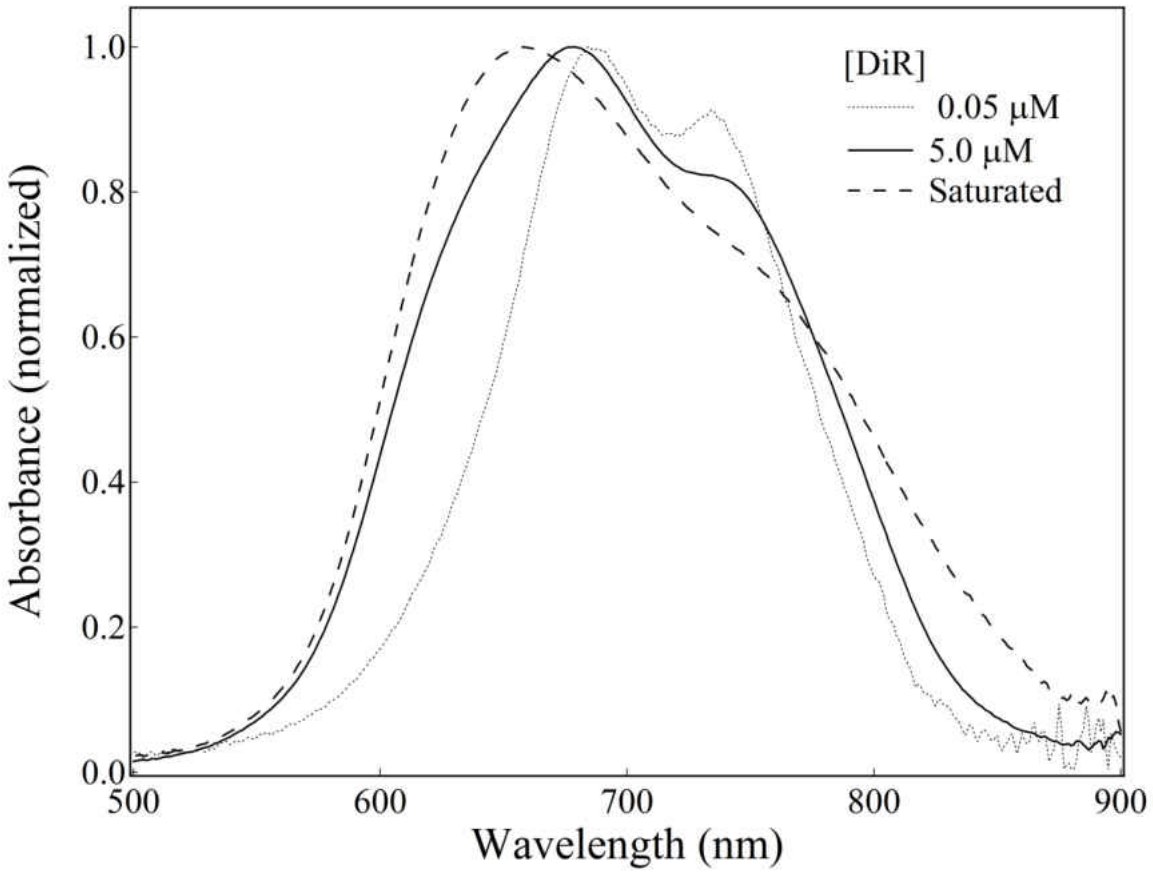

Fig 3.6.1 Absorption spectra of various concentrated DiR in water.

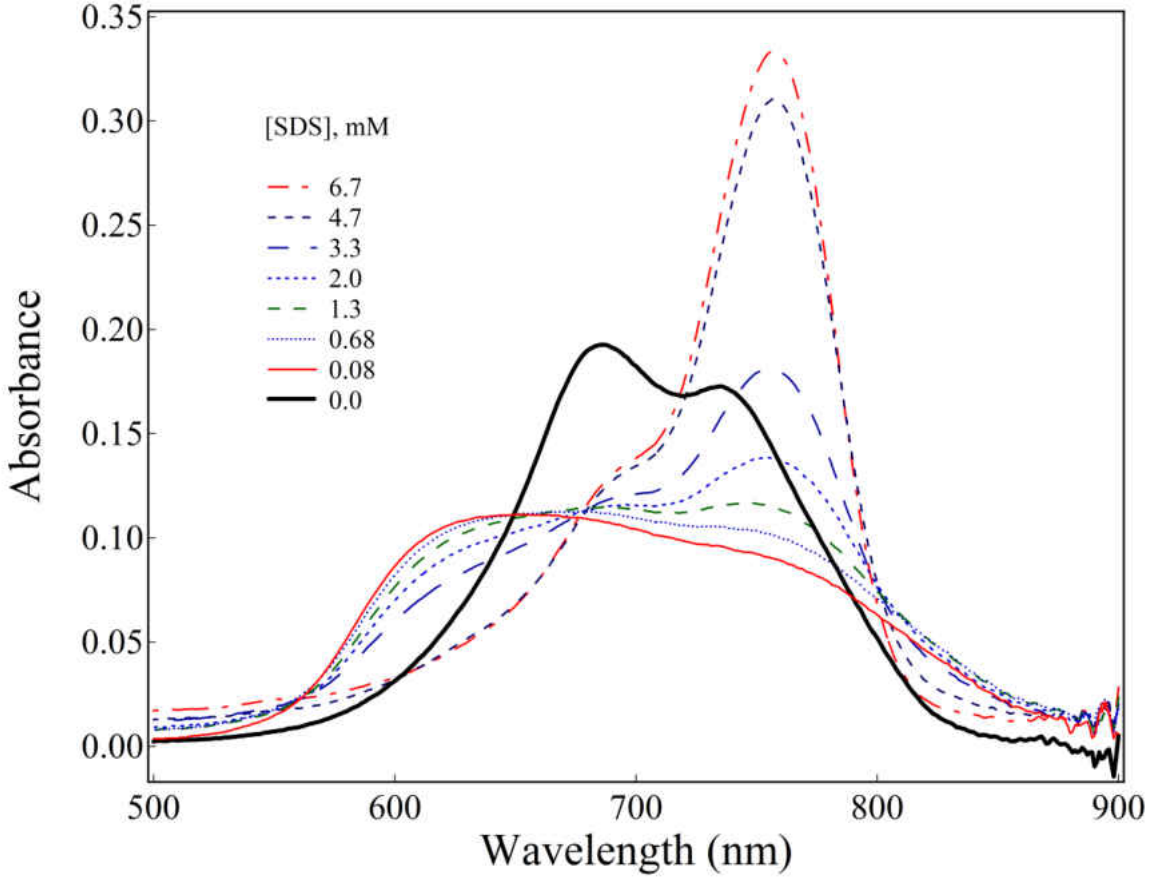

Fig 3.6.2 Effect of Sodium dodecyl sulfate (SDS) on the absorption spectra of DiR in water.

tion further increases.

We have found no evidences for DiR aggregation in any of the eight polar organic solvents used in this study (e.g. at least for DiR concentrations up to 5 μM; see Appendix C). On the other hand, here we have demonstrated that the DiR aggregates formed in water are easily broken apart when in the presence of a polar organic co-solvent in solution. Fig 3.6.3 shows the effect of ethanol concentration on the aggregation of DiR in water/ethanol mixtures (v:v, %). Upon increasing ethanol concentration, the contribution associated with the spectroscopic fingerprint characteristic of respective dye monomer increases, and this observation is in keeping with the inference that the aggregation of DiR in water counts with dominate contributions arising from the hydrophobic effect.

Regardless of the high aggregation tendency observed for DiR in aqueous media, as compared to HITC, the solvatochromic properties associated these two distinct dyes are highly comparable compare tables 3.5.1 and 3.6.1). This finding is not surprising, given the fact that the alkyl (methyl vs octadecyl) substituents associated with the respective differences in lipophilic character have at best negligible effect on the properties of the chromophoric groups of these molecules, which are the same in both cases. That is, the spectroscopic behaviors of these two distinct dyes are controlled by the delocalization of Π electrons throughout their respective (and largely comparable) molecular structures.

Solvent	Π*	α	β	λ_{max}(nm)	$\lambda_{shoulder}$(nm)	$\Delta\bar{\upsilon}$(cm^{-1})
Water	1.09	1.17	0.18	747	677	1338.7
Acetonitrile	0.75	0.19	0.31	748	679	1358.6
Acetone	0.72	0.08	0.48	749	681	1333.3
Methanol	0.6	0.93	0.62	748	679.5	1347.7
Ethanol	0.54	0.83	0.77	750	681	1351
n-Propanol	0.52	0.78	0.9	752	684	1322
i-Propanol	0.48	0.76	0.95	750	682	1329.4
n-Butanol	0.47	0.79	0.88	753	684.5	1329
n-Pentanol	0.4	0.84	0.86	755	685.5	1342.9

Table 3.6.1 Solvent effects on λ_{max}, $\lambda_{shoulder}$ and $\Delta\bar{\upsilon}$ for 5μM solutions of DiR.

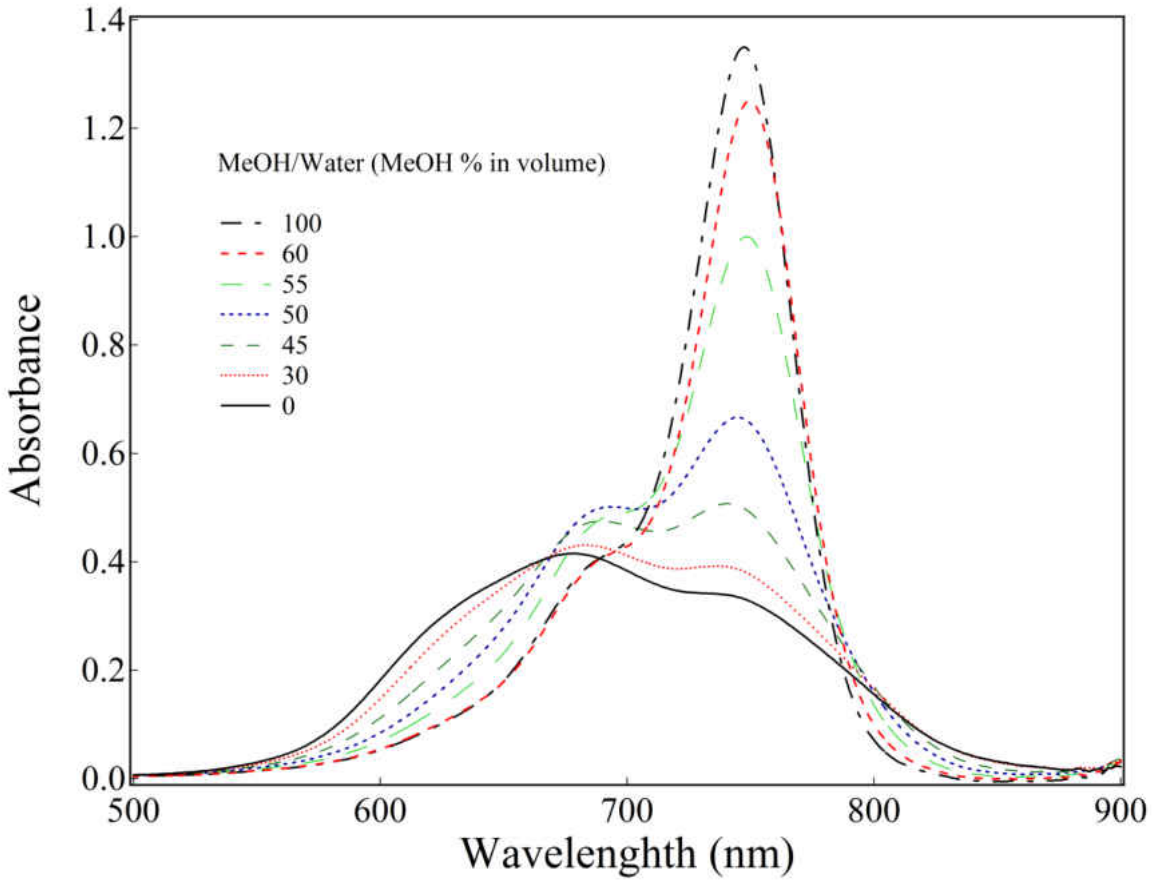

Fig 3.6.3 Absorption spectra of DiR in MeOH/Water mixture at various volume ratios

Figure 3.6.4 shows the absorption spectra of 5 μM DiR solutions prepared in nine distinct solvents. Although again in this case more abrupt changes were observed in the respective extinction coefficient at λ_{max} in going from water to organic solvents, here these changes are more satisfactory explained on basis of the overwhelmingly high tendencies of DiR to aggregate in water alone. That is, in this case the contributions arising from solvent solvatochromic properties can be considered mostly irrelevant as compared to those associated with DiR aggregation in water. However, when considering the organic solvent series alone, then only relatively modest solvent effects were observed (Fig. 3.6.4). In this study we have found that neither the extinction coefficients nor the wavelengths of maximum absorption of DiR in the solvent series investigated varies to an extent compatible to those expected for a desirable solvatochromic probe (Jones and Indig, 1996).

Accordingly, the effect of the Kamlet-Taft solvent solvatochromic parameters (Π*, α and β) on the wavelength of maximum DiR absorption, wavelength of absorption observed at the respective spectroscopic shoulder, and also the difference in frequency ($\Delta\bar{\upsilon}$) observed between the wavelengths of maximum and shoulder absorptions are all modest (Fig 3.6.5). For example, the observed changes in λ_{max} in going from acetonitrile (λ_{max} = 748 nm) to n-pentanol (λ_{max} = 755 nm) is just 7 nm. This exercise has been carried out with the objective of finding the most prominent spectroscopic changes associated with environmental effects. That is, the spectroscopic changes that most effectively could provide for the characterization of DiR interaction with the nanoscopic environments of polymeric micelles. However what we have

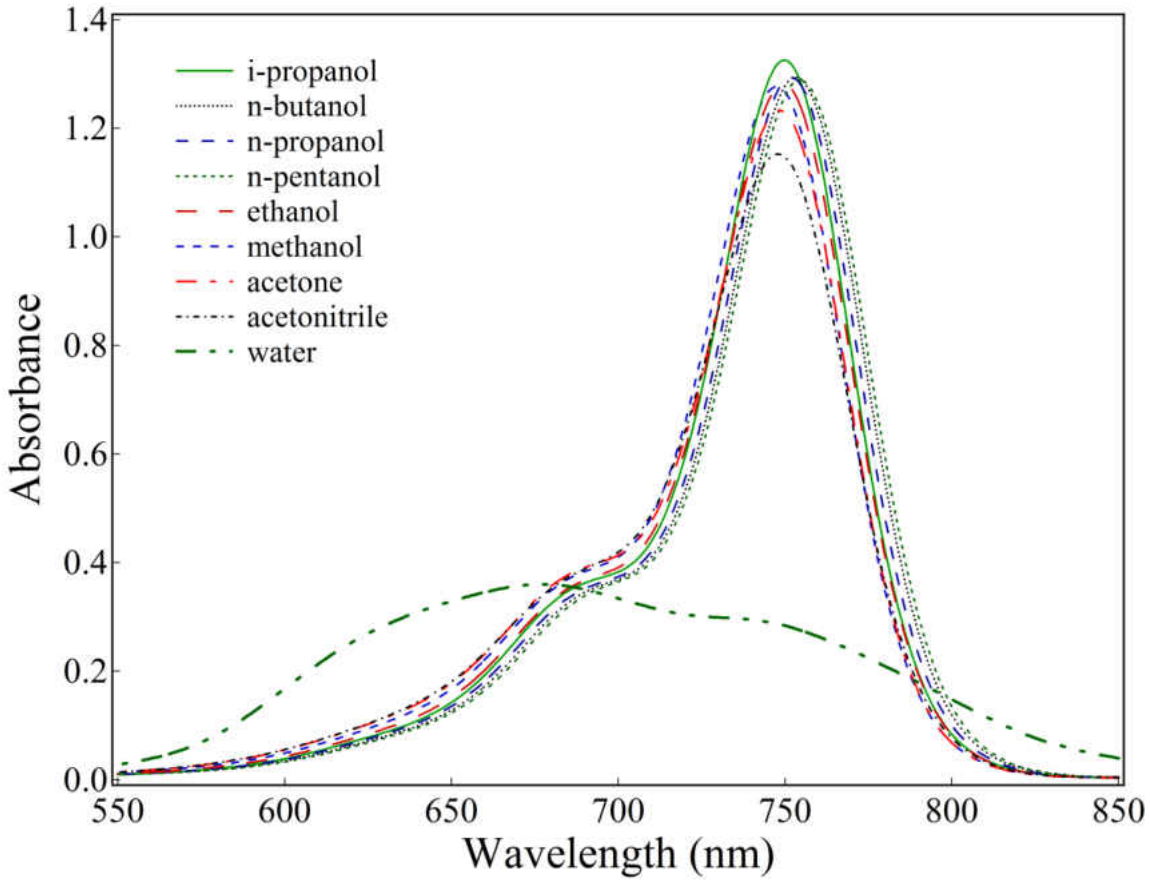

Fig 3.6.4 Absorption spectra of DiR in different solvents. [Dye] = 5μM.

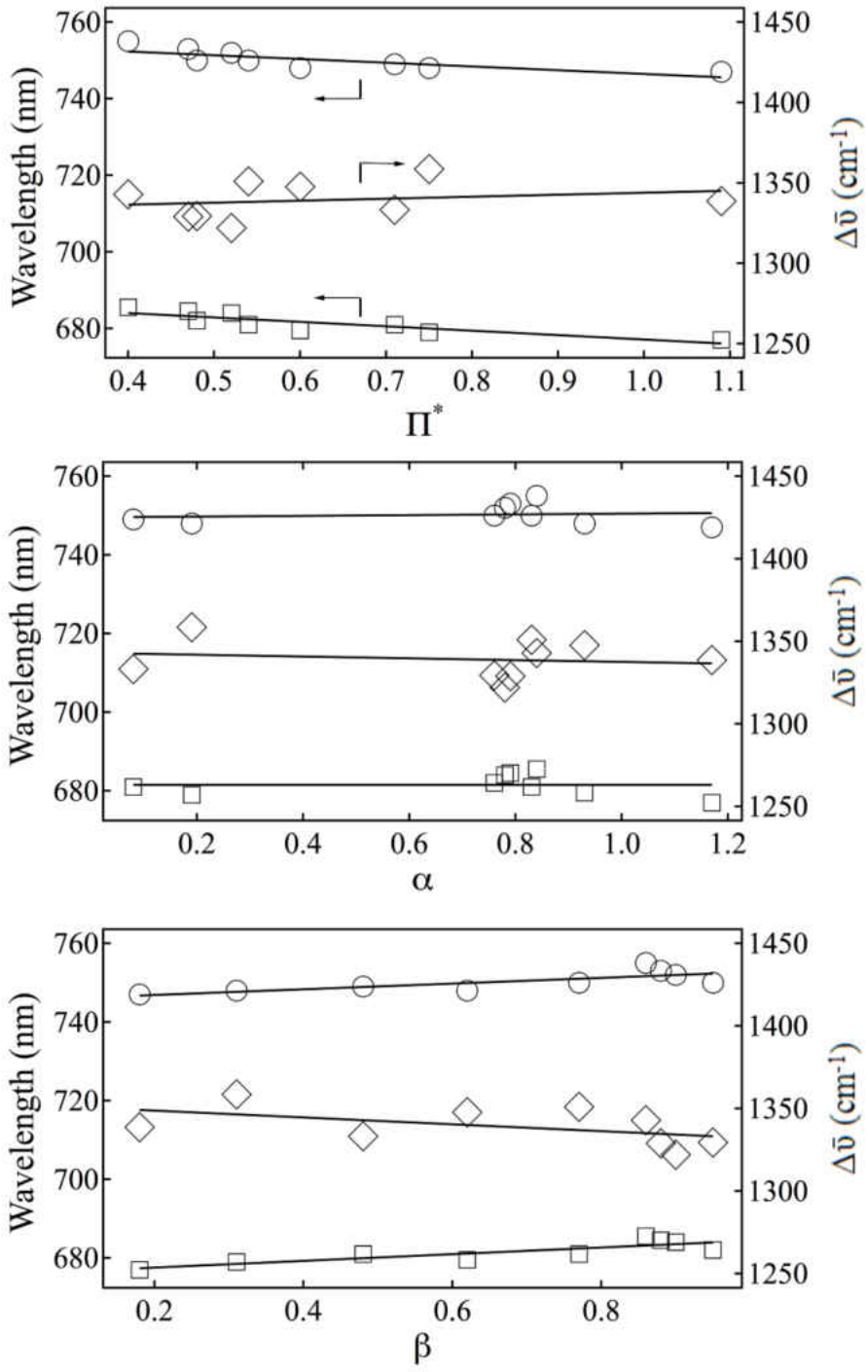

Fig 3.6.5 Solvatochromic effects on λ_{max}, $\lambda_{shoulder}$ and $\Delta\bar{\upsilon}$ for DiR. Empty circles, $\lambda_{max;}$ empty diamond, $\Delta\bar{\upsilon}$; empty square, $\lambda_{shoulder}$.

found was that, regardless of the parameter considered, environmental effects on the spectroscopic characteristics of DiR are just too small to be considered as useful tools for such characterization. For this dye, changes in total sample (dye) absorption observed for the original formulation, as compared to those associated with the respective purified micelles, and dye aggregation in the respective nanoscopic environments were found to provide more direct information on encapsulation efficiency (see section 4.3.1).

3.7 Cardiogreen

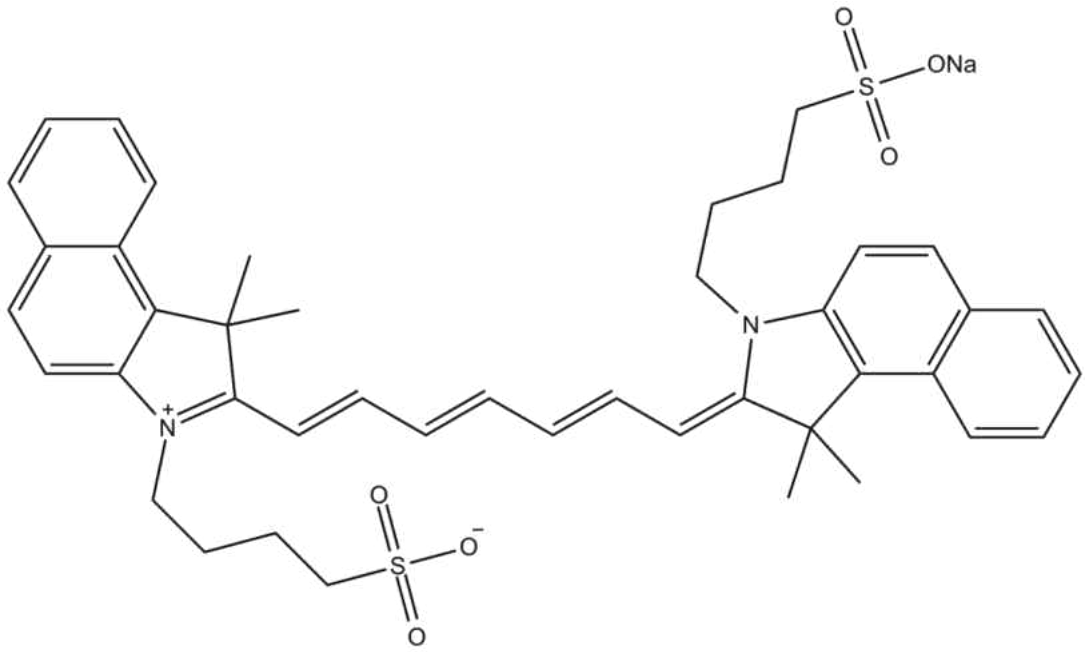

sodium 4-[2-[(1E,3E,5E,7Z)-7-[1,1-dimethyl-3-(4-sulfonatobutyl)benzo[e]indol-2-ylidene]hepta-1,3,5-trienyl]-1,1-dimethylbenzo[e]indol-3-ium-3-yl]butane-1-sulfonate (Indocyanine green)

Scheme 3.7.1 Structure of Cardiogreen

Cardiogreen (CG), also referred to as Indocyanine green, is a FDA approved fluorescent agent used in medical diagnostics, and it is considered one of the least toxic imaging agents currently administered to humans (Sheng et al., 2013). Although CG generates just minor amounts of phototoxic species upon excitation, it has been previously considered as a potential photosensitizer for use in photodynamic therapy (as most dyes sooner or later are; Kuo et al., 2012; Barth et al., 2011). Because CG shows high extinction coefficients in the near-IR region of the spectrum, and also easily measurable fluorescence emission in that region of the spectrum, this dye can be seen as a desirable near-IR imaging agent. That is, as an imaging probe well

suited to the detection of tumors located at deeper locations as compared to those provided by visible fluorescent probes (Kim et al., 2007; Zheng et al., 2011). A potential drawback associated with CG aqueous formulations is represented by its relatively limited thermostability and photostability in water. The decomposition of CG in water is significantly accelerated upon light exposure, and also upon increasing temperature (Saxena et al., 2003, 2004). Previous attempts to increase the (photo)stability of CG formulations have included formulations in which CG was incorporated into nanoparticles (Saxena et al., 2004; Larush and Magdassi , 2011)

Although relative aggregation tendencies cannot be attributed solely to the relative hydrophobic properties associated to any given dye in water (e.g. as measured via solubility and/or n-octanol/water partition coefficients; compare CV, MB and Rh-123), at least in some cases (perhaps the more extreme ones) the overall trend of higher aggregation tendencies appear to correlate well with a respective increase in hydrophobicity associated with the dominant organic backbone of otherwise comparable molecules (compare, for example, the cases of HITC and DiR). Cardiogreen (CG), a negatively charged "switerion" at pHs close to neutrality (i.e. CG displays one positive and two negative charges in that pH range). CG shows good water solubility and yet quite remarkable tendencies to aggregate in water, although not as prominent as the tendencies observed for DiR.

In CG the negative charges are not delocalized, but rather fixed at the respective sulfonate groups, and yet this dye shows significant tendencies to aggregate in water even when present in concentrations as low as 5 μM. The effect of concentration on the absorption spectra of CG in

water is shown in Fig 3.7.1. The spectroscopic fingerprint typical of the formation of H-type aggregates already start do dominate the shape of the respective absorption envelops when the CG concentration reaches the 50 μM to 100 μM range. In CG the larger (e.g. as compared to HITC) and "close to planar" aromatic rings apparently favorably offsets the expected repulsions associated with the localized (hard) sulfonate negative charges, and facilitates the formation of H-type dye aggregates in water. Interestingly, it has been previously demonstrated that at higher temperatures (e.g. 60^0C) CG aggregates tend to assume head-to-tail, J-type structure (Rotermund et al., 1997a, 1997b; Weigand et al., 1997). The data shown in Fig3.7.1 represent experiments carried out at room temperature.

Fig 3.7.2 shows how and to which extent different solvents affect the spectroscopic properties of CG in solution. Solvent effects have been found to be significantly more complex for CG as compared to any other dye considered in this study. Nonetheless, some trends are clear. The observed effect of the Kamlet-Taft solvent solvatochromic parameters (Π*, α and β) on the wavelength of maximum CG absorption, wavelength of absorption observed at the respective spectroscopic shoulder, and also the difference in frequency ($\Delta\bar{\upsilon}$) observed between the wavelengths of maximum and shoulder absorptions are all modest (Fig 3.7.3). For example, the observed changes in λ_{max} in going from acetonitrile (λ_{max} = 778 nm) to n-pentanol (λ_{max} = 780 nm) is just 2 nm, while a larger change in λ_{max} was observed when comparing acetonitrile and acetone ((λ_{max} = 785 nm; a 7 nm difference) (Table 3.7.1).

Solvent	Π*	α	β	λ_{max}(nm)	$\lambda_{shoulder}$(nm)	$\Delta\bar{\upsilon}$(cm^{-1})
Water	1.09	1.17	0.18	777	701	1287.0
Acetonitrile	0.75	0.19	0.31	778	708	1270.8
Acetone	0.72	0.08	0.48	785	712	1306.1
Methanol	0.6	0.93	0.62	778	707	1290.8
Ethanol	0.54	0.83	0.77	779	708	1287.3
n-Propanol	0.52	0.78	0.9	783	711	1293.3
i-Propanol	0.48	0.76	0.95	779	707	1307.3
n-Butanol	0.47	0.79	0.88	780	709.5	1273.9
n-Pentanol	0.4	0.84	0.86	780	710	1264.0

Table 3.7.1 Solvent effects on λ_{max}, $\lambda_{shoulder}$ and $\Delta\bar{\upsilon}$ for 5μM solutions of Cardiogreen. (exception, [Cardiogreen] = 10μM in acetone)

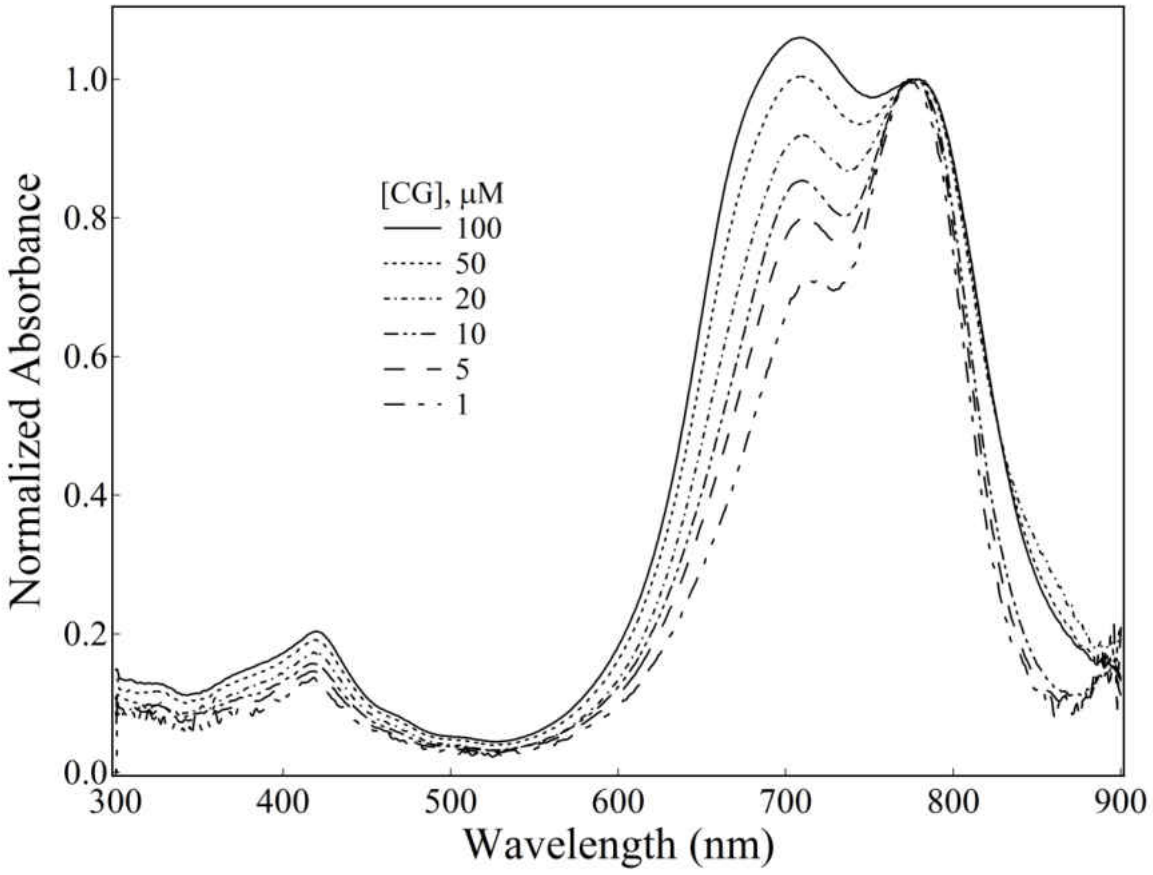

Fig 3.7.1 Effect of concentration on the absorption spectra of Cardiogreen in water.

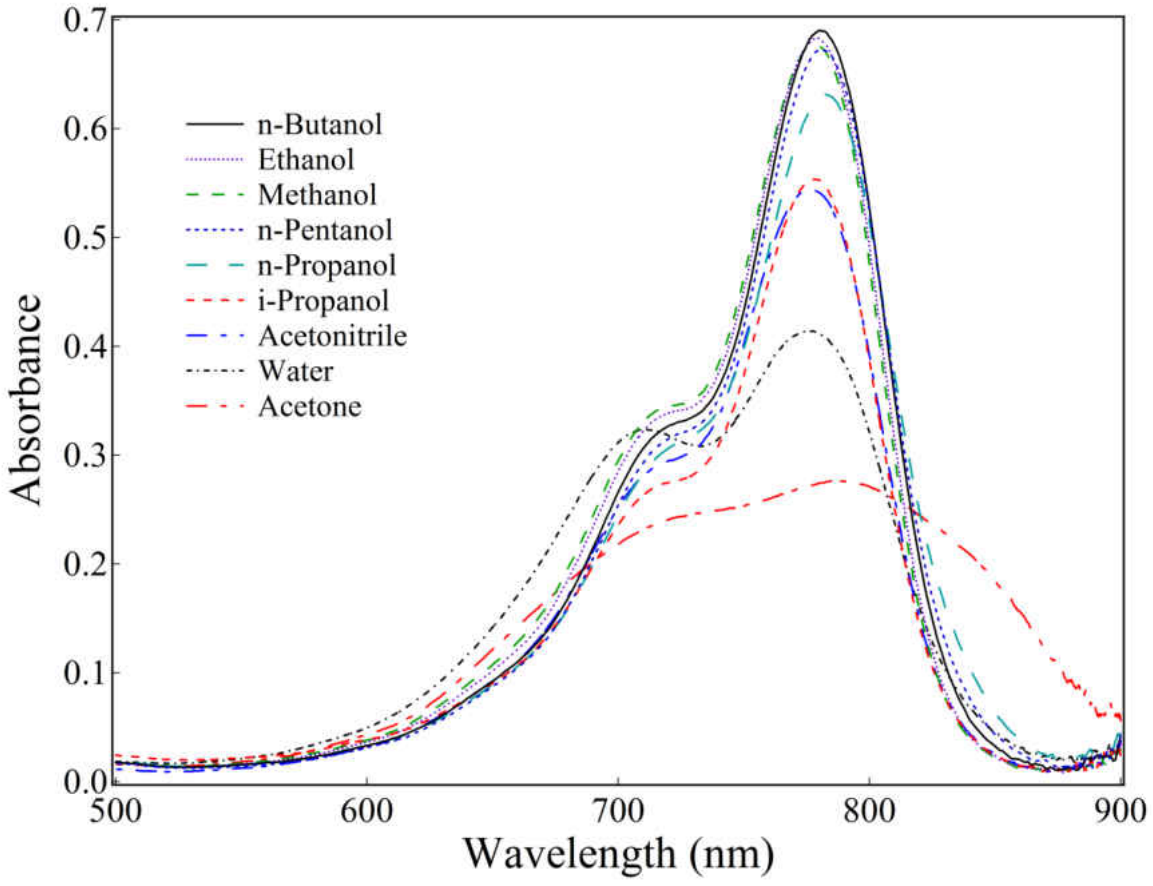

Fig 3.7.2 Absorption spectra of of Cardiogreen in different solvents. [Dye] = 5μM.

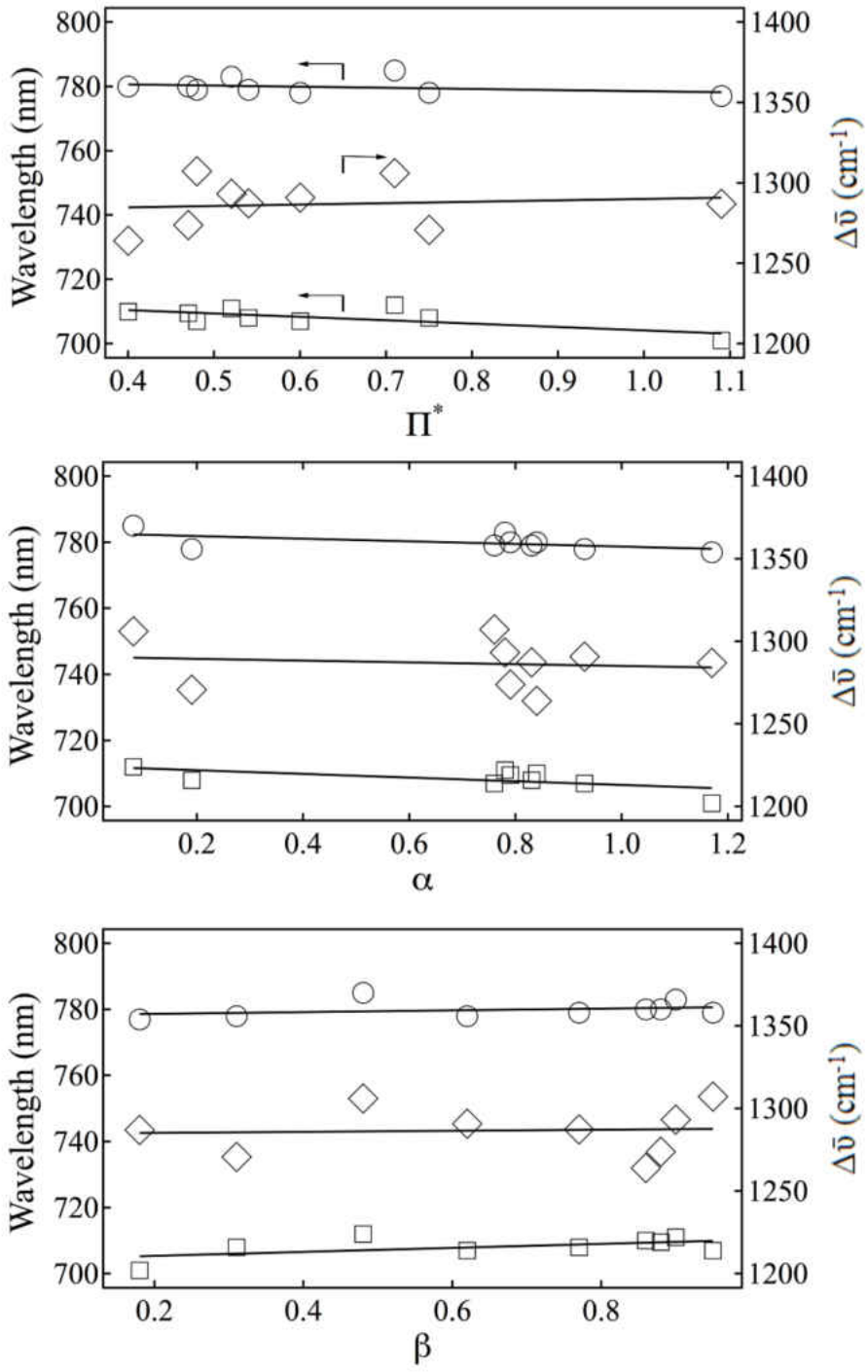

Fig 3.7.3 Solvatochromic effects on λ_{max}, $\lambda_{shoulder}$ and $\Delta\bar{\upsilon}$ for Cardiogreen. Empty circles, $\lambda_{max;}$ empty diamond, $\Delta\bar{\upsilon}$; solid square, $\lambda_{shoulder}$.

Again in this case, and in keeping with all others dyes considered in this study (with an exception made of Styryl 9M), environmental (solvent) effects on λ_{max}, $\lambda_{shoulder}$ and $\Delta\bar{\upsilon}$ are not likely to provide clear, unambiguous information on relative efficiencies of polymeric micelle encapsulation. Here, again, either changes in absorption between the original formulation, as compared to that of the respective purified micelles, or the characterization of the formation of dye aggregates in the nanoscopic polymeric micelle environments are bound to represent more reliable indications of encapsulation.

3.8 Concluding Remarks.

In this chapter we have explored how and to which extent concentration and solvent (i.e environmental) effects control the spectroscopic properties of seven cationic dyes of interest to this project. This exercise was performed in an attempt to find reliable spectroscopic parameters for the characterization of the encapsulation of these dyes into the nanoscopic environments of polymeric micelles (i.e. core and corona, respectively). Here, solvent (i.e. solvatochromic) effects were found to most typically provide either modest or just plain poor tools for such characterization, with exception made only to the case of styryl 9M. On the other hand, three out of the seven dyes studied here, namely MB, CG and, particularly, DiR were found to display high aggregation tendencies even when present at low concentrations in aqueous media. Therefore, the spectroscopic changes associated with either the de-aggregation of these dyes when in the presence of polymeric micelles (as compared to their respective aggregation states in water), or yet the identification of the respective aggregates spectroscopic fingerprints when in the presence of these micelles have been identified as potentially more promising experimental tools for the characterization of the respective micellar encapsulation. In addition, in this study we have also employed size-exclusion chromatography techniques in order to better explore and characterize the encapsulation (or lack thereof) of all dyes considered here into PEG-*b*-PCL polymeric micelles (see Chapter 4).

4. Studies on Relative Encapsulation Efficiency of Cationic Dyes into Polymeric Micelles.

This chapter describes studies aimed at the characterization of encapsulation (or lack thereof) of cationic dyes into Poly(ethylene glycol)-*b*-poly(ε-caprolactone) (PEG-*b*-PCL) polymeric micelles. Here, three distinct lines of evidence have been considered as indicators the occurrence of significant non-covalent interactions between these dyes and respective micelles. The first is represented here by initial comparisons on how and to which extent the wavelengths of maximum dye absorption (λ_{max}), wavelength of the shoulder typically observed at the left-hand side of the respective absorption envelops ($\lambda_{shoulder}$; only styryl 9M does not display such shoulder), and the difference in frequency (i.e. wavenumber) observed between λ_{max} and $\lambda_{shoulder}$ are affected by the presence of the micelles in the respective reaction media. These comparisons were performed using pairs of samples prepared exactly the same way, with the same dye concentrations (see methods), but with one prepared in the presence and the other prepared in the absence of PEG-*b*-PCL. The second represents a comparison of these same original samples, but with focus placed on changes in total absorption (i.e. extinction coefficient changes) and on changes in the respective spectral envelops as expected for the formation of dye aggregates when in the presence of polymeric micelles. The third, identified as the most powerful technique used in this study, is represented by the comparison of how much of the original dye present in such formulations elutes together with the respective micelles when these samples are subjected to size-exclusion chromatography analysis.

The results obtained for the seven distinct dyes considered in this study are presented in this chapter in three distinct categories. The first describes dyes to which no evidences of encapsulation were found, and not even evidences of any (i.e. measurable) weak dye interaction with the respective micelles (i.e. CV, MB and Rh123). The second describes dyes that interact with the micelles to measurable extents, but nevertheless show no evidence of stable non-covalent associations or micellar encapsulation (i.e. styryl 9M and HITC). The third, and last category, describes dyes to which strong evidences have been found for the respective encapsulation (or otherwise stable associations) into polymeric micelles (i.e. DiR, CG and Leuco Crystal Violet).

4.1 Dyes showing no evidence of significant interaction with polymeric micelles: Crystal Violet, Methylene Blue and Rhodamine 123.

The solvatochromic properties of CV, MB and Rh-123 are poor, and therefore any attempts to characterize the interaction of these dyes with polymeric micelles on basis of solvatochromic properties alone are unlikely to provide useful information. Accordingly, in this study no clear evidences for dye-micelle interactions were found on basis of these properties alone. Likewise, no experimentally measurable changes in total sample absorption, or in the ratio between λ_{max} and $\lambda_{shoulder}$ (a measure of dye aggregation) suggesting significant interactions were found. For these dyes, the ultimate demonstration of lack of any significant micellar interaction was provided by the respective assays involving size exclusion chromatography analysis.

Figure 4.1.1 shows the absorption spectra of crystal violet in the polymeric micelle

formulation before and after passing through a size-exclusion chromatographic column (see methods). Under the experimental conditions used in this assay, CV is entirely retained by the column, and only empty micelles are recovered in the respective eluted samples. This result indicates that the interaction of CV with the polymeric micelle is, at best, negligible.

Likewise, Figure 4.1.2 shows the absorption spectra of methylene blue in the polymeric micelle formulation before and after passing through a size-exclusion chromatographic column. Again in this case, the dye is entirely retained by the column, and only empty micelles are recovered in the respective eluted samples. The behavior of Rh-123 is not different from those observed for the cases of CV and MB (Fig. 4.1.3). Once again in this case only empty micelles are recovered from the respective column eluents after the respective Rh123/micelles samples are subjected to size exclusion chromatography. Therefore, the data obtained in studies involving these three cationic dyes quite strongly indicate that no significant interactions take place between these species and polymeric micelles, at least when considering the standard experimental conditions used in this comparative study. Whether measurable or significant dye-micelle interactions could develop under experimental conditions significantly different from those used here remains an open question, but yet irrelevant when considering the primary objectives of this comparative investigation.

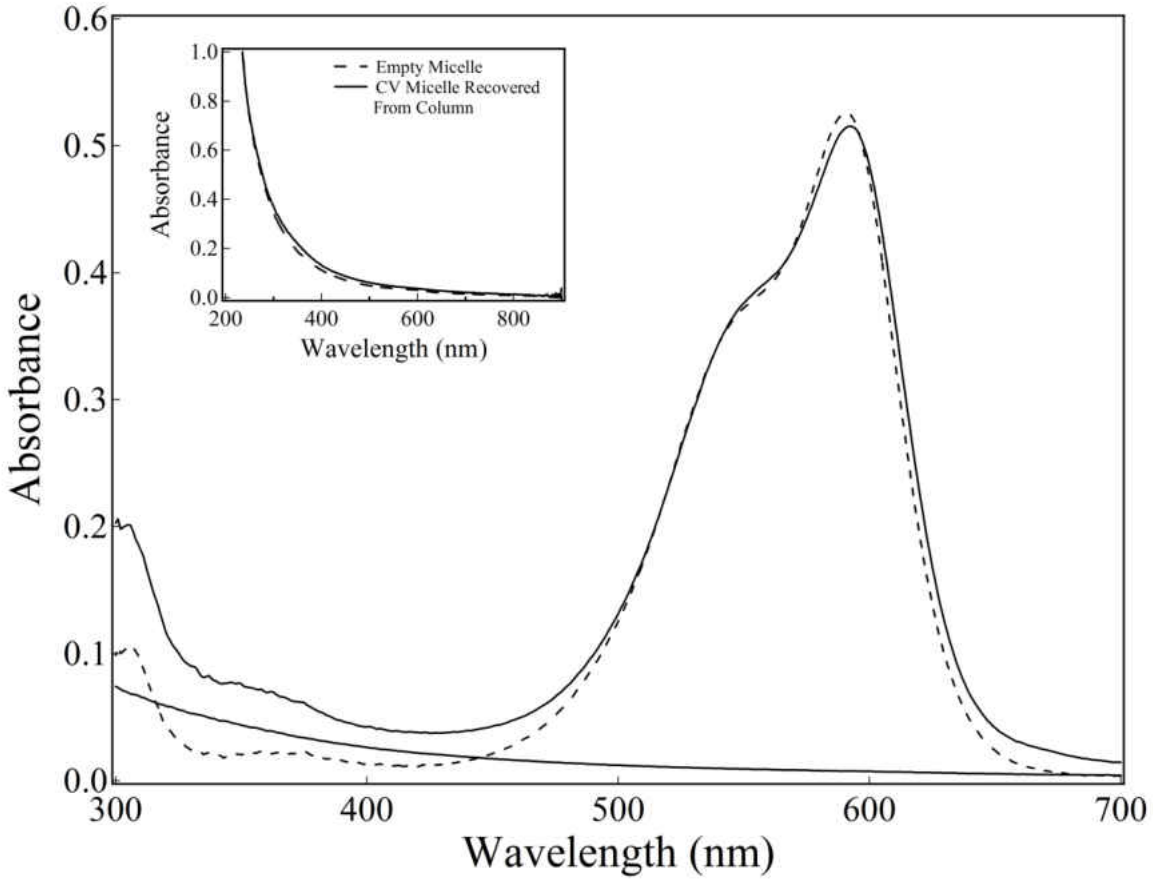

Fig 4.1.1 Absorption spectra of Crystal Violet in the polymeric micelle formulation before (top solid line λ_{max} = 592 nm) and after passing through a size-exclusion column (bottom solid line). The absorption spectrum of Crystal Violet in water is also shown (dashed line; λ_{max} = 591 nm). Inset: Absorption of total CV formulation micelles recovered from column (solid line) as compared to that of the respective empty micelles sample (dashed line).

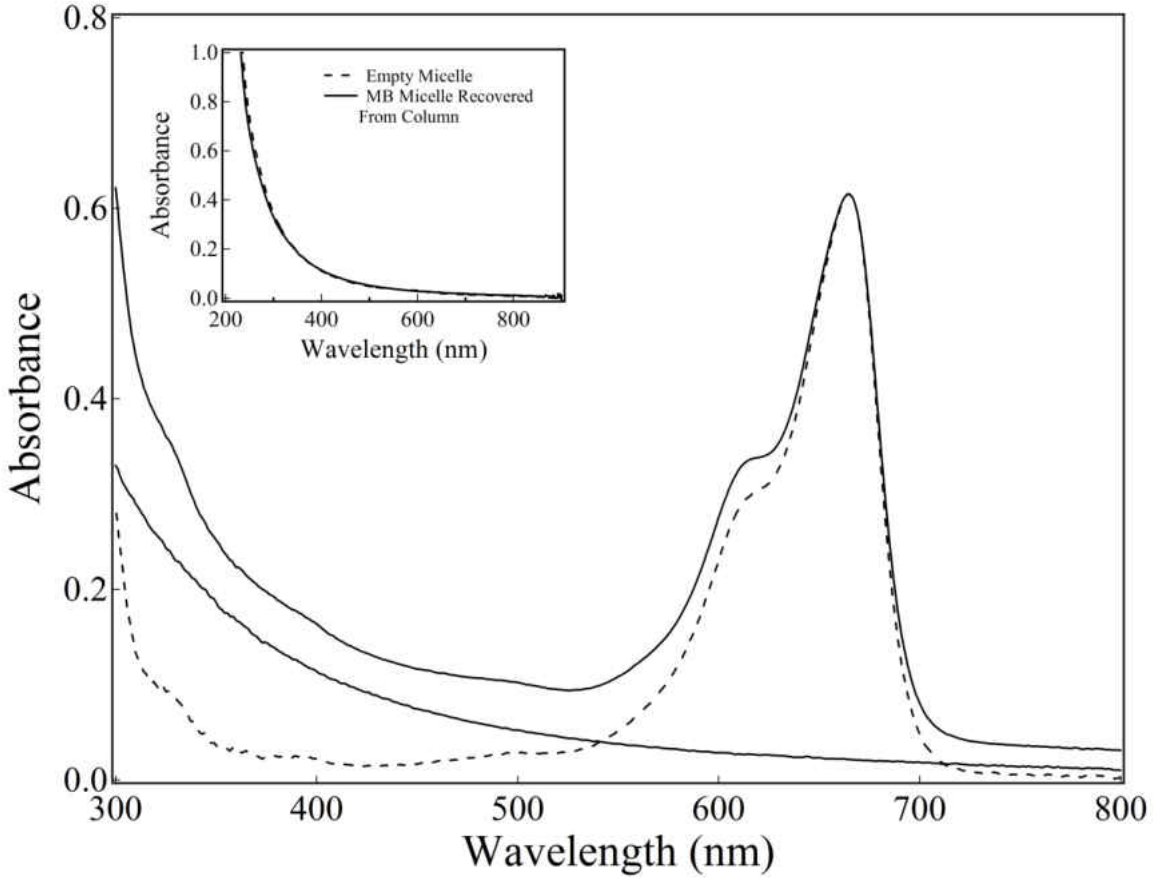

Fig 4.1.2 Absorption spectra of Methylene Blue in the polymeric micelle formulation before (top solid line λ_{max} = 665 nm) and after passing through a size-exclusion column (bottom solid line). The absorption spectrum of Methylene Blue in water is also shown (dashed line; λ_{max} = 665 nm) Inset: Absorption of total MB formulation micelles recovered from column (solid line) as compared to the respective empty micelles sample (dashed line)

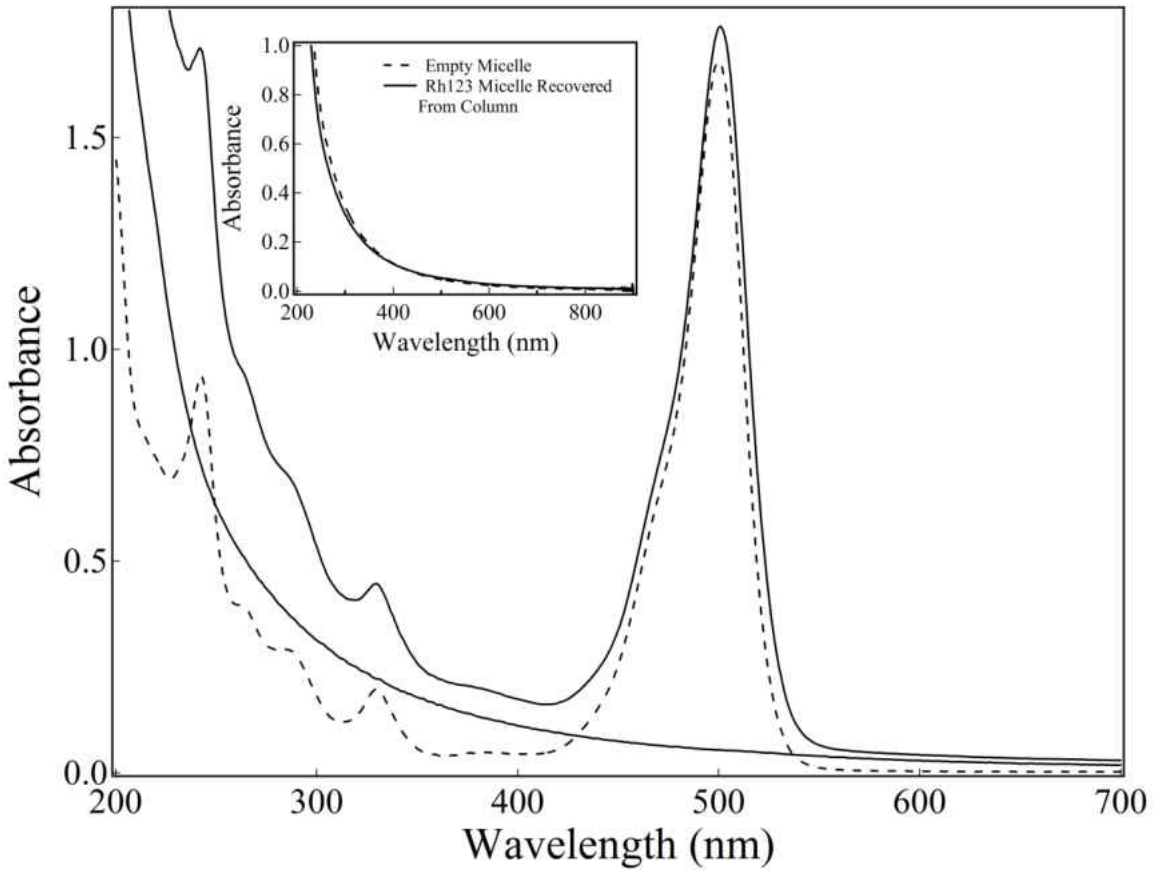

Fig 4.1.3 Absorption spectra of Rhodamine123 in the polymeric micelle formulation before (top solid line; λ_{max} = 501 nm) and after passing through a size-exclusion column (bottom solid line). The absorption spectrum of Rhodamine 123 in water is also shown (dashed line; λ_{max} = 500 nm). Inset: Absorption of total Rh123 formulation micelles recovered from column (solid line) as compared to the respective empty micelles sample (dashed line)

4.2 Dyes showing evidence of only modest interactions with polymeric micelles: Styryl 9M and HITC.

4.2.1 Styryl 9M

Styryl 9M is the most solvatochromic dye amongst all dyes considered in this study (see chapter 3). Accordingly, the absorption spectrum of this dye is significantly different in preparations containing PEG-*b*-PCL as compared to those which do not (Fig. 4.2.1.1). Following the standard protocol for the preparation of polymeric micelles (see methods), but yet comparing samples prepared in the presence and in the absence of PEG-*b*-PCL (i.e. samples subjected to the same treatment, but one in the presence and the other in the absence of polymeric micelles) the spectroscopic shift observed when in the presence of micelles suggest dye localization in (nano)environments less polar than that of the bulk aqueous media (Fig. 4.2.1.1). That is, a 19 nm red (batochromic) spectral shift is observed in polymeric micelle formulations as compared to the respective spectrum in pure water. This observation indicates some degree of interaction between Styryl 9M and the respective polymeric micelles. The subtraction of the spectrum representing the empty micelles alone from that representing the respective dye-micelle formulation suggests even a larger batochromic shift for Styryl 9M in the micellar environment (i.e. 21 nm; Fig. 4.2.1.1).

However, chromatographic assays have indicated that such interactions are very weak. That is, when micelle formulations containing styryl 9M are subjected to size exclusion chromatography the dye is promptly retained by the column, only empty micelles are recovered

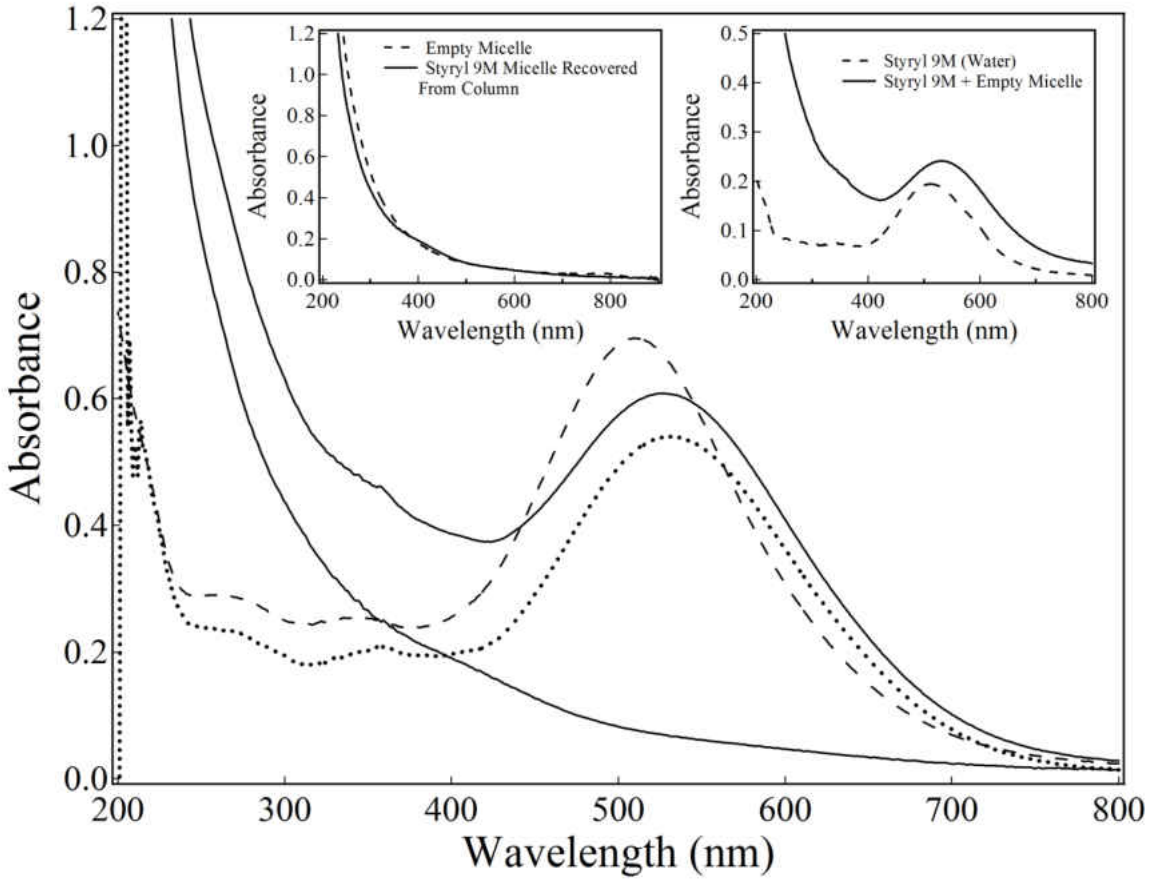

Fig 4.2.1.1 Absorption spectra of Styryl 9M in the polymeric micelle formulation before (top solid line; λ_{max} = 530 nm) and after passing through a size-exclusion column (bottom solid line). The absorption spectrum of Styryl 9M in water is also shown (dashed line; λ_{max} = 511 nm). The spectrum shown in doted line represents the difference between the spectrum of empty micelles and that of the original dye-micelle formulation (λ_{max} = 532 nm). Insets: Left panel, Absorption of total Styryl 9M formulation micelles recovered from column (solid line) as compared to that of the respective empty micelles sample (dashed line). Right panel, Absorption spectra of a physical mixture of Styryl 9M and empty micelles (solid line), compared to that of Styryl 9M in pure water (dashed line). [Styryl 9M] = ~20μM (i.e., saturated solution).

from the respective eluted samples (Fig 4.2.1.1). This observation suggests that Styryl 9M interact weakly and only with the corona region of the polymeric micelle. Further support to this inference was obtained from assays in which comparable solutions of Styryl 9M in water were just mixed with the respective comparable solutions containing only empty micelles (Fig 4.2.1.1, inset). That is, the mixture of aqueous (pure) dye and empty micelles samples.. Again, in this last case a 19 nm red spectroscopic shift was observed immediately after mixing, an observation that suggests the occurrence of only interfacial (corona) interactions. Note that micelle formation during solvent evaporation is the step in which dye encapsulation is expected to occur, and in this case none was observed.

It must be noted that the indications of the occurrence of weak Styryl 9M-micelle interaction described here are based solely on the respective spectroscopic shifts associated with this more solvatochromic dye. That is, they are not made evident when considering the ion-exchange chromatography assays alone. Therefore, the question of whether some sort of similarly weak dye-micelle interactions may also be observed when considering the cases of the less solvatochromic dyes described in the preceding section (i.e. CV, MB, and Rh123) cannot be properly addressed at this moment..

4.2.2 HITC

HITC is the first dye described in this report that shows both, measurable spectroscopic evidences and also ion-exchange chromatography evidences in support of its interaction with PEG-*b*-PCL polymeric micelles. Figure 4.2.2.1 shows the measurable differences observed both in λ_{max} and total absorption values observed between the respective samples prepared in the presence and in the absence of PEG-*b*-PCL. Some degree of dye aggregation when in the presence of polymeric micelles (as indicated by a decrease in the $\lambda_{max}/\lambda_{shoulder}$ ratio) is also made apparent. In addition, and more importantly, Fig. 4.2.2.1 also shows that measurable amounts of HITC elute along with the PEG-*b*-PCL micelles when the original dye-micelles formulations are subjected to ion-exclusion chromatography. That is, about 7 % of the total dye present in the original crude dye-micelle formulations are recovered along with the respective micelles upon exposure of the original samples to the size-exclusion chromatographic column. Besides, when the dye-micelle faction recovered from a first size exclusion column is subsequently subjected to a second column, still about 1 % of the original total dye content elutes, again, along with the respective micelles (Fig. 4.2.2.1).

These observations suggest that non-covalent interactions between HITC molecules and PEG-*b*-PCL micelles are significant, and lead to the formation of relatively stable association products. Whether these products are better described by loose associations of HITC with the corona region of these micelles or, otherwise, by dye partitioning into deeper micelle locations represents a question that cannot be unambiguously answered on basis of the experimental data

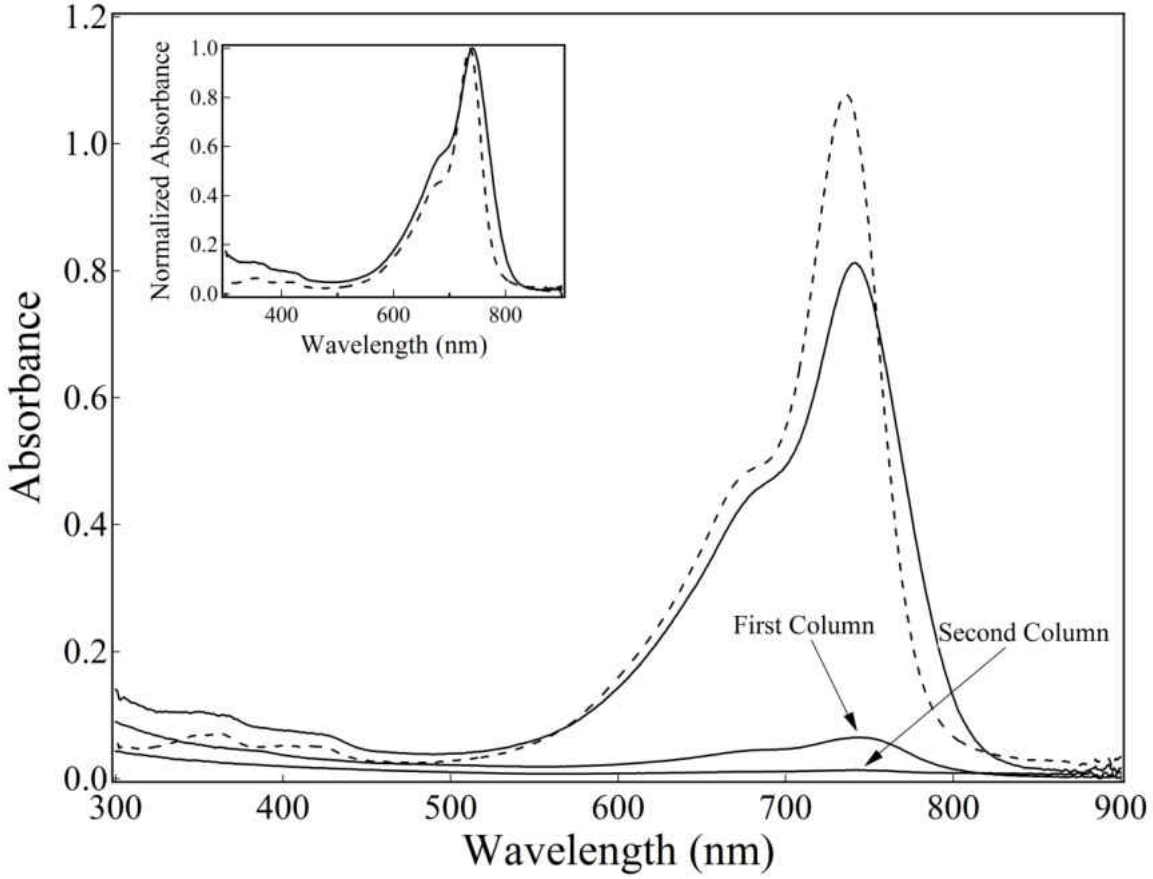

Fig 4.2.2.1 Absorption spectra of HITC in the polymeric micelle formulation before (top solid line; λ_{max} = 741 nm) and after passing through two consecutive columns (lower solid line) (lower solid line). Also shown is the absorption of HITC in pure water (dashed line; λ_{max} = 736 nm). Inset: normalized absorption spectra of HITC in the original micelle formulation (solid line) and in pure water (dashed line).

currently available. However, two lines of evidence appear to support the hypothesis of occurrence of at least some encapsulation during micelle formation. The first is represented by the resistance observed with regard to dye-micelle separation upon two subsequent size-exclusion assays, what suggest that some contribution arising from encapsulation may be at play in this case. Second, the spectroscopic differences observed in the physical mixtures of dye solutions with previously prepared empty micelle solutions are similar but not identical to those observed when the dye is exposed to the polymer during micelle assembly (compare Figs 4.2.2.1. and 4.2.2.2). A decrease in $\lambda_{max}/\lambda_{ratio}$ observed in the latter case, as compared to the ratio observed in pure water, suggest some degree of incorporation during micelle assembly, which cannot be reproduced in the respective dye/empty micelle physical mixtures.

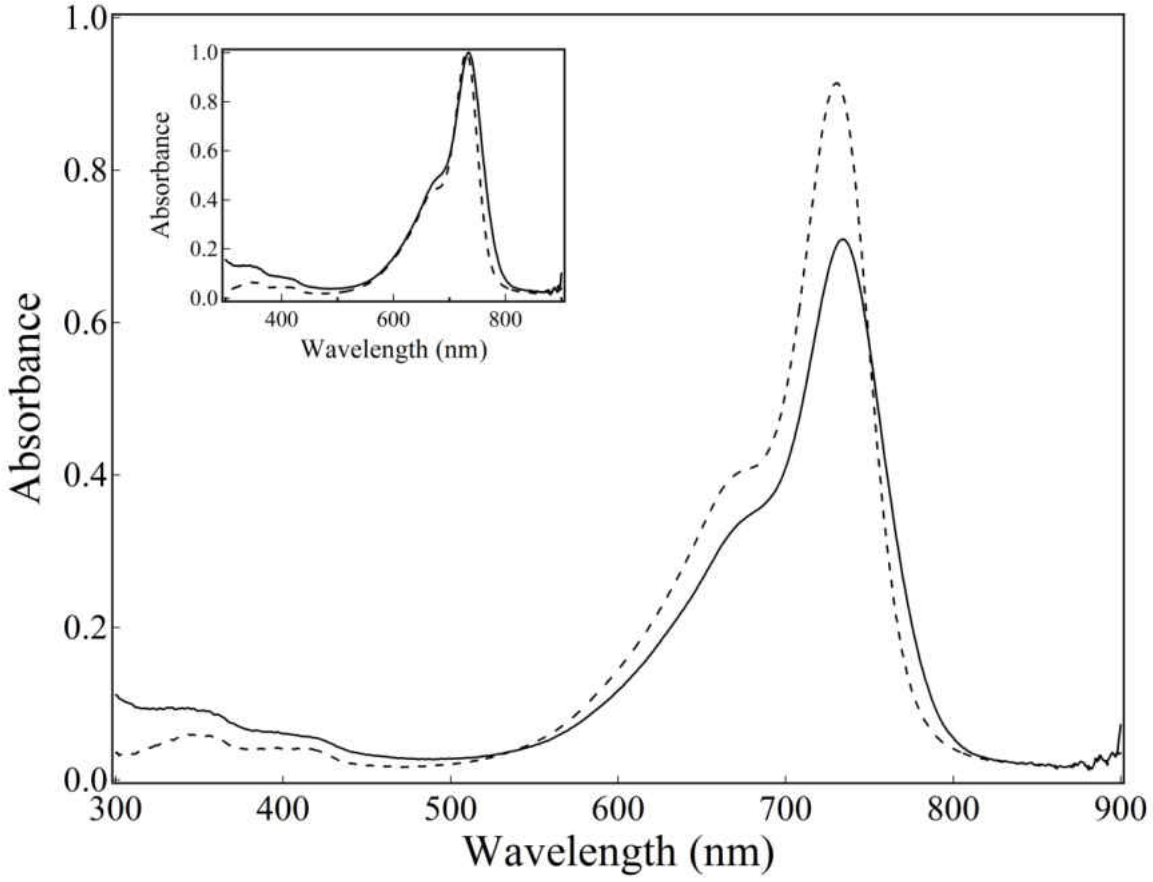

Fig 4.2.2.2 Absorption spectra of a physical mixture of HITC and empty micelles (solid line); λ_{max} = 739 nm), compared to that of HITC in pure water (dashed line; λ_{max} = 736 nm). Inset: respective normalized spectra.

4.3. Dyes showing significant encapsulation into polymeric micelles: DiR, Cardiogreen and Leuco-Crystal Violet.

4.3.1 DiR

DiR is a lipophilic dye that shows very limited solubility in water, and also great tendencies to aggregate in this solvent. Low water solubility and high hydrophobicity represent properties particularly well suited for the effective encapsulation of this dye into polymeric micelles. Figure 4.3.1.1 shows the absorption spectra of DiR in pure water and also in a polymeric micelle formulation. The differences observed in the absorption spectra of DiR in these two distinct samples are remarkable, and indicate a great deal of solubilization (encapsulation) of DiR into PEG-*b*-PCL micelles when these micelles are prepared using the standard formulation conditions described in Chapter 2. The DiR aggregates observed in water are mostly gone in the polymeric micelle formulation. In this last case, the dominant spectroscopic feature is that of the respective dye monomer (λ_{max} = 754 nm), in keeping with the respective λ_{max} values observed in organic solvents showing low polarity (e.g. n-butanol and n-pentanol; see Table 3.6.1). However, in these DiR-micelle formulations spectroscopic contributions are also observed at the left-hand side of the respective absorption envelope, suggesting the presence of DiR aggregates in the micellar environment (Fig. 4.3.1.1).

The strength of the association of DiR with these micelles is demonstrated by the results obtained in size-exclusion chromatography assays (Fig. 4.3.1.2). When the original DiR-micelle formulation is subjected to size-exclusion chromatography, about 77 % of the original dye elutes

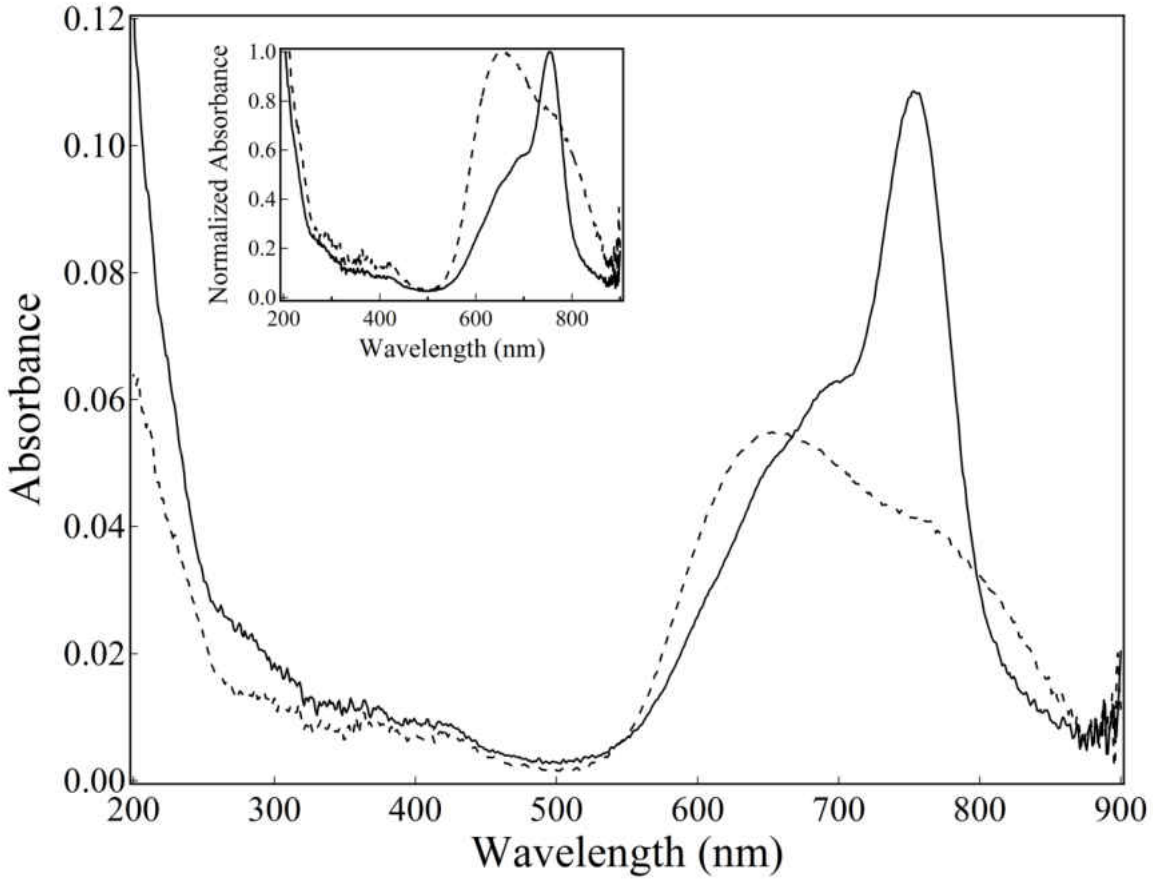

Fig 4.3.1.1 Absorption spectra of DiR in a polymeric micelle formulation (molar ratio, DiR:polymer, 74:100; solid line; λ_{max} = 754 nm) and DiR in pure water (dashed line; λ_{max} = 653 nm). Spectra recorded after the respective original solutions were diluted 30 times (optical path = 1.0 cm). Inset: normalized spectra of DiR micelles formulation (solid line) and DiR in water (dashed line).

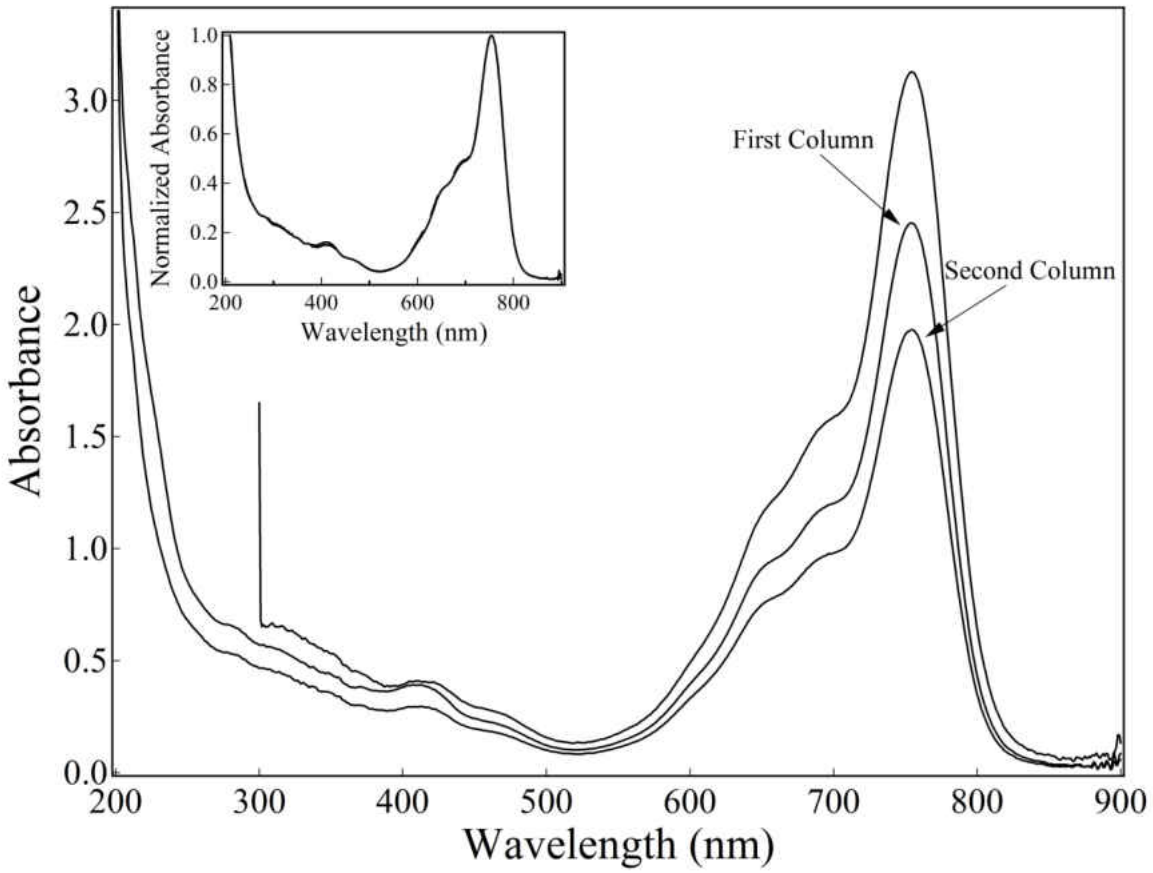

Fig 4.3.1.2 Absorption spectra of DiR in polymeric micelle formulation (molar ratio of DiR: polymer is 74:100) before (top solid line) and after passing through two consecutive columns (lower solid lines). From top to bottom (λ_{max}, nm): 754, 753, 755. Inset: Normalized spectra of DiR in polymeric micelle formulation before (solid line) and after passing through a size-exclusion column (dashed lines).

associated with the micelle. In addition, when the sample recovered from the first chromatographic column is subjected to a second column, still about 61 % of the original dye is recovered along with the micelles. The normalize spectra of these samples are presented in the inset of Fig. 4.3.1.1.

Interestingly, the contributions observed at the left-hand side of the respective spectra do not change with respect to the absorption observed at the respective λ_{max} values (Fig. 4.3.1.2, inset). This observation not only suggests that some aggregation takes place in the micellar environment, but also that such aggregates are retained by the micelles at comparable proportions as the respective monomers are upon column chromatography treatment. This last observation is somehow counterintuitive. If one considers that the column chromatography treatment is more effective in removing "free" dye molecules form the respective initial (raw) formulations; that is, dye molecules not strongly associated to the respective micelles, than the respective $\lambda_{max}/\lambda_{shoulder}$ ratios should, accordingly, change upon column treatment, but they do not. A speculative explanation for this last observation is represented by the hypothesis that in the original formulations DiR molecules are encapsulated into the polymeric micelles with a high degree of efficiency, perhaps close to 100%, but significant amounts of the original supramolecular assemblies are somehow lost in the respective column chromatography experiments. In support to this speculative hypothesis, a set of experimental observations deserves attention. First, upon column treatment of all formulations involving dyes showing low to negligible micelle association (i.e. CV, MB, Rh-123, styryl-9M, and HITC), the respective dye

retentions were observed at the very top regions of the respective columns (observations based on visual inspection alone). Second, for the DiR-micelle formulation cases a faint and continuous smear was observed along and throughout the respective columns, suggesting some sort of nonspecific association of cationic charged micelles (i.e. dye loaded micelles) with the respective solid phase of the columns used in this study. In case a fraction of the original dye-loaded micelles are indeed retained by these columns, then the observed decreased in total DiR/micelle concentration leaving the column would be in keeping with the otherwise constant composition of such micelles. It is appropriate to note here that when pure DiR aqueous samples are subjected to column treatment all dye is retained by the respective column. Although the hypothesis described above will require further investigation, it nevertheless satisfactorily supports our observations of how DiR loading affects both the spectroscopic and fluorescence properties of the respective formulations (see below).

Considerable DiR-PEG-*b*-PCL micelle interactions were also observed in the respective physical mixtures. That is, in mixtures prepared via simple mixture of DiR solutions in pure water with solutions of empty micelles also in pure water. Fig. 4.3.1.3 shows the absorption spectrum of such a mixture kept at room temperature for about 145 hours before analysis. In this case, the spectrum of the mixture still shows a major contribution associate with the presence of DiR aggregates in water, but it also shows evidence of considerable partitioning of DiR into the polymeric micelle domains. When the original physical mixture is subjected to size-exclusion chromatography, most of the contributions observed at shorter wavelengths disappear, indicating

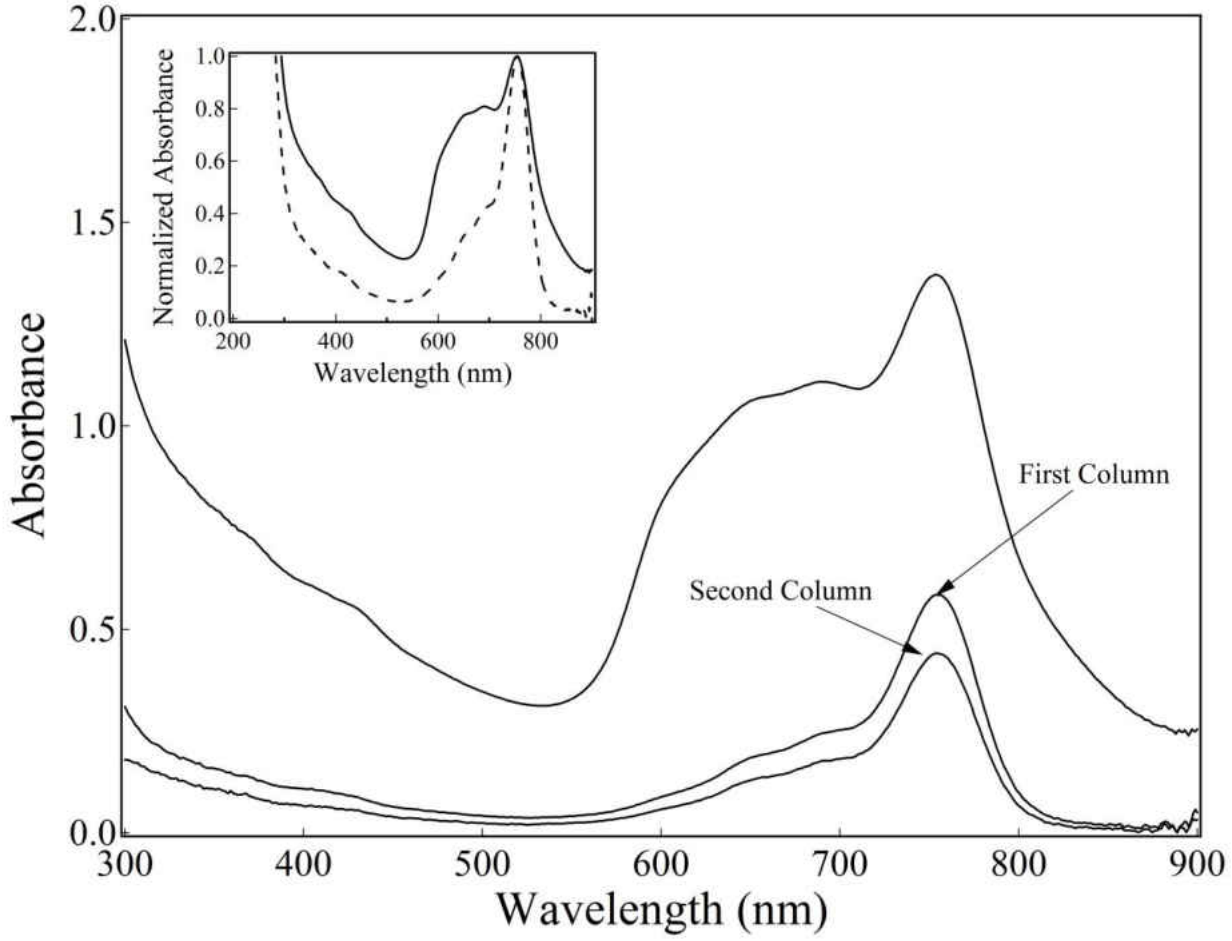

Fig 4.3.1.3 Absorption spectra of a physical mixture of DiR and empty micelles (molar ratio of DiR:polymer = 36:100) before (top solid line) and after passing through two consecutive columns (lower solid lines). Inset: normalized absorption spectra of the mixture before (solid line) and after (dashed line) passing through the first size-exclusion column.

that the aggregates found in pure water are efficiently removed from the mixture by the column. On the other hand, the comparison between the absorbance observed at λ_{max} before and after column treatment indicates that a significant fraction of the dye initially present in the mixture remains associated with the micelles (Fig. 4.3.1.3). That is, about 43% the original absorbance at λ_{max} is recovered in the respective eluted sample. In addition, when the DiR-micelle sample recovered from the first column is subjected to a second column, still about 32 % of the original absorbance at λ_{max} is recovered. These results indicate that DiR can interact with PEG-b-PCL micelles to generate stable final assemblies via simple mixture of the respective solutions in water, but with far lower efficiencies than those observed when such preparations are prepared using the standard solvent evaporation method (see Methods).

Because the normalize spectra of DiR-micelle formulations prepared using the solvent evaporation method do not change as a result of column treatment (Fig. 4.3.1.2, inset), it is reasonable to infer that under the standard conditions used in this study the efficiency of encapsulation is very high, and includes some degree of DiR aggregation in the micellar nanoscopic domains. Experiments carried out using formulations prepared with a constant amount of polymer, but with variable dye concentrations (Fig.4.3.1.4), have indicated that the formation of such aggregates varies significantly with the degree of micellar loading. That is, with the increase in the ratio between the amount of dye and amount of polymer used to prepare such formulations. Indeed, the respective blue contributions observed at the respective absorption envelops (i.e. the respective $\lambda_{shoulder}/\lambda_{max}$ ratio) increase as the dye content (loading)

increases in the respective formulations (Fig.4.3.1.5).

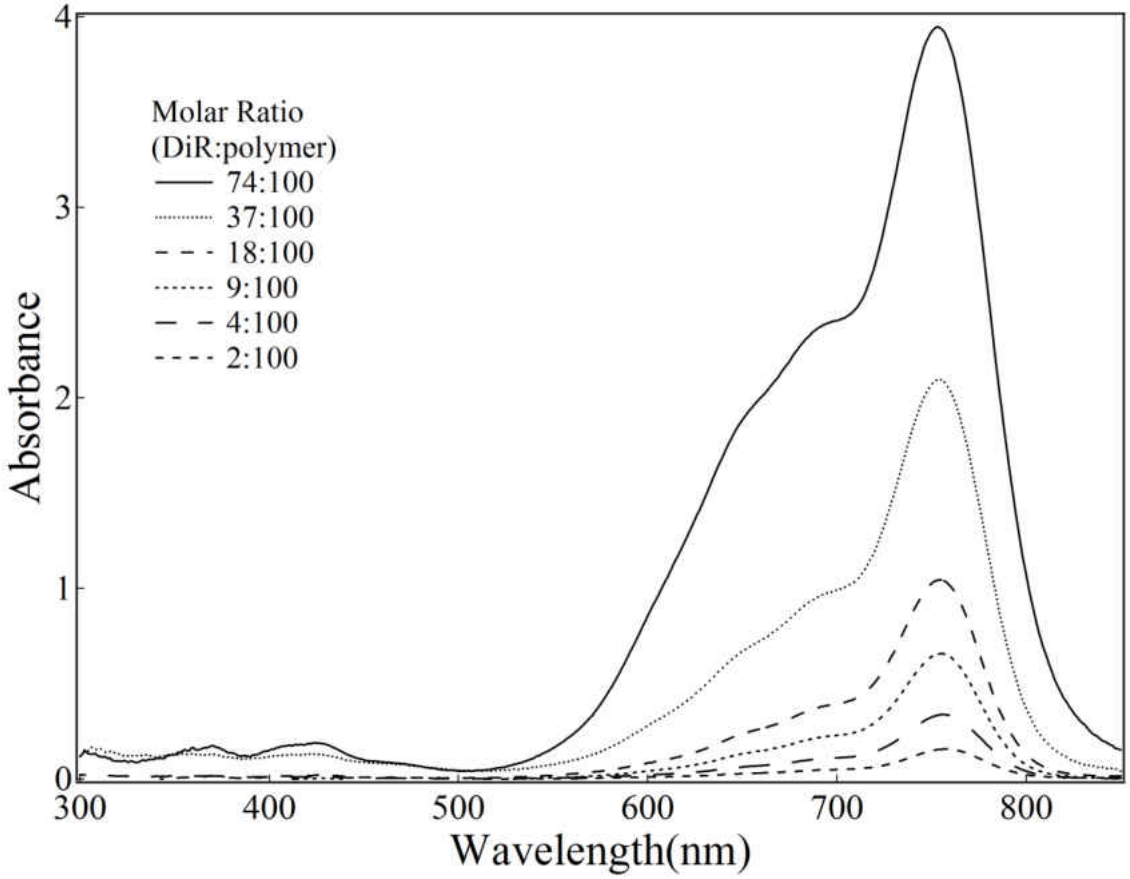

Fig 4.3.1.4 Absorption spectra of DiR in polymeric micelle formulation at different Dye:polymer molar ratios. From top to bottom the molar ratio of DiR to polymer is: 74:100, 37:100, 18:100, 9:100, 4:100 and 2:100. Because the top two spectra were taken in 0.2 cm cuvettes (instead of 1.0 cm cuvettes), the absorbance values are relative. All original (experimental) values were below 2.0.

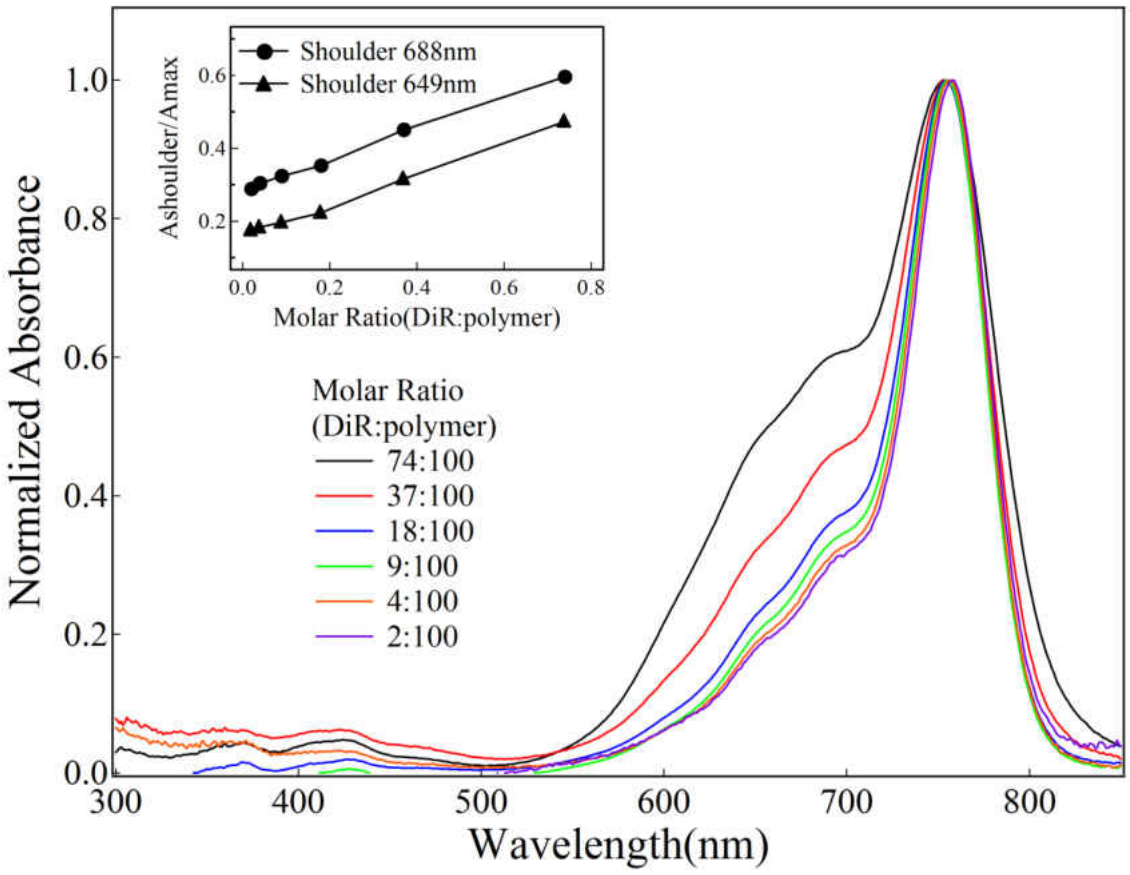

Fig 4.3.1.5 Normalized absorbance spectra of DiR in distinct polymeric micelle formulations. At 700 nm, from top to bottom, the molar ratio of DiR to polymer is: 74:100, 37:100, 18:100, 9:100, 4:100 and 2:100. Inset: Relative degrees of dye aggregation as a function of [DiR]/[polymer] ratios, as indicated by the respective $\lambda_{shoulder}/\lambda_{max}$ ratios.

The formation of H-type DiR aggregates in the micellar environment is bound to lead to fluorescence quenching. Indeed, as shown in Fig. 4.3.1.6, upon increasing micelle loading (i.e. increasing the [DiR]/[polymer] ratio in the respective formulations), the respective quantum yield tends to decrease upon increasing dye aggregation. While for formulations with molar ratios in the 2:100 and 4:100 (DiR:polymer) range the fluorescence quantum yield is close to constant (in keeping with just minor aggregation), the DiR fluorescence quantum yield is just about 2% of that observed for the 2:100 ratio when the loading reaches the 74:100 ratio. The observed fluorescence quenching is apparently too high to be explained only on basis of dye aggregation alone though. In other words, only on basis of the static (aggregation) quenching mechanisms. The magnitude of the observed quenching suggests significant and concurrent contributions arising from dynamic mechanisms of fluorescence quenching mechanisms (either collisional/Dexter or long distance/Forster mechanisms). Inferences of this hypothesis are presented below.

Considering, at least as a first approximation, that under the standard micelle preparation conditions used in this study the efficiency of DiR encapsulation is close to 100%, then the DiR concentration in the micellar environment(s) can be calculated as follows. The diameter of the core region of these PEG-*b*-PCL micelles has been previously estimated to fall within the 10 nm range, while the diameter of the entire micelle (i.e. core plus corona) has been previously estimated to fall within the 50 nm range (Cho et al., 2012),. In addition, the aggregation number associated with the formation of such micelles has been previously estimated as 200 polymer molecules per micelle

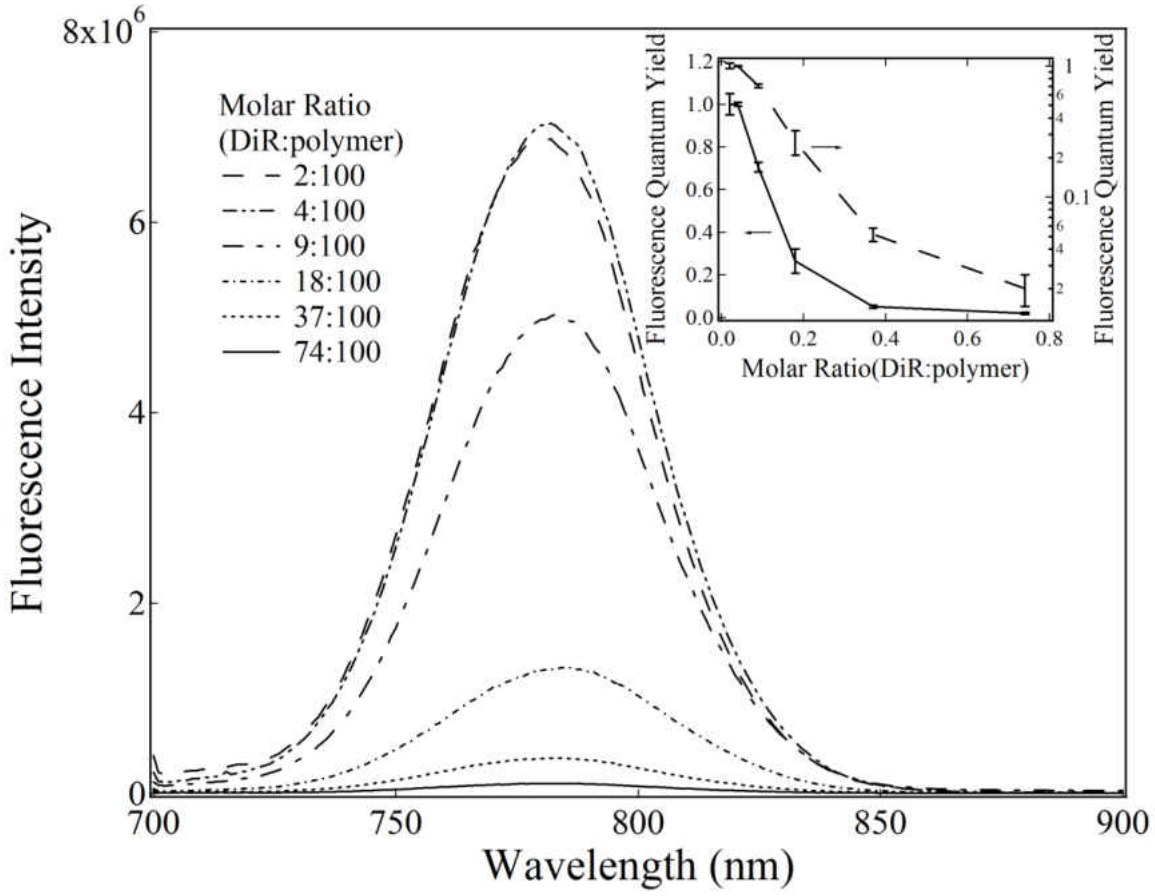

Fig 4.3.1.6 Fluorescence spectra of DiR in polymeric micelle formulation at different molar ratios. From top to bottom, the [DiR]/[polymer] ratio is: 2:100, 4:100, 9:100, 18:100, 37:100 and 74:100. Inset: Solid line: relative quantum yield of DiR micelle formulation at different molar ratio in regular scale (solid line) and in log scale (dashed line). λ_{exc} = 690nm.

(Cho et al., 2012). On basis of these previous estimates, and considering 100% encapsulation efficiency under our experimental conditions, the number of encapsulated DiR molecules per micelle has been be calculated for all distinct formulations investigated in this study (Table 4.3.1.1). Here, and for the sake of simplicity, two extreme (boundary) conditions have been considered. The first is represented the hypothetic case in which all dye molecules are encapsulated exclusively in the core region of these micelle, while the second considers homogeneous dye distribution along both, the core and corona regions of these micelles. Although none of these two extreme conditions should be expect to rigorously represent what indeed takes place in the micellar environment, they still provide valuable insights on upper and lower limits for the fluorescence quenching parameters of interest and under consideration here.

Accordingly, when considering only the core region of these micelles as the region in which DiR molecules localize (diameter = 10 nm; volume = 5.24×10^{-22} L), the calculated dye concentrations inside the polymeric micelle core were found to vary from 12 mM (2:100 molar ratio) to 470 mM (74:100 molar ratio) (Table 4.3.1.1). Analogously, if homogeneous distribution of DiR within these micelles is otherwise considered (diameter = 50 nm; volume = $6.54*10^{-20}$ L), then the respective concentrations were found to vary from 0.10 mM to 3.76 mM (Table 4.3.1.1). The relatively high DiR concentrations found in both cases (specially in the core-only localization model) supports the hypothesis that at least some contributions arising from dynamic quenching on the observed total fluorescence quenching may be at play here.

DiR : Polymer				
Weight Ratio	**Molar Ratio**	**[DiR]/[micelle]**	**C_{DiR} in Core**	**C_{DiR} in micelle**
1:20	74:100	148	470mM	3.76mM
1:40	37:100	74	235mM	1.88mM
1:100	18:100	30	94mM	0.76mM
1:200	9:100	15	47mM	0.38mM
1:400	4:100	7	24mM	0.18mM
1:800	2:100	4	12mM	0.10mM

Table 4.3.1.1 DiR concentration within PEG-*b*-PCL polymeric micelles as evaluated on basis of two distinct premises. First, that all dye molecules are encapsulated into the core regions of these micelles (C_{DiR} in Core), and second, that the dye is found homogeneously distributed along the two distinct domains of these micelles (i.e. core plus corona; C_{DiR} in micelle).

Table 4.3.1.2 describes the observed values of relative fluorescence quantum yields as a function of the respective micellar loading, along with the respective absorption values both at the wavelength of maximum absorption and at the respective wavelength of excitation of the respective samples (690 nm). The simplest and most classical model to describe fluorescence quenching is represented by the Stern-Volmer formalism. According to this formalism, in cases in

$[DiR]_{total}$	$[DiR]_{core}$	A_{690}	A_{max}	A_{690}/ A_{max}	Φf
3.76mM	**470mM**	**2.37**	**3.95**	**0.6**	**0.02**
1.88mM	**235mM**	**0.96**	**2.09**	**0.46**	**0.05**
0.76mM	**94mM**	**0.37**	**1.04**	**0.36**	**0.26**
0.38mM	**47mM**	**0.22**	**0.66**	**0.33**	**0.7**
0.18mM	**24mM**	**0.1**	**0.34**	**0.29**	**1**
0.10mM	**12mM**	**0.05**	**0.16**	**0.31**	**1**

Table 4.3.1.2 Fluorescence quantum yields of distinct DiR/ micelles formulations as a function of micellar loading. Also shown are the respective relative values of absorbance at the wavelengths of maximum sample absortpitons and those measured at the λ_{exc} = 690nm

which either dynamic or static quenching are the only (or at least vastly dominant) mechanisms of fluorescence quenching the experimentally observed decrease in fluorescence of the original fluorophore when in the presence of a quencher (Q) present in solution can be rigorously described by the equation:

$$\Phi_{f0}/ \Phi_f = 1+ K [Q] \qquad \text{eq. 4.3.1.1}$$

In equation 4.3.1.1 Φ_{f0} and Φ_f represent quantum yields in the absence (Φ_{f0}) and in the presence of a quencher, (Φ_f) respectively, while the constant K represents two distinct physical phenomena depending upon the mechanism of quenching. For purely dynamic quenching, K (here

also known as the classical Stern-Volmer constant, K_{sv}) represents the product of the bimolecular rate constant of the quenching process (K_q) by the fluorescence lifetime of the respective fluorophore in the absence of the quencher (τ_0). In other words, $K = K_{sv} = K_q \times \tau_0$. On the other hand, when the quenching is 100% static, K represents the equilibrium constant (K_{eq}) describing the non-covalent association of the fluorophore and respective quencher in solution. Therefore, in both extreme cases considered here, the effect of quencher concentration on fluorescence can be expected to follow a linear relationship, with the respective plots showing Y intercept numerically equal to 1 and respective slopes representing either K_{sv} of K_{eq}, depending upon the respective quenching mechanism. Upward deviations from these expected limiting linear behaviors represent strong evidences of the simultaneous occurrence of both mechanisms of quenching, and perhaps additional contributions as well (e.g. environmental/solvent effects).

Figure 4.3.1.7 shows a classical Stern-Volmer plot built on basis of the DiR fluorescence quenching observed in this study as a function of increasing DiR concentration in the core micellar environment. The steep upward curvature of the plot presented in Fig. 4.3.1.7 suggests significant contributions arising from distinct mechanisms of quenching. Note worth here is the fact that the respective Stern-Volmer plot as built on basis of homogeneous distribution of DiR along the entire micelle (i.e. core plus corona) shows exactly the same profile, with the only difference between the two plots being the values of DiR concentrations represented in the X axis of the respective plots.

Although the data presented in Fig 4.3.1.7 can generate a variety of speculative interpretations for the experimentally observed DiR micellar concentration effects, the classical

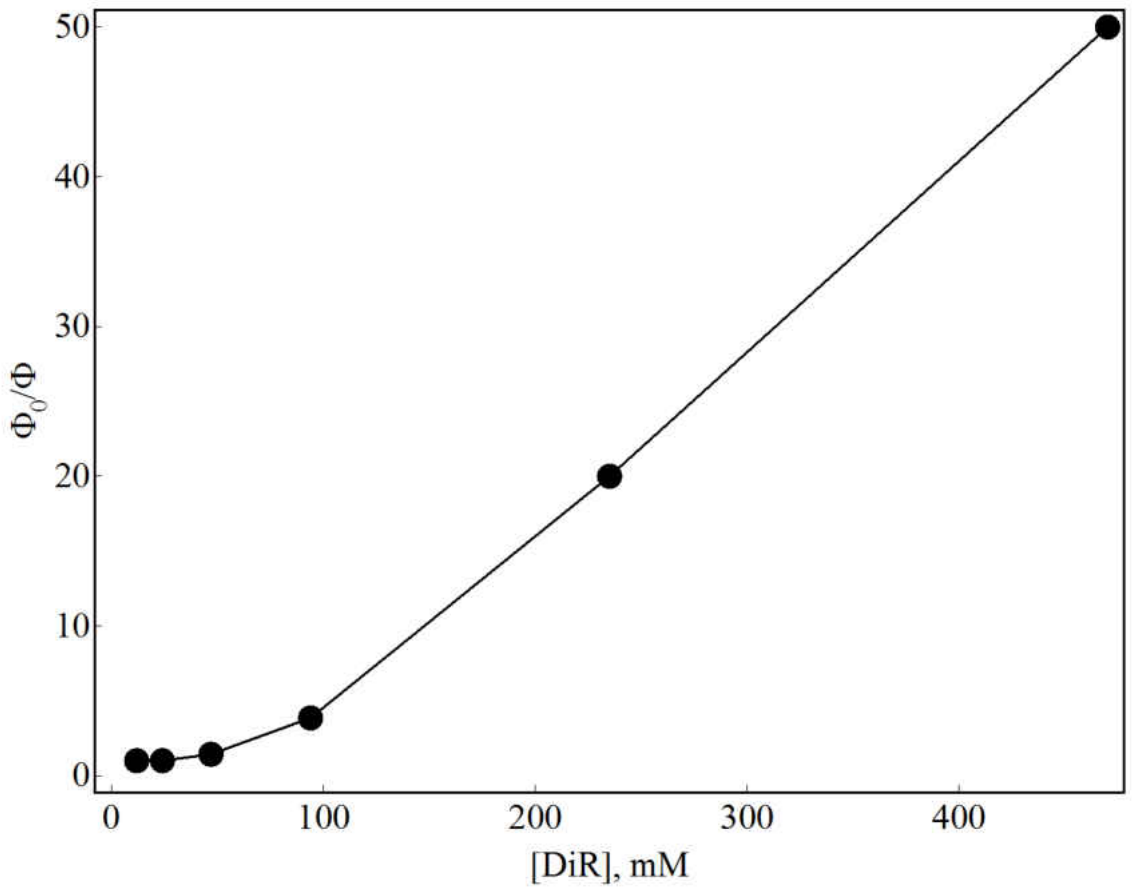

Fig. 4.3.1.7 Classical Stern-Volmer plot for the quenching of DiR fluorescence as a function of dye concentration in the core region of PEG-*b*-PCL polymeric micelles.

dynamic plus static quenching interpretation represents the most common interpretation of the upward bound (e.g quadratic) concentration dependence of quenching. The experimental data present here represent, therefore, strong evidence that the observed fluorescence quenching as a function of increasing micelle loading cannot be explained solely on basis of DiR aggregation in the micellar environment. That is, additional and concurrent mechanisms of fluorescence quenching can be expected be at play in this system.

4.3.2. Cardiogreen (CG)

Cardiogreen is typically more soluble in water than in organic solvents. However, this dye still shows far higher tendencies to aggregate in water than it does in any of the organic solvents considered in this study (see Fig 3.7.1 and Appendix D). The high aggregation tendencies of CG in water facilitate the characterization of the respective interaction with polymeric micelles *via* the observation of "de-aggregation" tendencies when this dye is formulated in the presence of PEG-*b*-PLC micelles. For example, Fig 4.3.2.1 shows the absorption spectrum of a 32 μM solution of CG in water along with that of a standard CG-micelle formulation containing the same concentration of this dye. The observation here is a sharp decrease in the $\lambda_{shoulder}/\ \lambda_{max}$ ratio when in the presence of micelles, what represents an indication of CG micellar solubilization/encapsulation. Fig. 4.3.2.1 also shows how the absorption spectrum of the original (raw) dye-micelle formulation if affected by size-exclusion chromatography treatment. On basis of the comparison between values of maximum absorption alone, and as measured before and after size exclusion chromatography treatment, the data presented in Fig. 4.3.2.1 indicates that at least 55% of the dye present in the original formulation elutes along with the polymeric micelles through the first column. Likewise, when the CG-micelle sample recovered from the first column is subjected to a second column, still about 29 % of the original absorbance at λ_{max} is recovered. These results indicate that CG can be formulated with PEG-b-PCL micelles to generate stable final supramolecular assemblies.

The data presented in Fig. 4.3.2.2 suggests that the composition of the original CG-micelle

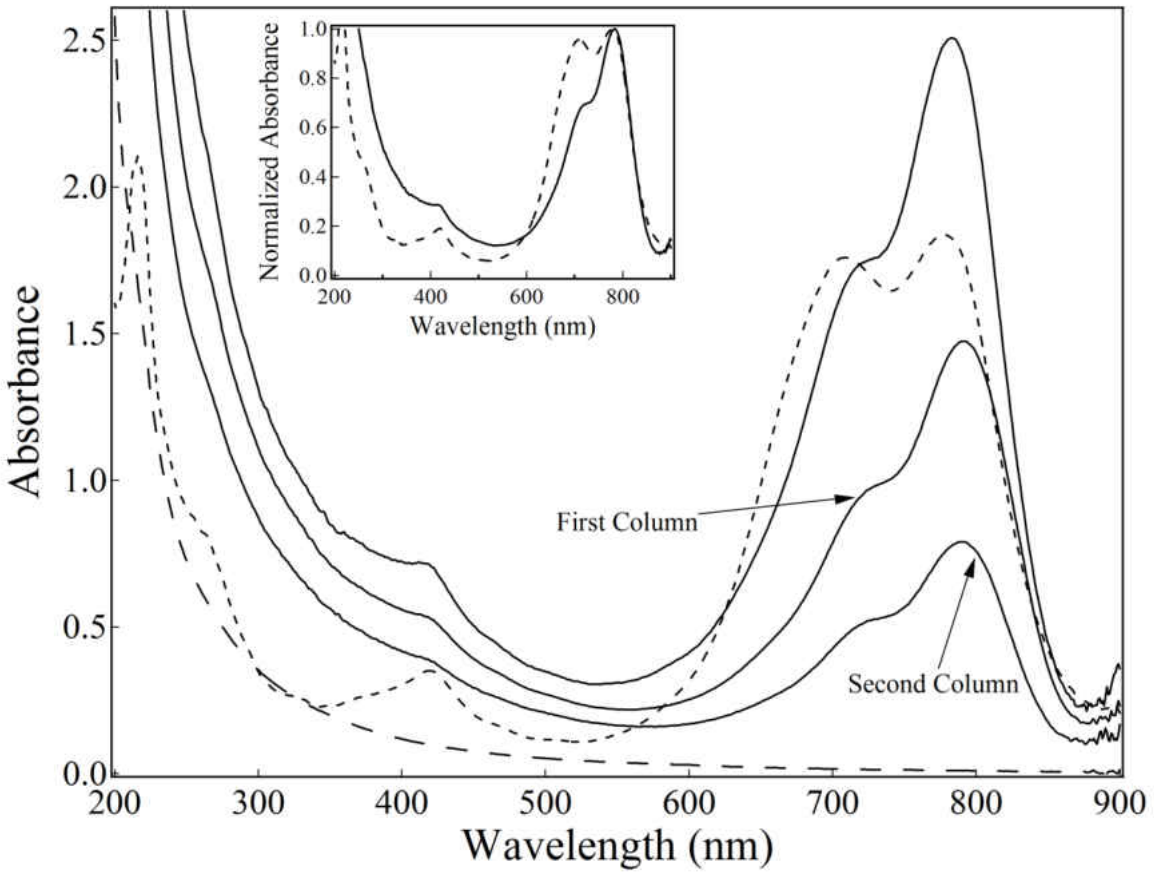

Fig 4.3.2.1 Absorption spectra of Cardiogreen in the polymeric micelle formulation before (top solid line) and after passing through two consecutive columns (lower solid lines). Also shown is the absorption of Cardiogreen in pure water (top dashed line) and the spectrum of empty micelles (bottom dashed line). Inset: normalized absorption spectra of Cardiogreen in the original micelle formulation (solid line) and in pure water (bottom dashed line). λmax: Solid line (top to bottom): 783nm, 790nm, 789nm; Dashed line: 778nm; $[CG]_{water}$ = 32μM.

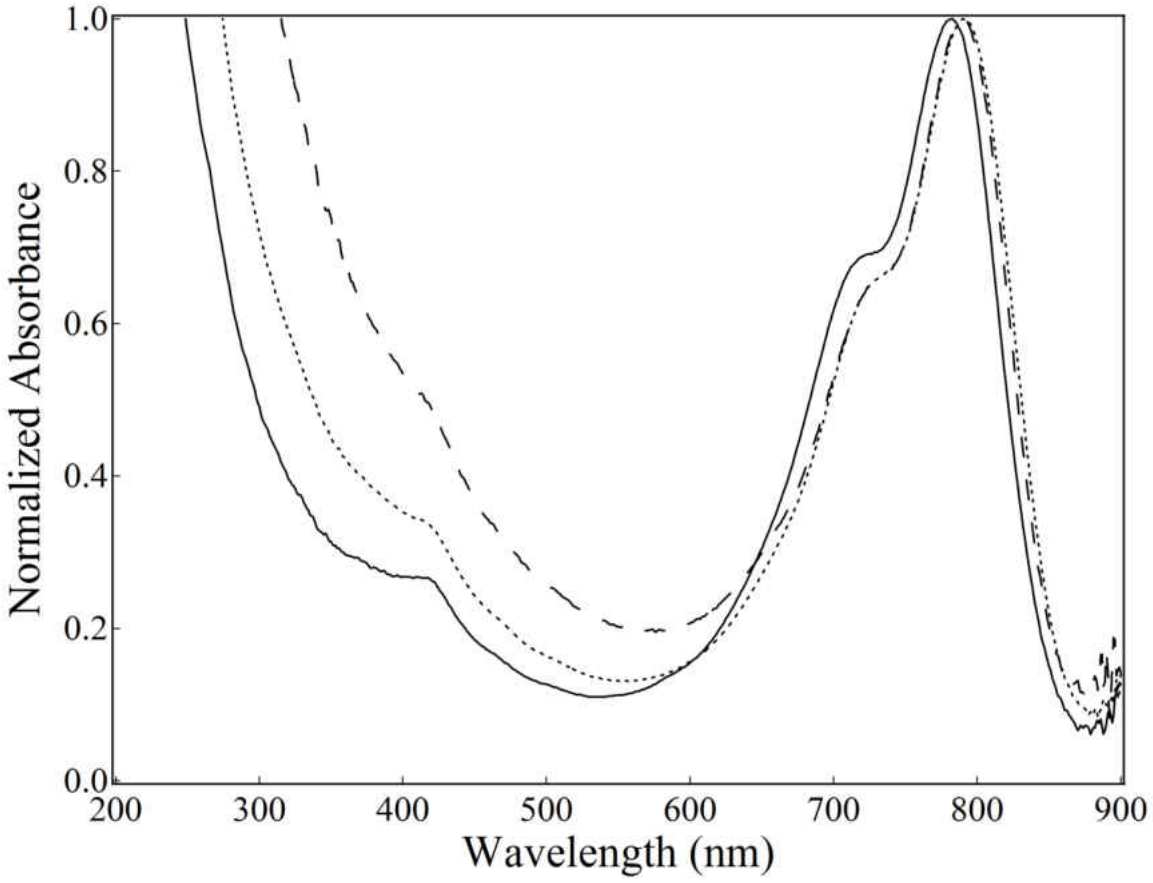

Fig 4.3.2.2 Absorption Spectra of Cardiogreen in the polymeric micelle formulation before (solid line) and after passing through first (bottom dashed line) and second (top dashed line) size-exclusion chromatographic columns.

formulation varies to a measurable extent upon column treatment. That is, the data presented in Fig. 4.3.2.2 suggests that a sub-population of the dye molecules present in the original (raw) formulation are more efficiently retained by the column than others. That is, while λ_{max} and the $\lambda_{shoulder}/\lambda_{max}$ ratio varies measurably in going from the original formulation to the first column eluent, apparently the total amount of dye-loaded micelle recovered from both columns contains, proportionally, less dye than the original (raw) formulation (note higher UV contribution associated with the latter). This observation may indicate the presence of a sub-population of CG dye molecules either free in the aqueous media or just loosely associated with more surficial regions of the corona moiety of the polymeric micelles. In other words, apparently micelle encapsulation and the respective supramolecular product stability are lower for CG as compared to DiR.

A somehow complicating factor associated with the study of PEG-*b*-PCL/CG formulations, as proposed in this study, and following the standard formulation protocol used here, is represented by the fact that when aqueous solutions of CG are warmed up to about 60 ^{o}C and higher temperatures, the respective H-Type dye aggregates tend to re-orient into the respective J-Type aggregates (Rotermund et al., 1997a). CG J-type aggregates show λ_{max} in the 890nm region of the spectrum. In this study the formation of J-Type CG aggregates in pure water has indeed been observed, but with no consequences with respect to the respective dye encapsulation/interaction with the polymeric micelles.

4.3.3. Leuco Crystal Violet

In this study, initial attempts were made to evaluate the extent to which more hydrophilic cationic imaging agents (e.g. Rh-123) and photosensitizers (e.g. CV and MB) could possibly be efficiently encapsulated into PEG-*b*-PCL polymeric micelles. Initial considerations involving ion-pairs as potential micellar loading species (i.e. ion pairs involving highly delocalized cationic dyes and the large soft anion tetrhaphenylborate) have not provided clear guidelines for the achievement of the desired objectives (see Chapter 3). Likewise, all attempts described in this study to encapsulate these last (free) dyes alone into polymeric micelles have failed (see section 4.1). On the other hand, many cationic species can be easily transformed into more hydrophobic derivatives *via* simple reduction. It is reasonable to infer that these more hydrophobic dye derivatives would have better chances to show higher and more desirable polymeric micelle encapsulation efficiencies than those associated with the respective parent cationic dyes.

Here the reduced form of Crystal Violet (that is, Leuco-Cystal Violete (L-CV)) has been used as a model molecule to explore the potential of this strategy. L-CV is a largely hydrophobic compound, show just minor solubility in water, and can be re-oxidized back to the parent dye cation (CV) by the action of Reactive Oxygen Species and peroxidases (Mottola et al., 1970; Cohn et al., 2005, 2006). Fig. 4.3.3.1 shows the absorption spectrum of L-CV in pure water and also the respective spectrum of a L-CV/PEG-*b*-PCL micelle formulation prepared using the standard solvent evaporation method described in Chapter 2. The amount of L-CV

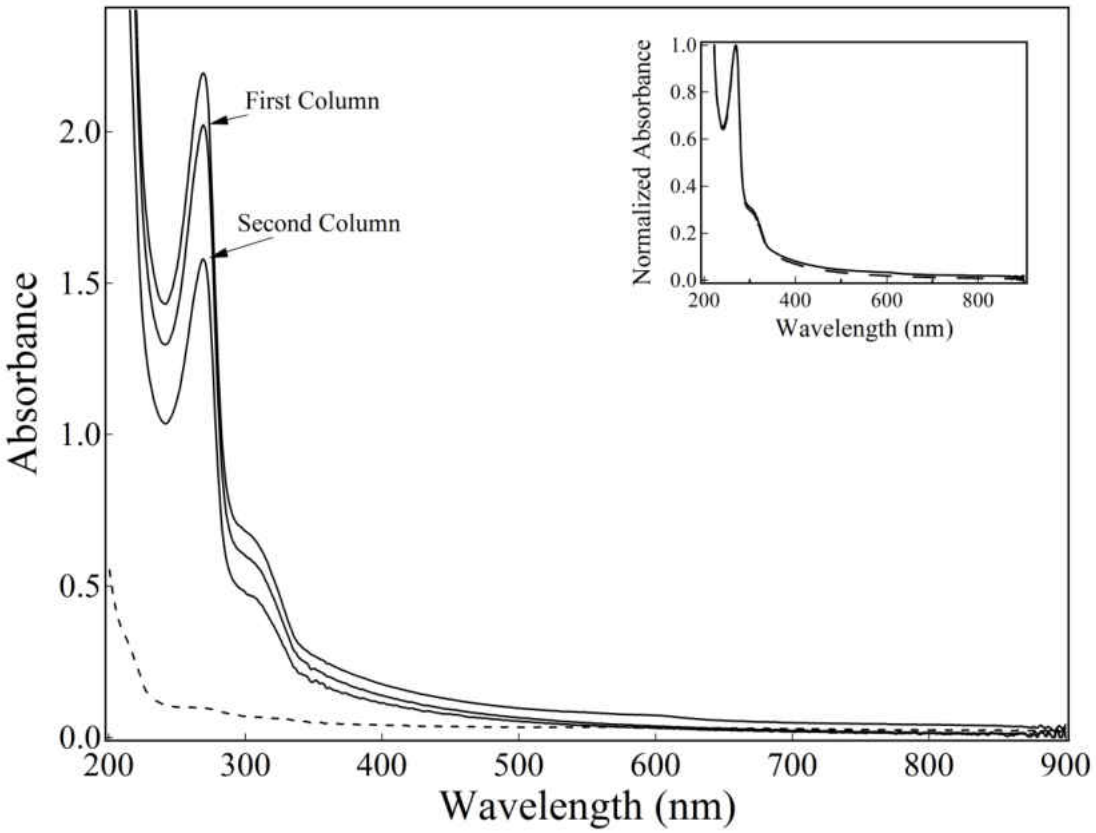

Fig 4.3.3.1 Absorption spectra of Leuco Crystal Violet in a standard polymeric micelle formulation before (top solid line) and after passing through two consecutive ion-exchange chromatographic columns (lower solid line). The absorption spectrum of Leuco Crystal Violet in pure water is also shown (dashed line). Inset: Normalized absorption spectra of Leuco Crystal Violet micelle formulation before (solid line) and after (dashed line) passing through a size-exclusion column.

solubilized in the micellar environment was found to be around 16 fold higher than that observed in pure water. This observation represents an indication of efficient encapsulation of L-CV into PEG-*b*-PCL micelles. In addition, upon exposure of the original L-CV/micelle formulation to two consecutive size-exclusion chromatographic columns, most of the L-CV present on the original formulation was still present in the eluted fractions recovered from these columns along with the respective micelles, indicating strong associations of the guest molecules with the host micelles. That is, around 92% of the L-CV presented in the original formulation eluted along with the micelles when exposed to the first column, and about 72% of the original amount was recovered along with the respective micelles from the second column (Fig. 4.3.3.1). Interestingly, again in this case, the composition of the supramolecular assemblies apparently do not change upon column treatment (see inset of Fig. 4.3.3.1), suggesting the possibility that a fraction of the original L-CV loaded micelles may be somehow lost in the column chromatography experiments.

The observed enhanced solubility of L-CV in the micellar environment along with the stability of the respective L-CV/micelle assemblies, as indicated by the column chromatography experiments, satisfactorily supports the hypothesis that the reduced derivatives of some cationic dyes may represent far better alternatives for micellar encapsulation then the respective parent cationic species. In these cases, the reduced forms of the respective desirable “drugs” would represent classical examples of “prodrugs”. That is, species that would need to be metabolic (or otherwise) activated before displaying their desirable “therapeutic” properties.

5. Fluorescence Properties of Visible and Near-IR absorbing dyes

This chapter describes the fluorescence spectroscopic distributions of all cationic dyes considered in this study. This chapter also describes attempts to compare the fluorescence quantum yields of the dyes showing the most desirable levels of micellar encapsulation, namely DiR and Cardiogreen. Here the difficulties associated with a rigorous (accurate) characterization of fluorescence quantum yields are explored and highlighted.

5.1 Fluorescence spectroscopic characteristics of all cationic dyes considered in this study.

The library of cationic dyes used in this study includes dyes showing absorption and fluorescence distributions in most of the visible and also in significant regions of the near-IR regions of the electromagnetic spectrum (Fig 5.1). That is, dyes showing maximum absorption from the 507 nm to the 778 nm regions of the spectrum (in methanol), and maximum (uncorrected) fluorescence emissions from the 525 nm to the 808 nm regions of the spectrum (in methanol). This library, therefore, includes representative agents that can be used in both spectroscopic regions of current interest for imaging and phototherapy. While near-IR agents can be expected to provide for the imaging and phototherapy of tumor located at deeper tissue locations (as compared to more superficial malignancies), fluorescence quantum yields are typically higher for agents that absorb light in the visible region of the spectrum, and the respective photosensitization efficiencies are also most typically higher as compared to those associated with Near-IR dyes (Debbage et al., 2008; Park et al., 2009). Examples of recent developments in Visible and Near-IR intra-operative tumor imaging are represented by a current

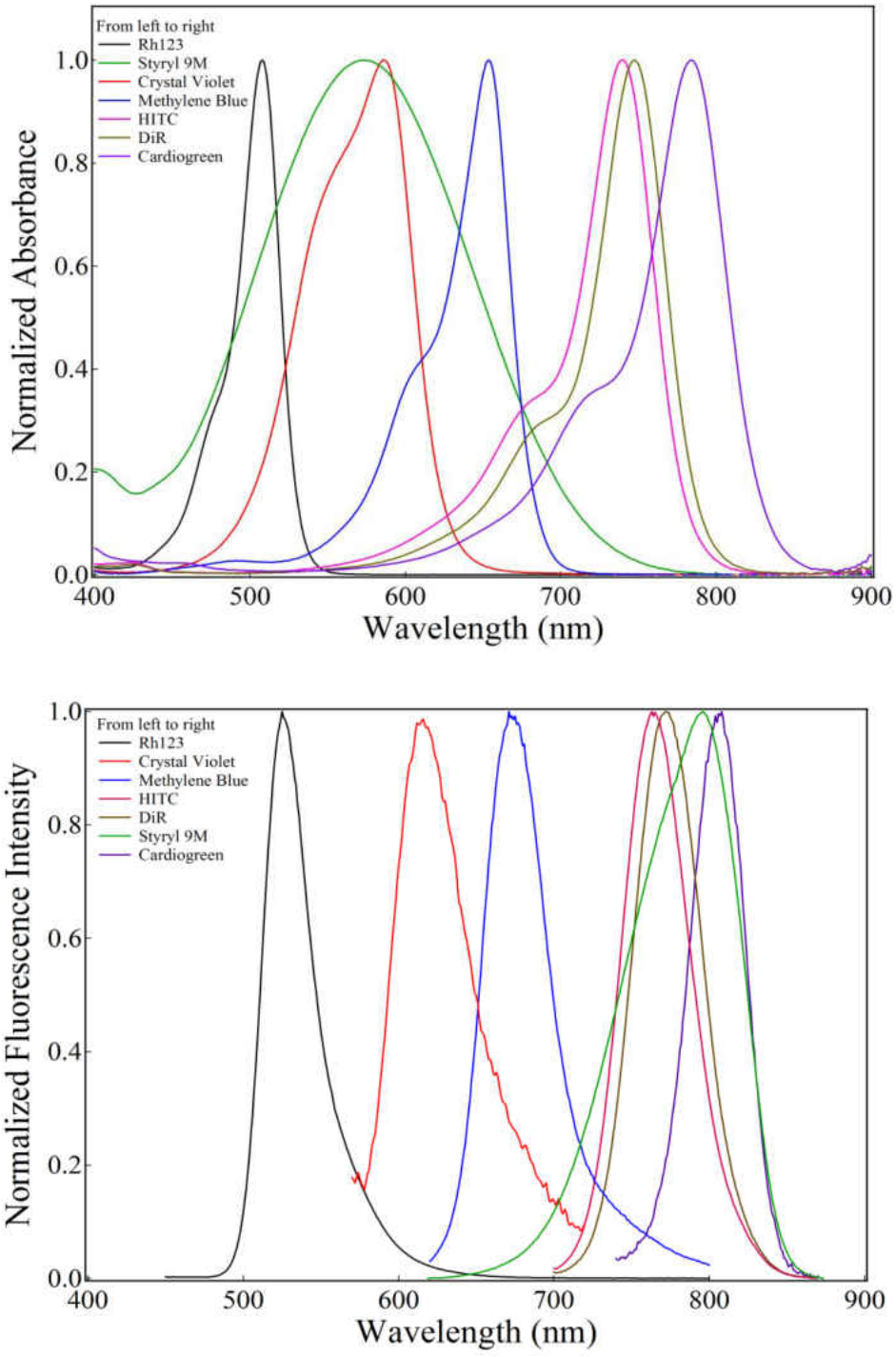

Fig 5.1 Top panel: Absorption spectra of visible and Near-IR absorbing dyes in methanol. From left to right (λ_{max}, nm): Rh123 (507), Styryl 9M (573), CV (587), MB (654), HITC (740), DiR(748) and Cardiogreen (778). Bottom panel: respective fluorescence spectra in methanol, from left to right (λ_{max} and $\lambda_{excitation}$, nm): Rh123 (525, 440); CV (615, 550); MB (673, 610); HITC (764, 690); DiR (772, 690); Styryl 9M (796, 570); Cardiogreen (808, 690).

human clinical trial in which the visible fluorescent dye fluorescein is used as imaging agent (van Dam G.M. et al., 2011), and by current pre-clinical (animal model-based) studies in which DiR is used as the respective Near-IR imaging agent (Cho and Kwon, 2011; Cho et al., 2012, 2014).

Amongst all dyes investigated here the best imaging agent, as far as the visible range is concerned, is Rh-123 ($\phi_f \sim 0.8$ in a variety of distinct environments/solvents) (Kubin and Fletcher, 1983). The other visible dyes considered here (e.g. CV and MB) show relatively low fluorescence quantum yields ($3.0*10^{-5}$(ACN) and 0.04(methanol) respectively; Baptista and Indig, 1998; Moreira et al., 2012), but this last characteristic just represents a (indirect) requirement for high photosensitization efficiency. That is, photosensitization efficiency most typically steels from fluorescence quantum yield via enhanced intersystem crossing (ISC) efficiency. In this study, attempts to encapsulate photosensitizers into micelles were not performed on basis of their imaging properties, but rather on their photodynamic therapeutic properties.

On the other hand, reasonably accurate values of fluorescence quantum yields for near-IR dyes are scant in the literature, and yet in this study the comparison between the fluorescence quantum yields of the imaging dyes showing the highest levels of micellar encapsulation (i.e. DiR and CG, respectively) are of significant interest. The reasons why accurate values of fluorescence quantum yield for Near-IR dyes are rare in the literature are discussed in the following section of this document. The primary objective of the exercise described below is not

to measure "absolute" values of fluorescence quantum yield, but rather to compare the fluorescence quantum yields of DiR and Cardiogreen to an extent that would provide for a satisfactory inference on which one of them is higher, and approximately by how much.

5.2 Evaluation of fluorescence quantum yields of interest.

Fluorescence spectroscopy is a technique made notorious by the number of experimental artifacts that can be easily avoided in order to generate reliable and accurate fluorescence data. These would include, but would not be restricted to, problems associated with inner filter effects and the required corrections for differences in refractive index and absorbances/concentrations observed amongst any set of samples to be compared. For instance, the artifacts associated with inner filter effects (i.e. spectroscopic distortions and quantum yield measurement flaws) can be easily avoided by keeping the absorbance of any and all samples under investigation very low, preferably below the 0.05 absorption units limit at the wavelength of excitation and also at any other longer wavelength within the respective absorption envelopes (Lakowics 2006; Demas and Crosby 1971; Parker and Rees, 1962). Because very low absorption values (e.g. below 0.05 absorption units) typically represent very diluted solutions, in most cases concentration effects (i.e. self-quenching effects) are negligible under such conditions. Likewise, in quantum yield measurements corrections for differences in refractive index, differences in light intensity from excitation light source at different wavelength when distinct samples are excited at different wavelengths, and also for differences in absorption values at the wavelength of excitation between distinct samples are all taken into consideration and by the formalism presented in

Demas and Crosby (1971; equation 2.2.1). Accordingly, when inner filter effects are avoided, and all other corrections described in equation 2.2.1 are taken into consideration, then the measurement of fluorescence quantum yields can be expected to be highly accurate, but yet unfortunately that is not always the case. The reason for this last inference is based on the fact that the efficiency with which any spectrofluorometer is capable of detecting emitted photons is not constant throughout the spectrum, but rather a wavelength dependent variable.

The accuracy associated with the response of any spectrofluorometer depends primarily on the properties of its respective detection system, namely the combination of its monochromator and photomultiplier (or, in some cases, other photodetector devices such as a diode-array detector). In other words, the accuracy of spectrofluorometers depends primarily on the wavelength-dependent efficiency with which the respective monochromator directs light to the respective photomultiplier through the equipment optical pathway, and also on the wavelength-dependent quantum efficiency of the respective photomultiplier. Most commercially available spectrofluorometers are designed to show maximum response by or near the center region of the visible spectrum. The detection system of the equipment used in this study is composed of a monochromator biased at 500 nm (1200 lines/cm) and a photomultiplier with maximum quantum efficiency around 500 nm, but with significant lower efficiencies beyond the 600 nm region of the spectrum. Accordingly any comparative evaluation of relative fluorescence quantum yields between samples emitting at different wavelengths using this specific (although typical) spectrofluorometer would represent a futile exercise unless proper corrections are made

with regard to equipment response. Such correction became even more important when comparing samples that emit at different wavelengths beyond the 600 nm range, region in which the decrease in photomultiplier quantum efficiency is more pronounced. This is the reason why reliable values of fluorescence quantum yields for Near-IR fluorescent compounds are rare in the literature. They are difficult to measure using typical commercially available spectrofluorometers.

For the sake of comparison, Fig. 5.2.1 shows the raw (uncorrected) fluorescence spectrum of Rh-123 in water along with the respective corrected spectrum (correction parameters from 400 nm to 600 nm provided by *Photon Technologies International, Inc*., the equipment builder). The data presented in Fig. 5.2.1 highlights the fact that even when working within the optimum spectral range of any given spectrofluorometer, still detectable changes in fluorescence spectra are most typically observed upon correction of the respective raw data for the response of the respective detection system. Accordingly, Fig. 5.2.1 shows a 2nm red-shift in the corrected spectrum as compared to the uncorrected one, although the respective fluorescence integrals have assumed virtually the same value (i.e. less than 0.1 % increase in total area for the case of the corrected spectrum). Because the equipment used in this study is optimized to operate in the 400 nm to 600 nm range, and because a reliable correction curve is also available for that range, reliable relative values of fluorescence quantum yields can be obtained in that range, but not in any other spectroscopic range without proper correction.

Figure 5.2.2 shows the absorption and fluorescence spectra of HITC, Cardiogreen and DiR

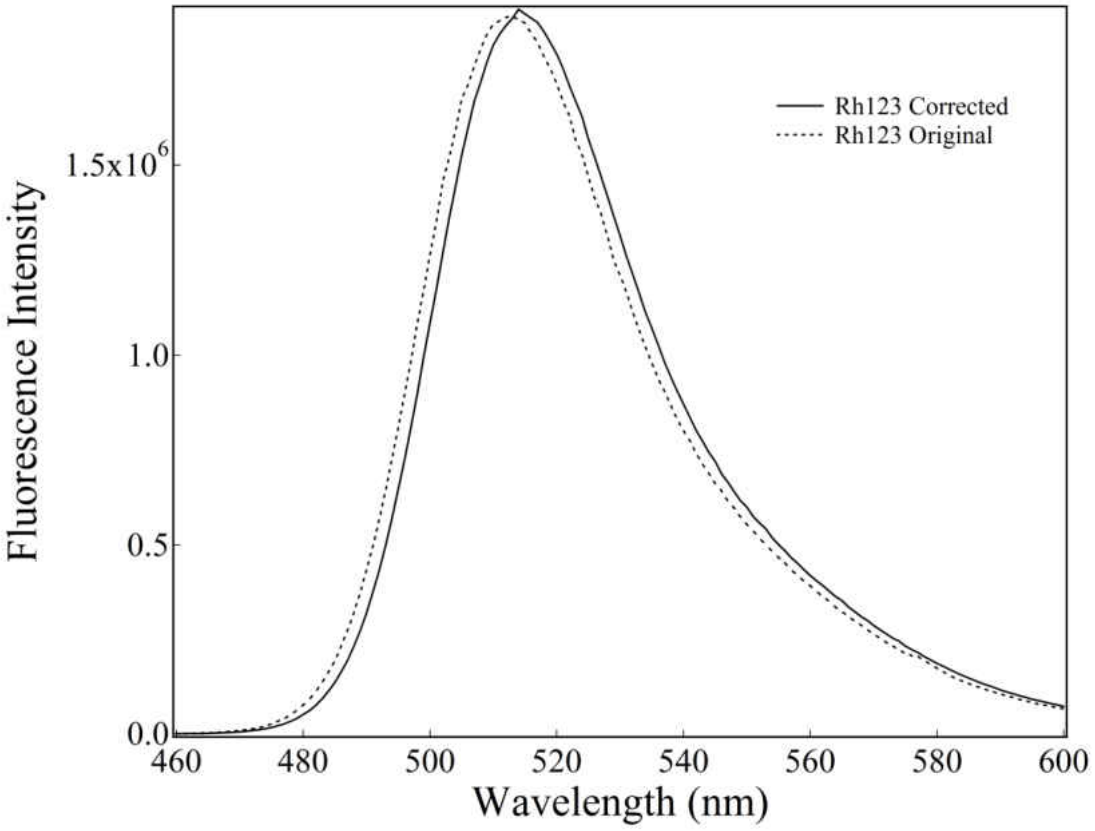

Fig 5.2.1 Uncorrected (doted line; λ_{max}=512nm) and correct (solid line; λ_{max}=514nm) fluorescence spectra of Rhodamine 123 in water. λ_{exc} = 450 nm.

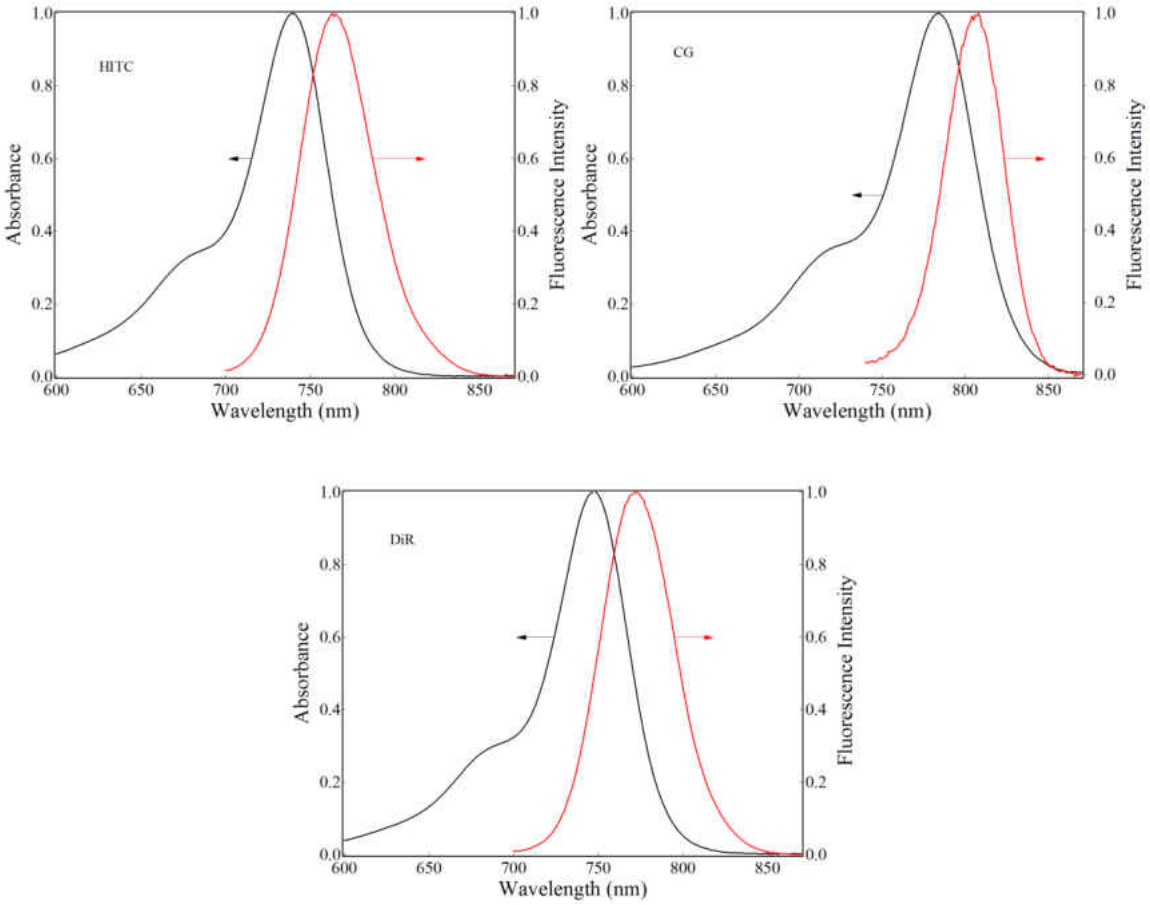

Fig 5.2.2 Normalized absorption (left) and fluorescence spectra (right) of Near-IR absorbing dyes in methanol. Clockwise, from top left panel (λ_{max} of absorption, λ_{max} of fluorescence, nm): HITC (740, 764), Cardiogreen (778, 808) and DiR (748, 772). λ_{exc} = 690 nm

in methanol. In all cases, significant overlaps are observed between the absorption and respective fluorescence spectra, what highlights the need to work with diluted solutions in order to avoid inner-filter effects. Fig. 5.2.2 also shows that the fluorescence of these dyes appear at wavelengths quite significantly longer than 600 nm, with the respective maximum (uncorrected) varying from 764 nm (HITC) to 808 nm (Cardiogreen). That is, these dyes fluoresce at wavelengths far from the region of optimum equipment response.

The attempts to compare fluorescence yields described here were facilitated by (i) the excitation of all samples at the same wavelength (therefore no need for corrections arising from different excitation lamp intensities at different wavelength; (ii) preparing all solution in the same solvent (no need for corrections due to differences in refractive index); (iii) preparing samples with low absorption values and correcting any small differences in absorption at wavelength of excitation by normalizing the respective spectra (no need for further correction based on absorption values. With these actions, Eq. 2.2.1 is then reduced to the following equation:

$$\Phi_X = \Phi_R (B_R/B_X) \qquad \textbf{Equation } 5.2.1$$

Therefore, here the relative quantum yields of samples X and R can be obtained by the simple comparison of the integral areas of the respective corrected fluorescence spectra (B_R and B_X, respectively).

Fig. 5.2.3 shows the normalized raw fluorescence spectra (i.e. raw fluorescence spectra already corrected for small difference in absorption at the wavelength of excitation) of HITC,

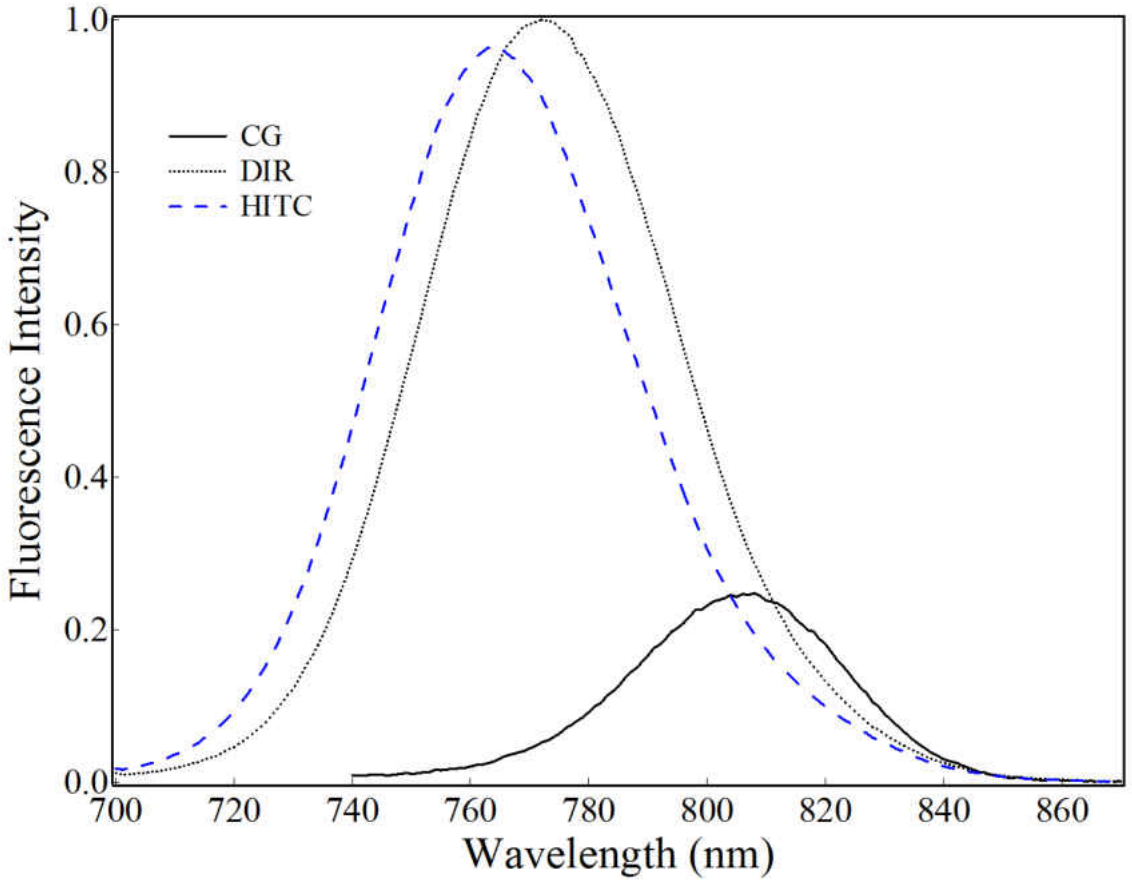

Fig 5.2.3 Fluorescence spectra of HITC (λ_{max}=764nm), DiR (λ_{max}=772nm) and Cardiogreen (λ_{max}=808nm) in methanol. Relative intensities for solutions showing the same absorption at the wavelength of excitation (690 nm). Data not corrected for the wavelength-dependent response of the detection system (monochromator grading and photomultiplier; see text).

DiR and Cardiogreen in methanol. In Fig. 5.2.3 relative values of fluorescence integral (i.e. in the areas under the respective fluorescence envelops) represent, therefore, the respective relative values of (uncorrected) fluorescence quantum yields. On basis of the data shown in Fig. 5.2.3, the relative uncorrected fluorescence quantum yields for Cardiogreen, DiR and HITC were found to be 1.0, 4.8, and 4.9, respectively. That is, on basis of uncorrected fluorescence spectra, the experimental data suggests that DiR is about five-fold more fluorescent than Cardiogreen, while showing largely comparable fluorescence yield compared to HITC. This last observation is not surprising, given the fact that the chromophoric group is the same in DiR and HITC. The only structural difference between these two last dyes is represented by the size of the alkyl groups linked to the respective quaternary ammonium moieties. While actadecyl substituents are present in DIR, the respective substituents in HITC are methyl groups. Besides, the fluorescence spectra of both HITC and DiR are observed mostly in the same spectroscopic region, therefore minimizing correction needs at least for an initial evaluation of the respective relative quantum yields.

While the uncorrected fluorescence data suggest that the quantum yield of DiR is about five-fold higher than that of Cardiogreen, the fluorescence distribution of these two dyes are observed at significantly different spectroscopic regions (Fig. 5.2.3). For this reason, in order to better compare the relative quantum yields of DiR and Cardiogreen, the correction of the respective fluorescence spectra for the response of the detection system of the spectrofluorometer used in this study is of essence.

The experimental determination of correction curves for the response of the detection system of spectrofluorometers is, in principle, almost trivial. It only requires the experimental acquisition of the fluorescence raw spectrum of a standard fluorescent compound using the spectrofluorometer under analysis, and the comparison of that spectrum with the spectroscopic distribution of that same fluorescence standard as previously rigorously characterized by reference agencies or laboratories. Recent publications have provided quite robust protocols for that correction (including appropriate software), along with information on standard compounds and respective spectroscopic distributions, but only for the visible region of the spectrum (Würth, C et al., 2013). However, unfortunately, the availability of standard data for fluorescent compounds that emit in the Near-IR region of the spectrum remain largely scant in the literature. In this study one of these rare compounds has been used as standard, namely LDS 751 (Lakowicz, 2006). Fig. 5.2.4 shows the experimental absorption and fluorescence spectra of LDS 751 in methanol, along with the respective standard (corrected) fluorescence spectrum as found in the current literature (Lakowicz, 2006). The simple ratio between the respective experimental and standard (published) fluorescence spectra provides therefore the desired correction parameters for the response of the detection system of the spectrofluorometer used in this study. This exercise has provided reliable information for the correction of fluorescence spectra within 646 nm to 844 nm spectroscopic range. The respective correction curve is shown in Fig. 5.2.5.

The correction of the raw fluorescence data presented in Fig. 5.2.3 was then carried out by the simple multiplication of the respective spectra by the correction curve shown in Fig. 5.2.5.

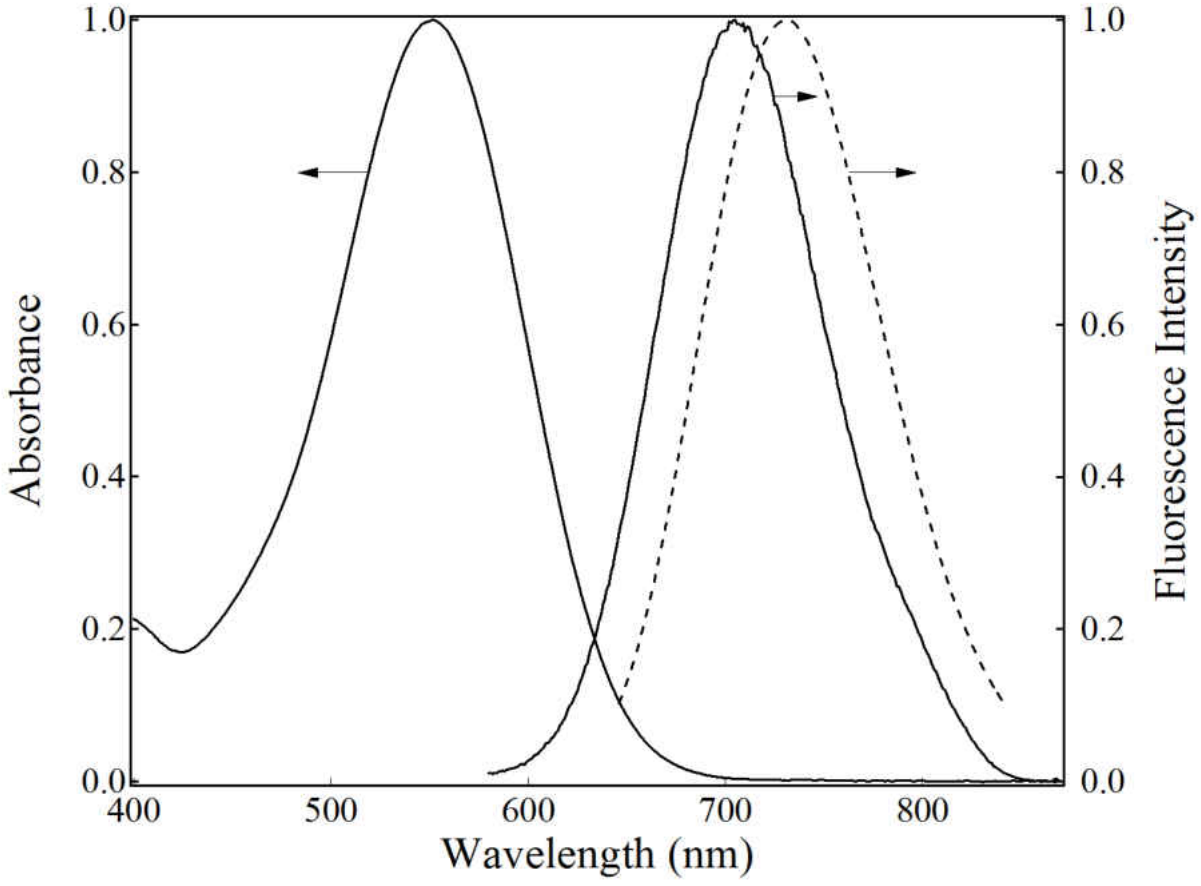

Fig 5.2.4 Normalized absorption (λ_{max}=550nm) and fluorescence spectra (λ_{max}=705nm) of LDS 751 in methanol (solid lines). λ_{exc} = 550 nm. Also shown is the respective standard (corrected) fluorescence spectrum as found in the current literature (dash lines; λ_{max}=730nm; see text).

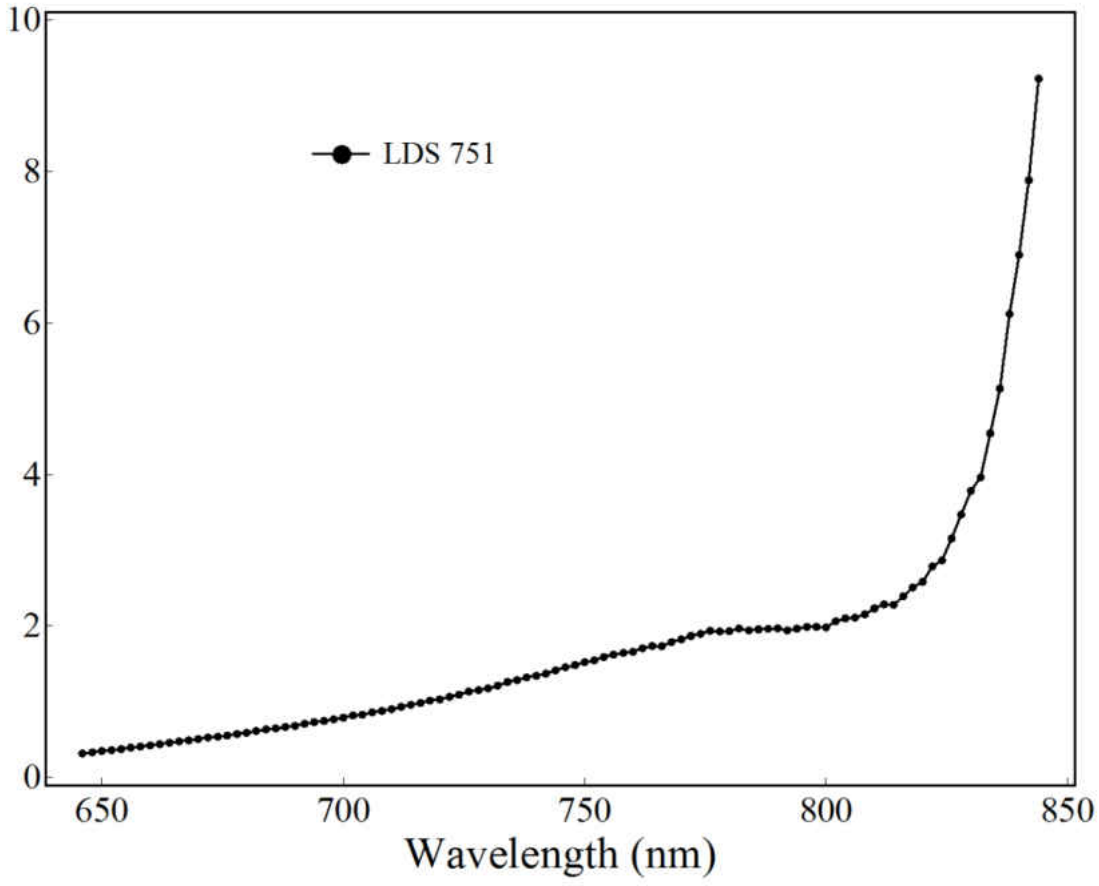

Fig. 5.2.5 Correction curve for the spectrofluorometer detection system used in this study (monochromator grading and photomultiplier) generated by the data presented in Fig 5.2.4.

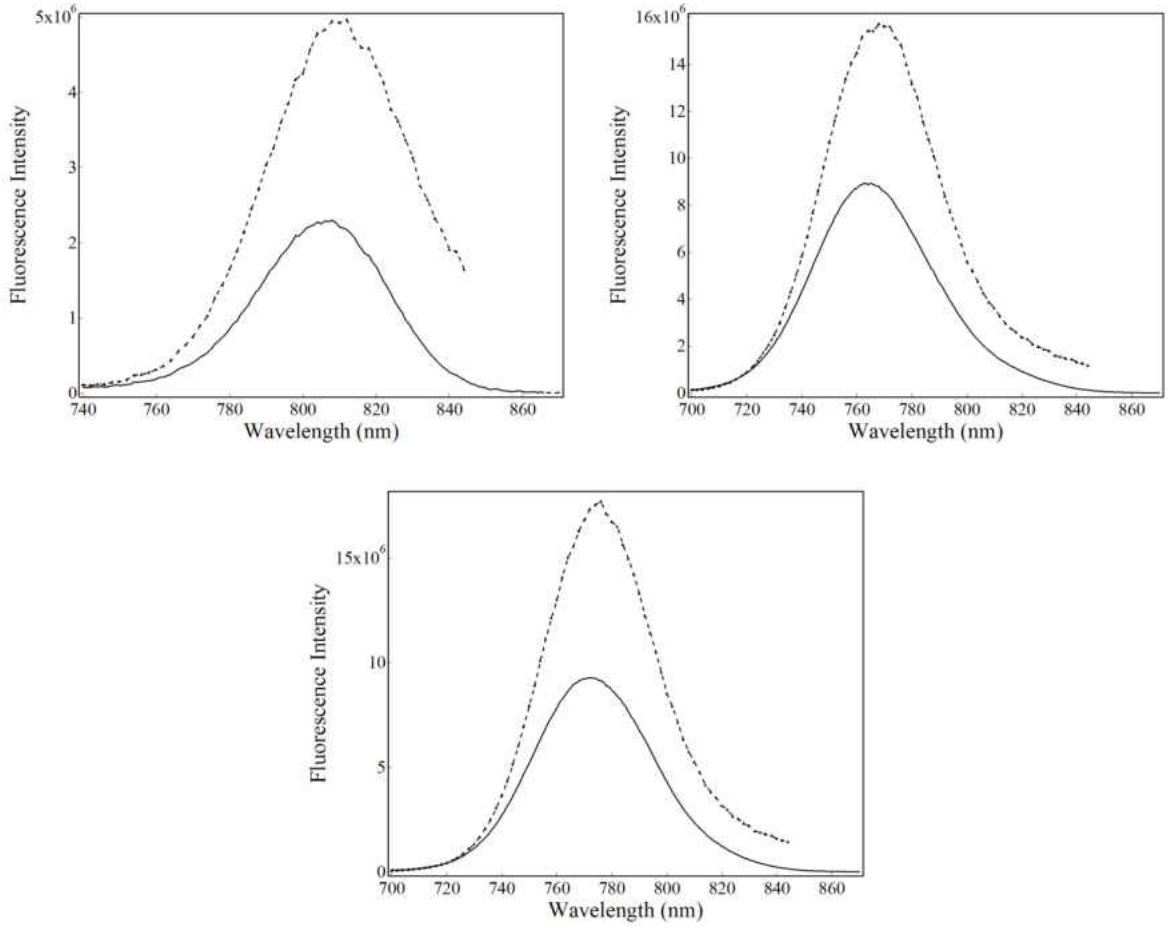

Fig. 5.2.6 Clockwise from the top left panel: Uncorrected (solid lines) and "correct" (doted lines) spectra of Cardiogreen, HITC and DiR according to the correction curve shown in Fig. 5.2.5. Uncorrected/corrected fluorescence maximums (nm): Cardiogreen (808/812), HITC (764,768), DiR (772,776).

The results of such corrections are shown if Fig. 5.2.6. It must be noted here that the correction curve generated by using LDS 751 as an standard compound does not actually corrects for the entire fluorescence envelops of all dyes of interest in this study. The very long wavelength tailing regions of the respective spectra are not always corrected to desirable extents, but nevertheless this limitation is bound to have just minor impact on the comparative evaluations considered here. Based on the respective integrated fluorescence areas alone, the respective relative values of fluorescence quantum yields were found to follow the sequence: Cardiogreen (1.0), HITC (3.6) and DiR (3.9). That is, based on this correction, the DiR quantum yield has been found to be around four-fold higher than that of Cardiogreen, in contrast with the five-fold evaluation based solely on the respective uncorrected fluoresce spectra. Here yet another attempt was made to further compare such values, and with the objective of somehow avoiding the limitations provided by the LDS 751 correction curve. In this final effort, it has been considered that the fluorescence emission spectra of the dyes under consideration here are highly symmetric (see Fig. 5.2.3). That is, that the areas of the first halves of these spectra (i.e. with λ_{max} representing the middle spectroscopic point) are comparable to the areas represented by the respective second halves (i.e. the longer wavelength halves). In this effort the area of the first half of each spectrum was measured and then multiplied by 2 in order to evaluate total fluorescence area. Following this procedure, the relative values of fluorescence quantum yields were found to follow the sequence: Cardiogreen (1.0), HITC (3.0) and DiR (3.3). Therefore, it is apparent safe to state that, in methanol, the fluorescence quantum yield of DiR is between 3.3 and 3.9 times (with this last

value defined using total corrected areas) higher than that of Cardiogreen, and not 4.9 times higher as suggested by the respective analysis involving uncorrected fluorescence spectra. That is, about four-fold higher instead of five-fold higher as suggested by uncorrected fluorescence spectra considerations.

5.3. Concluding Remarks

In this chapter the spectroscopic fluorescence distributions of all cationic dyes considered in this study have been described. The dye series considered here include dyes with potential applications both in the visible and Near-IR regions of the electromagnetic spectrum. In addition, here significant effort has been placed on the comparison of the fluorescence quantum yields of DiR and Cardiogreen. The best estimate arising from this study indicates that, at least in methanol, the fluorescence quantum yield of DiR is at best only four-fold higher than that of Cardiogreen.

6. Conclusions

In this study the extent to which concentration and solvent (i.e environmental) effects control the spectroscopic properties of seven cationic dyes of interest to this project have been explored. This exercise was performed in an attempt to find reliable spectroscopic parameters for the characterization of encapsulation (or lack thereof) of these dyes into PEG-*b*-PCL polymeric micelles. Accordingly, here attempts were also made to characterize spectroscopic signatures that would more properly describe just minor interactions (rather than encapsulation) of these dyes with PEG-*b*-PCL polymeric micelles. Based on the spectroscopic information alone, three out of the seven dyes considered here were found to show significantly altered properties when in the presence of polymeric micelles (Styryl 9M, DiR and Cardiogreen). However only two out of these three dyes (DiR and Cardiogreen) where found to actually form stable supramolecular assemblies with these micelles.

The findings described in this study appear to support the current working hypothesis that polymeric micelles represent superior drug delivery vehicles only (or at least most typically) for the formulation of drugs showing very low aqueous solubility. Indeed, this study describes the highly efficient micellar encapsulation of a reduced (water insoluble) derivative of one of the cationic dyes studied here that otherwise shows no evidences of any significant (measurable) interactions with PEG-*b*-PCL polymeric micelles (i.e. Crystal Violet). On the other hand, this study has also provided strong evidences for the efficient encapsulation of a significantly water soluble cationic dye (i.e. Cardiogreen) into these micelles. Interestingly, Cardiogreen was found to

aggregate in aqueous media even when present at very low concentrations, a characteristic shared by another significantly water soluble cationic dye, methylene blue. On the other hand, while no evidences where found for MB micellar encapsulation, the encapsulation of Cardiogreen into PEG-*b*-PCL polymeric micelles was made evident by the experimental results obtained in this study.

While no "absolute" correlation has been found in this preliminary study on how and to which extent water solubility (or hydrophobic character) controls micellar encapsulation, the observed trend appear to support the hypothesis that the lower the water solubility the higher the encapsulation efficiency, although the remarkable exception represented by the Cardiogreen case will require and deserve further investigation.

This initial "screening" exercise (as carried out under a single standard condition) has also suggested higher encapsulation efficiency and higher supramomelucar assembly stability for the case in which DiR is the host dye in PEG-*b*-PCL polymeric micelles as compared to the case in which Cardiogreen is the host dye. Likewise, the best estimate on relative fluorescence quantum yields between DiR and Cardiogreen described in this study indicates that at least under the comparable conditions used here DiR shows fluorescence quantum yield about four-fold higher than that of Cardiogreen. Therefore, on basis of this initial set of experimental data it is reasonable to infer that DiR may represent a more adequate imaging agent for intraoperative imaging of tumors when delivered to the respective targeted areas with the use of polymeric micelles then Cardiogreen would most likely be.

The fluorescence quantum yield of DiR in distinct PEG-*b*-PCL micelle formulations was found to decrease upon increasing dye aggregation in the nanonscopic domain(s) of the respective polymeric micelles. However, dye aggregation alone cannot explain the magnitude of the observed fluorescence quenching. Accordingly, the treatment of the original fluorescence quenching data using the classical Stern-Volmer formalism indicates that at least two distinct mechanism of quenching are likely to operate simultaneously in these formulations. Given the relatively high dye concentrations in the micellar environment, energy transfer mechanisms (Dexter/collisional or Forster/resonance energy transfer) are likely to significantly contribute to the observed quenching effects.

7. Proposed Future Work

At least when considering polymeric micelles as drug delivery shuttles, the body of experimental evidences described in this work suggests that amongs all cationic dyes considered here DiR is the one showing the highest potential as intraoperative Near-IR imaging agent. However, to better fine-tune the fluorescence properties of the respective formulations more will need to be understood on how and to which extent polymeric loading affects the fluorescence quantum yield of this dye in distinct polymeric micelle formulations. A systematic study aimed at the characterization of the distinct mechanisms of fluorescence quenching at play in these formulations represents, therefore, a natural extention of this initial work.

Likewise, more rigorous comparisons between the properties of DiR formulations with those of the respective Cardiogreen formulations represent a subject of significant interest. Although the initial indications of higher fluorescence quantum yield of DiR (as compared to Cardiogreen), along with its potentially higher micellar loading and respective supramolecular assemble stability could potentially limit further interest in Cardiogreen. However, Cardiogreen has already been approved by the US-FDA as an imaging agent for use in humans. Therefore, drug formulations involving this last dye are far more likely to reach pre-clinical and subsequent clinical use on a timely basis than those currently based on DiR. More hydrophobic Cardiogreen analogs (e.g. as rerpresented by the simple replacement of the respective four-carbon amino-substituents by substituents containig larger carbon chains) may provide for more stable,

better polymeric micelle formulations, and the investigation of this last inference also represents a subject of current interest.

8. References

Abboud, J.L., Kamlet, M.J., and Taft, R.W. (1977) Regarding a Generalized Scale of Solvent Polarities, *J. Am. Chem. Soc.* 1977; 99(25):8325-8327

Adams ML, Lavasanifar A, Kwon G.S.(2003). Amphiphilic block copolymers for drug delivery. *J Pharm Sci*. 2003;92:1343–55.

Aliabadi H. M. and Lavasanifar A.,(2006). Polymeric micelles for drug delivery *Expert Opin. Drug Delivery*, 2006, 3, 139.

Amaral, E., Guatimosim, S., & Guatimosim, C. (2011). Using the fluorescent styryl dye FM1-43 to visualize synaptic vesicles exocytosis and endocytosis in motor nerve terminals. In *Light Microscopy* (pp. 137-148). Humana Press.

Baptista, M.S.; Indig, G.L. (1997). Mechanism of Photobleaching of Ethyl Violet Non-Covalently Bound to Bovine serum Albumin" *Chemical Communications*, 1997, 1791-1792

Baptista, M.S.; Indig, G.L. (1998). Effect of BSA Binding on Photophysical and Photochemical Properties of Triarylmethane Dyes. *J. Phys. Chem. B*, 1998, *102* (23), pp 4678–4688

Barth B. M., Altinoglu E. I., Shanmugavelandy S. S., Kaiser J. M., Crespo-Gonzalez D., DiVittore N. A., McGovern C., Goff T. M., Keasey N. R., Adair J. H., Loughran T. P.Jr., Claxton, D. F. and Kester M., (2011) Targeted indocyanine-green-loaded calcium phosphor-silicate nanoparticles for in vivo photodynamic therapy of leukemia", *Acs Nano* 5(7), 5325-5337 (2011).

Bartlett, J. A. and Indig, G. L. (1999), Effect of Self-association and Protein Binding on the Photochemical Reactivity of Triarylmethanes. Implications of Noncovalent Interactions on the Competition between Photosensitization Mechanisms Type I and Type II. *Photochemistry and Photobiology*, 70: 490–498.

Belostotsky, I., Da Silva, S.M., Paez, M.G. and Indig, G.L.(2011). Mitochondrial targeting for photochemotherapy. Can selective tumor cell killing be predicted based on n-octanol/water distribution coefficients?.*Biotechnic & Histochemistry*, 2011, *86*(5), pp.302-314.

Chawla B., Pollack S. K., Lebrilla C. B., Kamlet M. J., Taft R. W.(1981), Use of carbon-13 substituent chemical shifts to scale nonhydrogen-bonding dipolar interactions of protonic solvents, *J. Am. Chem. Soc.*, 1981, 103 (23), pp 6924–6930

Chen L.B.(1988). Mitochondrial membrane potential in living cells. *Annu Rev Cell Biol.*1988; 4:155-81.

Chen L.B.(1989). Fluorescent labeling of mitochondria. *Methods Cell Biol.* 1989;29:103-23.

Cho H. and Kwon G.S. (2011). Polymeric micelles for neoadjuvant cancer therapy and tumor-primed optical imaging. *ACS Nano*. 2011; 5(11):8721-9.

Cho, H., Cho, C.S., Indig, G.L., Lavasanifar, A., Vakili,M.R., Kwon, G.S., (2014). Polymeric Micelles for Apoptosis-Targeted Optical Imaging of Cancer and Intraoperative Surgical Guidance. *PLoS ONE* 9(2): e89968.

Cho H, Indig GL, Weichert J, Shin HC, Kwon GS.,(2012). In vivo cancer imaging by poly(ethylene glycol)-b-poly(ε-caprolactone) micelles containing a near-infrared probe. *Nanomedicine.* 2012 Feb;8(2):228-36.

Choi H. S., Liu W., Misra P., Tanaka E., Zimmer J. P., Ipe B. I., Bawendi M. G. and Frangion J. V. (2007). Renal clearance of quantum dots, *Nat.Biotechnol.*, 2007, 25, 1165.

Chung, E.J., Cheng, Y., Morshed, R., Nord, K., Han, Y., Wegscheid, M.L., et al. (2014). Fibrin-binding, peptide amphiphile micelles for targeting glioblastoma. *Biomaterials* 35, 1249–1256.

Cohn, C.A., Pak, A., Schoonen, M.A.A. and Strongin, D.R., (2005). Quantifying hydrogen peroxide in iron-containing solutions using leuco crystal violet. *Geochemical Transactions*, 2005, *6*(3), pp.47-52.

Cohn, C.A., Laffers, R., Simon, S.R., O'Riordan, T. and Schoonen, M.A., (2006). Role of pyrite in formation of hydroxyl radicals in coal: possible implications for human health. *Particle and Fibre Toxicology*, 2006, *3*(1), p.16.

Croy, S.R., and Kwon, G.S. (2006). Polymeric micelles for drug delivery. *Curr. Pharm.Des.* 12, 4669–4684.

da Silva, J.S., Junqueira, H.C. and Ferreira, T.L., (2014). Effect of pH and dye concentration on the n-octanol/water distribution ratio of phenothiazine dyes: a microelectrode voltammetry study. *Electrochimica Acta*, 2014, *144*, pp.154-160.

Davis S, Weiss M.J, Wong J.R, Lampidis T.J, Chen L.B.(1985). Mitochondrial and plasma membrane potentials cause unusual accumulation and retention of rhodamine 123 by human breast adenocarcinoma-derived MCF-7 cells. *J Biol Chem.* 1985;260(25):13844-50.

Debbage P. and Jaschke W., Molecular imaging with nanoparticles: giant roles for dwarf actors, Histochem. *Cell Biol.* 130 (2008) 845 – 875.

Delaey E., Van Laar F., De Vos D., Kamuhabwa A., Jacobs P., and De Witte P., *J.* (2000). A comparative study of the photosensitizing characteristics of some cyanine dyes. *Photochem. Photobiol., B*, 2000; **55**, 27–36.

Demas, J.N. and Crosby, G.A.,(1971). Measurement of photoluminescence quantum yields-Review. *Journal of Physical Chemistry*,1971, *75*(8), p.991.

Di, L., Fish, P.V.,and Mano, T.(2012).Bridging solubility between drug discovery and development. *DrugDiscov.Today* 17, 486–495.

Di, L., Kerns, E.H.,and Carter, G.T.(2009).Drug-like property concepts in pharmaceutical design. *Curr.Pharm.Des.* 15, 2184–2194.

Dilgin Y., Nişli G. (2005). Fluorimetric determination of ascorbic acid in vitamin C tablets using methylene blue. *Chem Pharm Bull (Tokyo)*. 2005;53(10):1251-4.

Drexhage, K. H. (1976). Fluorescence Efficiency of Laser Dyes. *J. Res. Natl. Bur. Stand*. A 1976, 80A, 421–428

Du W, Nystrom AM, Zhang L, Powell KT, Li Y, Cheng C, et al (2008). Amphiphilic hyperbranched fluoropolymers as nanoscopic 19F magnetic resonance imaging agent assemblies. *Biomacromolecules*.2008;9:2826–33.

Folkman, J. (1995). Angiogenesis in cancer, vascular, rheumatoid and other disease. *Nat.Med.* 1, 27–31.

Fonge, H., Huang, H., Scollard, D., Reilly, R.M., and Allen, C. (2012). Influence of formulation variables on the biodistribution of multifunctional block copolymer micelles. *J. Control.Release* 157, 366–374.

Fortina, P., Delgrosso, K., Sakazume, T., Santacroce, R., Moutereau, S., Su, H. J., Graves D., McKenzie S. and Surrey, S. (2000). Simple two-color array-based approach for mutation

detection. *European Journal of Human Genetics*, 2000; *8*(11), 884-894.

Fukukawa K, Rossin R, Hagooly A, Pressly ED, Hunt JN, Messmore BW, et al. Synthesis and characterization of core-shell star copolymers for in vivo PET imaging applications. *Biomacromolecules*.2008;9:1329–39.

Gilani, A.G., Salmanpour, M. and Ghorbanpour, T., (2013). Solvatochromism, dichroism and excited state dipole moment of azure A and methylene blue.*Journal of Molecular Liquids*, 2013, *179*, pp.118-123.

Gohy, J.F., (2005). Block copolymer micelles. In *Block copolymers II* (pp. 65-136). Springer Berlin Heidelberg.

Green F.J. (1990).The Sigma–Aldrich Handbook of Stains, Dyes and Indicators *Aldrich Chemical Co., Inc, Milwaukee* (1990), pp. 300–301

Gülçür, E., Thaqi, M., Khaja, F., Kuzmis, A., and Önyüksel, H. (2013).Curcumin in VIP-targeted sterically stabilized phospholipid nanomicelles: a novel therapeutic approach for breast cancer and breast cancer stem cells. *DrugDeliv.Transl. Res.* 3, 562–574.

Guttmann, P. and Ehrlich. P. (1891) "Über die Wirkung des Methylenblau bei Malaria" (On the effect of methylene blue on malaria), *Berliner Klinische Wochenschrift*, 1891; 28: 953-956.

Hideaki A., US Patent 6,261,352 (2001).

Hobbs S.K., Monsky W.L., Yuan F., Roberts,W.G., Griffith, L., Torchilin, V.P., et al. (1998). Regulation of transport pathways in tumor vessels: role of tumor type and microenvironment. *Proc.Natl.Acad.Sci.U.S.A.* 95, 4607–4612.

Indig, G. L., Anderson, G. S., Nichols, M. G., Bartlett, J. A., Mellon, W. S. and Sieber, F. (2000), Effect of molecular structure on the performance of triarylmethane dyes as therapeutic agents for photochemical purging of autologous bone marrow grafts from residual tumor cells. *J. Pharm. Sci.*, 89: 88–99.

Istomin Y. P., Alexandrova E. N., Zhavrid E. A., Samtsov M. P., Kaplevsky K. N., and Lugovsky A. A. (2006). The effect of hypoxia on photocytotoxicity of tics tricaebocyanine dye in vitro. *Exp. Oncol.*,2006; **28**, 80–82

Iyer,A.K., Khaled,G., Fang,J., and Maeda,H.(2006). Exploiting the enhanced permeability and retention effect for tumor targeting. *DrugDiscov.Today* 11, 812–818.

Jain, R.K. (1987).Transport of molecules across tumor vasculature. *Cancer MetastasisRev.* 6, 559–593

Jhaveri, A.M. and Torchilin, V.P. (2014). Multifunctional polymeric micelles for delivery of drugs and siRNA. *Front Pharmacol.* 2014; 5: 77.

Jin, C., Yang, W., Bai, L., Wang, J., and Dou, K. (2011). Preparation and characterization of targeted DOX-PLGA-PEG micelles decorated with bivalent fragment HAb18 F(ab')2 for treatment of hepatocellular carcinoma. *J. Control.Release* 152(Suppl.1),e14–e15

Johnson, L. V., Walsh, M. L., & Chen, L. B. (1980). Localization of mitochondria in living cells with rhodamine 123. *Proceedings of the National Academy of Sciences*, 1980;*77*(2), 990-994.

Johnson, L. V., Walsh, M. L., Bockus, B. J., & Chen, L. B. (1981). Monitoring of relative mitochondrial membrane potential in living cells by fluorescence microscopy. *The Journal of Cell Biology*, 1981; *88*(3), 526-535.

Jones, G. and Indig G.L.(1996). Spectroscopic and chemical binding properties of humic acids in water, *New J.Chem.*, 1996, 20,221-232

Jones, M. and Leroux, J. (1999). Polymeric micelles—a new generation of colloidal drug carriers. *Eur.J.Pharm.Biopharm.* 48, 101–111.

Kalchenko, V., Shivtiel, S., Malina, V., Lapid, K., Haramati, S., Lapidot, T., Brill A. and Harmelin, A. (2006). Use of lipophilic near-infrared dye in whole-body optical imaging of hematopoietic cell homing. *Journal of biomedical optics*, 2006; 11(5), 050507-050507.

Kamaly, N., Xiao, Z., Valencia, P.M., Radovic-Moreno ,A.F., and Farokhzad, O.C. (2012). Targeted polymeric therapeutic nanoparticles: design, development and clinical translation. *Chem.Soc.Rev.* 41, 2971–3010.

Kamlet, M.J., Abbound, J.L. and Taft, R.W. (1977), The solvatochromic comparison method. 6. The .pi.* scale of solvent polarities. *J. Am. Chem. Soc.*, 1977, *99* (18), pp 6027–6038

Kamlet, M.J., Hall, T.N., Boykin, J. and Taft, R.W.(1979a), Linear solvation energy relationships. 6. Additions to and correlations with the .pi.* scale of solvent polarities. *J. Org. Chem.*, 1979, *44* (15), pp 2599–2604

Kamlet, M.J. and Taft, R.W.(1979b) Linear solvation energy relationships. Part 3. Some reinterpretations of solvent effects based on correlations with solvent π* and α values. *J. Chem. Soc., Perkin Trans. 2*, 1979, 349-356

Kamlet, M. J., Abboud, J.-L. M. and Taft, R. W. (1981) An examination of linear solvation energy relationships, *Prog. phys. org. Chem.* 13, 485−630 (1981).

Kandela, I. K., Bartlett, J. A., and Indig, G. L. (2002). Effect of molecular structure on the selective phototoxicity of triarylmethane dyes towards tumor cells. *Photochemical & Photobiological Sciences*, 2002;*1*(5), 309-314.

Kandela, I.K., Lee, W. and Indig, G.L., (2003). Effect of the lipophilic/hydrophilic character of cationic triarylmethane dyes on their selective phototoxicity toward tumor cells. *Biotechnic & Histochemistry*, 2003, *78*(3-4), pp.157-169.

Kaprelyants A.S., Gottschal J.C., Kell D.B. (1993). Dormancy in nonsporulating bacteria. *FEMS Microbiol Rev* 1993,104: 271–286.

Kasha M. (1947), Phosphorescence and the Role of the Triplet State in the Electronic Excitation of Complex Molecules. *Chem. Rev.*, 1947, *41* (2), pp 401–419

Kasha M. (1963), Energy transfer mechanisms and the molecular exciton model for molecular aggregates. *Radiat Res*. 1963 Sep; 20:55-70.

Kasha M., Rawls H. R. and Ashraf El-Bayoumi M.(1965), The exciton model in molecular spectroscopy, *Pure Appl. Chem.*, 1965, Vol. 11, No. 3-4, pp. 371-392

Kataoka K., Kwon G. S., Yokoyama M., Okano T. and Sakurai Y. (1993). Block copolymer micelles as vehicles for drug delivery. *J. Controlled Release*, 1993, 24, 119

Kell D.B,, Kaprelyants A.S., Weichart D.H., et al. (1998). Viability and activity in readily culturable bacteria: a review and discussion of the practical issues. *Antonie Van Leeuwenhoek* 1998; 73: 169–187.

Khemtong C, Kessinger CW, Togao O, Ren J, Takahashi M, Sherry AD, et al (2009). Off-resonance saturation magnetic resonance imaging of superparamagnetic polymeric micelles. *Conf Proc IEEE Eng Med Biol Soc*. 2009:4095–7.

Kim G., Huang S. W., Day K. C., O'Donnell M., Agayan R. R., Day M. A., Kopelman R. and Ashkenazi S.(2007), Indocyanine-green-embedded PEBBLEs as a contrast agent for photoacoustic imaging", *J. Biomed. Opt*.12(4), 044020 (2007).

Kubin, R. F., & Fletcher, A. N. (1983). Fluorescence quantum yields of some rhodamine dyes. *Journal of Luminescence*, 1983; *27*(4), 455-462.

Kuo W. S., Chang Y. T., Cho K. C., Chiu K. C., Lien C. H., Yeh C. S. and Chen S. J.,(2012) Gold nanomaterials conjugated with indocyanine green for dual-modality photodynamic and photothermal therapy, *Biomaterials* 33(11), 3270-3278 (2012).

Kwon G. K. and Forrest M. L.,(2006). Amphiphilic block copolymer micelles for nanoscale drug delivery. *Drug Dev. Res.*, 2006, 67, 15.

Lakowics, J., (2006). Principles of Fluorescence Spectroscopy, Springer. *New York*.

Larush L.and Magdassi S. (2011), "Formation of nearinfrared fluorescent nanoparticles for medical imaging", *Nanomedicine* 6(2), 233-240 (2011).

Lee H, Hoang B, Fonge H, Reilly RM, Allen C. *In vivo* distribution of polymeric nanoparticles at the whole-body, tumor, and cellular levels. *Pharm Res* (2010).

Lewis L.M. and Indig, G.L. (2000). Solvent effects on the spectroscopic properties of triarylmethane dyes, *Dye Pigment*, 2000,46(3),, pp. 145-154

Lewis, L.M. and Indig, G.L. (2002). Effect of dye aggregation on triarylmethane-mediated photoinduced damage of hexokinase and DNA. *Journal of Photochemistry and Photobiology B: Biology*, 2002, *67*(3), pp.139-148.

Lu J, Ma S, Sun J, Xia C, Liu C, Wang Z, et al. Manganese ferrite nanoparticle micellar nanocomposites as MRI contrast agent for liver imaging. *Biomaterials*. 2009;30:2919–28.

Lu, Y. and Park, K., (2013). Polymeric micelles and alternative nanonized delivery vehicles for poorly soluble drugs. *International journal of pharmaceutics*, *453*(1), pp.198-214.

Maeda, H., Wu, J., Sawa, T., Matsumura, Y., and Hori, K. (2000). Tumor vascular permeability and the EPR effect in macromolecular therapeutics: a review. *J. Control.Release* 65, 271–284.

Mellish K.J., Cox R.D., Vernon D.I., Griffiths J., Brown S.B. (2002). In vitro photodynamic activity of a series of methylene blue analogues. *Photochem Photobiol.* 2002 Apr;75(4):392-7.

McRae, E. G. and Kasha, M. Enhancement of Phosphorescence Ability upon Aggregation of Dye Molecules, *J. Chem. Phys.*, 28, 721 (1958).

Miura, Y., Takenaka, T., Toh, K., Wu, S., Nishihara, H., Kano, M.R.,et al. (2013). Cyclic RGD-linked polymeric micelles for targeted delivery of platinum anticancer drugs to glioblastoma through the blood-brain tumor barrier. *ACSnano* 7, 8583–8592.

Moon, E.W.; Lee, B.G.; Kim, K.J. (1988). Medium Effect on the Formation of Ion-Pair between Methylene Blue and Tetraphenylborate in Dilute Solutions. *Bull. Korean Chem. Soc*., 1988. vol.9. pp.209

Moraes-Souza H, Bordin JO.(1996). Strategies for prevention of transfusion-associated Chagas' disease. *Transfus Med Rev.* 1996 Jul;10(3):161-70.

Moreira, L.M., Romani, A.P., Severino, D., de Oliveira, H.P., Lyon, J.P. and Rodrigues, M.R., (2012). *Phenotiazinium dyes as photosensitizers (PS) in photodynamic therapy (PDT): spectroscopic properties and photochemical mechanisms*.

Mottola, H.A., Simpson, B.E. and Gorin, G., (1970). Absorptiometric determination of hydrogen peroxide in submicrogram amounts with leuco crystal violet and peroxidase as catalyst. *Analytical chemistry*, 1970, *42*(3), pp.410-411.

Nie, S., Xing, Y., Kim, G.J., and Simons, J.W. (2007). Nanotechnology applications in cancer. *Annu.Rev.Biomed.Eng.* 9, 257–288.

Oh S.Y., Lee B.G., Kim K.J. (1988). Surfactant Effect on the Hydrophobic Interaction between Rhodamine 6G and Sodium Tetraphenylborate. *Bull. Korean Chem. Soc*., 1988. vol.9. pp.308

Padera,T.P., Stoll,B.R., Tooredman,J.B., Capen,D., DiTomaso,E., and Jain,R.K. (2004). Pathology: cancer cells compress intratumour vessels. *Nature* 427, 695.

Park, J.H., Lee, S., Kim, J.H., Park, K., Kim, K., and Kwon, I.C. (2008). Polymeric nano-medicine for cancer therapy. *Prog.Polym.Sci.* 33, 113–137.

Park K., Lee S., Kang E., Kim K., Choi K., Kwon I.C., Newgeneration ofmultifunctional nanoparticles for cancer imaging and therapy, *Adv. Funct. Mater*. 19 (2009) 1553 – 1566.

Parker C. A. and Rees W. T.(1962) Fluorescence spectrometry. A review. *Analyst*, 1962,87, 83-111

Pressly ED, Rossin R, Hagooly A, Fukukawa K, Messmore BW, Welch MJ, et al. Structural effects on the biodistribution and positron emission tomography (PET) imaging of well-defined (64)Cu-labeled nanoparticles comprised of amphiphilic block graft copolymers. *Biomacromolecules.* 2007;8:3126–34.

Qiu, L.Y., Yan, L., Zhang, L., Jin, Y.M., and Zhao, Q.H. (2013). Folate- modified poly(2-ethyl-2-oxazoline) as hydrophilic corona in polymeric micelles for enhanced intracellular doxorubicin delivery. *Int.J.Pharm.* 456, 315–324.

Ramirez LE, Lages-Silva E, Pianetti GM, Rabelo RM, Bordin JO, Moraes-Souza H.(1995). Prevention of transfusion-associated Chagas' disease by sterilization of Trypanosoma cruzi-infected blood with gentian violet, ascorbic acid, and light. *Transfusion*. 1995 Mar;35(3):226-30.

Reichardt C. and Welton T. (2010). Solvents and Solvent Effects in Organic Chemistry. 4th Edtion,2010

Rice L.; Wainwright M.; Phoenix D.A. (2000). Phenothiazine Photosensitizers. III. Activity of Methylene Blue Derivatives against Pigmented Melanoma Cell Lines. *Journal of chemotherapy* 12.1 (2000): 94-104.

Riehle, R.D., Cornea, S., Degterev, A., and Torchilin, V. (2013). Micellar formulations of pro-apoptotic DM-PIT-1 analogs and TRAIL *in vitro* and *in vivo*. *Drug. Deliv.* 20, 78–85.

Roberts W.G. and Palade G.E. (1997). Neovasculature induced by vascular endothelial growth factor is fenestrated. *Cancer Res.* 57, 765–772.

Rotermund, F., Weigand, R. and Penzkofer, A., (1997a). J-aggregation and disaggregation of indocyanine green in water. *Chemical physics*, 1997, *220*(3), pp.385-392.

Rotermund, F., Weigand, R., Holzer, W., Wittmann, M. and Penzkofer, A., (1997b). Fluorescence spectroscopic analysis of indocyanine green J aggregates in water. *Journal of Photochemistry and Photobiology A: Chemistry*, 1997, *110*(1), pp.75-78.

Samtsov, M. P., Tikhomirov, S. A., Lyashenka, L. S., Tarasau, D. S., Buganov, O. V., Galievsky, V. A., Stasheuski A. S. and Voropay, E. S. (2013). Photophysical and photochemical properties of HITC indotricarbocyanine dye molecules in solutions. *Journal of Applied Spectroscopy*, 2013; *80*(2), 170-175.

Sawant, R.R., Jhaveri, A.M., Koshkaryev, A., Qureshi, F., and Torchilin, V.P. (2013a). The effect of dual ligand-targeted micelles on the delivery and efficacy of poorly soluble drug for cancer therapy. *J. DrugTarget.* 21, 630–638.

Sawant, R.R., Jhaveri, A.M., Koshkaryev, A., Zhu, L., Qureshi, F., and Torchilin, V.P. (2013b). Targeted transferrin-modified polymeric micelles: enhanced efficacy *in vitro* and *in vivo* in ovarian carcinoma. *Mol.Pharm.* 11, 375–381.

Saxena V, Sadoqi M, Shao J. (2003). Degradation kinetics of indocyanine green in aqueous solution. *J Pharm Sci* 2003;92:2090-7

Saxena V, Sadoqi M, Shao J. (2004). Enhanced photo-stability, thermal-stability and aqueous stability of indocyanine green in polymeric nanoparticulate systems. *J Photochem Photobiol B Biol* 2004;74:29-38

Schirmer R.H., Coulibaly B., Stich A., Scheiwein M., Merkle H., Eubel J., Becker K., Becher H., Müller O., Zich T., Schiek W., Kouyaté B. (2003). Methylene blue as an antimalarial agent. *Redox Rep.* 2003;8(5):272-5.

Schutters K., Reutelingsperger C., (2010) Phosphatidylserine targeting for diagnosis and treatment of human diseases. *Apoptosis* 15: 1072–1082.

Sheng Z.H., Hu D.H., Xue M.M., He M., Gong P., Cai L.T.,(2013) Indocyanine Green Nanoparticles for Theranostic Applications. *Nano-Micro Letters*, 2013, 5, 145-150

Severino, D., Junqueira, H.C., Gugliotti, M., Gabrielli, D.S. and Baptista, M.S. (2003). Influence of Negatively Charged Interfaces on the Ground and Excited State Properties of Methylene Blue¶. *Photochemistry and photobiology*, 2003,*77*(5), pp.459-468.

Shim, S. H., Xia, C., Zhong, G., Babcock, H. P., Vaughan, J. C., Huang, B., Wang X., Xu C., Bi G.Q. & Zhuang, X. (2012). Super-resolution fluorescence imaging of organelles in live cells with photoswitchable membrane probes. *Proceedings of the National Academy of Sciences*, 2012; *109*(35), 13978-13983.

Starkey, J. R., Makarov, N. S., Drobizhev, M., & Rebane, A. (2012). Highly sensitive detection of cancer cells using femtosecond dual-wavelength near-IR two-photon imaging. *Biomedical optics express*, 2012; *3*(7), 1534-1547.

Sun, L., Yang, Y., Dong, C.M., and Wei, Y. (2011). Two-photon-sensitive and sugar-targeted nanocarriers from degradable and dendritic amphiphiles. *Small* 7, 401–406.

Sutton, D., Nasongkla, N., Blanco, E., and Gao, J. (2007). Functionalized micellar systems for cancer targeted drug delivery. *Pharm.Res.* 24, 1029–1046.

Taft, R.W. and Kamlet, M.J. (1976), The solvatochromic comparison method. 2. The .alpha.-scale of solvent hydrogen-bond donor (HBD) acidities. *J. Am. Chem. Soc.*, 1976, *98* (10), pp 2886–2894

Taft, R.W. and Kamlet, M.J. (1979), Linear solvation energy relationships. Part 4. Correlations with and limitations of the α scale of solvent hydrogen bond donor acidities. *J. Chem. Soc., Perkin Trans. 2*, 1979, 1723-1729

Talelli M, Rijcken CJ, Lammers T, Seevinck PR, Storm G, van Nostrum CF, et al. (2009). Superparamagnetic iron oxide nanoparticles encapsulated in biodegradable thermosensitive polymeric micelles: toward a targeted nanomedicine suitable for image-guided drug delivery. *Langmuir.* 2009;25:2060–7.

Takada N., Sonoda T.,Kobayashi H. (1983). Spectrophotometric determination of tetraarylborate anions of minute concentration in aqueous solutions based upon aggregate formation with cationic dye. *Bunseki Kagaku.* 1983; 32:191.

Tardivoa J.P., Giglioa A.D., Oliveirab C.S., Gabriellib D.S., Junqueirab H.C. , Tadab D.B., Severinob D., Turchiellob R.F., Baptista M.S. (2005). Methylene blue in photodynamic therapy: From basic mechanisms to clinical applications. *Photodiagnosis and photodynamic therapy* , 2005, Vol.2(3), p.175-191

Texier I, GoutayerM, Da Silva A, Guyon L, Djaker N, Josserand V, Neumann E., Bibette J., Vinet F., (2009). Cyanine-loaded lipid nanoparticles for improved in vivo fluorescence imaging. *J Biomed Opt* 2009;14:054005-2.

Torchilin, V.P. (2001). Structure and design of polymeric surfactant-based drug delivery systems. *J. Control.Release* 73, 137–172.

Torchilin, V.P. (2007). Micellar nanocarriers: pharmaceutical perspectives. *Pharm. Res.* 24, 1–16.

Torchilin, V.P., Lukyanov, A. N., Gao, Z., and Papahadjopoulos-Sternberg, B. (2003). Immunomicelles: targeted pharmaceutical carriers for poorly soluble drugs. *Proc.Natl.Acad.Sci.U.S.A.* 100, 6039–6044.

Torchilin V.P., Frank-Kamenetsky MD, Wolf GL. (1999) CT visualization of blood pool in rats by using long-circulating, iodine-containing micelles. *Acad Radiol*. 1999;6:61–5.

Trotter M.J, Chaplin D.J, Olive P.L. (1989) Use of a carbocyanine dye as a marker of functional vasculature in murine tumours. *Br J Cancer* 1989;59:706-9.

van Dam, G.M., Themelis, G., Crane, L.M., Harlaar, N.J., Pleijhuis, R.G., Kelder, W., Sarantopoulos, A., de Jong, J.S., Arts, H.J., van der Zee, A.G. and Bart, J., (2011). Intraoperative tumor-specific fluorescence imaging in ovarian cancer by folate receptor-[alpha] targeting: first in-human results.*Nature medicine*, *17*(10), pp.1315-1319.

Wainwright, M., Phoenix, D. A., Rice, L., Burrow, S. M., & Waring, J. (1997). Increased cytotoxicity and phototoxicity in the methylene blue series via chromophore methylation. *Journal of Photochemistry and Photobiology B: Biology*, 1997;*40*(3), 233-239.

Wainwright, M. Photosensitizers in Biomedicine. Wiley, Oxford; 2009.

Weigand, R., Rotermund, F. and Penzkofer, A., (1997). Degree of aggregation of indocyanine green in aqueous solutions determined by Mie scattering.*Chemical physics*, 1997, *220*(3), pp.373-384.

Williams, H.D., Trevaskis, N.L., Charman, S.A., Shanker, R.M., Charman, W.N., Pouton, C.W., et al.(2013).Strategies to address low drug solubility in discovery and development. *Pharmacol.Rev.* 65, 315–499.

Wu, Y., Yeh, F. L., Mao, F., & Chapman, E. R. (2009). Biophysical characterization of styryl dye-membrane interactions. *Biophysical journal*, 2009; *97*(1), 101-109.

Würth, C., Grabolle, M., Pauli, J., Spieles, M. and Resch-Genger, U., (2013). Relative and absolute determination of fluorescence quantum yields of transparent samples. *Nature protocols*, *8*(8), pp.1535-1550.

Xu,W., Siddiqui,I.A., Nihal,M., Pilla,S., Rosenthal,K., Mukhtar,H.,et al. (2013). Aptamer-conjugated and doxorubicin-loaded unimolecular micelles for targeted therapy of prostate cancer. *Biomaterials* 34, 5244–5253.

Yang, R., Meng, F., Ma, S., Huang, F., Liu, H., and Zhong, Z. (2011). Galactose-decorated cross-linked biodegradable poly(ethyleneglycol)-b-poly(epsilon-caprolactone) block copolymer micelles for enhanced hepatoma-targeting delivery of paclitaxel. *Biomacromolecules* 12, 3047–3055.

Yang, C., Zhao, H., Yuan, H., Yu, R., and Lan, M. (2013). Preparation and characterization of thermosensitive and folate functionalized Pluronic micelles. *J. Nanosci.Nanotechnol.* 13, 6553–6559.

Yokoyama, M., Satoh, A., Sakurai, Y., Okano, T., Matsumura, Y., Kakizoe, T., et al. (1998). Incorporation of water-insoluble anticancer drug into polymeric micelles and control of their particlesize. *J. Control.Release* 55, 219–229.

Yoon K. J. and Kim K. J. (1985) Double Ion-Pair Formation in Aqueous Solutions of Methylene Blue and Tetraphenylborate. *Bull. Kor. Chem. Soc*, 6, 149. (1985).

Yu, S.S., Lau, C.M., Barham, W.J., Onishko, H.M., Nelson, C.E., Li, H., et al. (2013). Macrophage-specific RNA interference targeting via “click,” mannosylated polymeric micelles. *Mol.Pharm.* 10, 975–987.

Zhao, J., Mi, Y., and Feng, S.S. (2013). Targeted co-delivery of docetaxel and siPlk1 by herceptin-conjugated vitamin E TPGS based immunomicelles. *Biomaterials* 34, 3411–3421.

Zheng X., Xing D., Zhou F., Wu B. and Chen W. R.(2011), Indocyanine green-containing nanostructure as near infrared dual-functional targeting probes for optical imaging and photothermal therapy, *Mol. Pharm.* 8(2), 447-456 (2011).

Appendix A: Absorption spectra of Styryl 9M in various solvents. Panels at left: top curve: 10μM, bottom curve: 5μM. Panels at right: respective normalized absorption spectra. The noise observed in acetone is due to the high absorption of this solvent below 280nm.

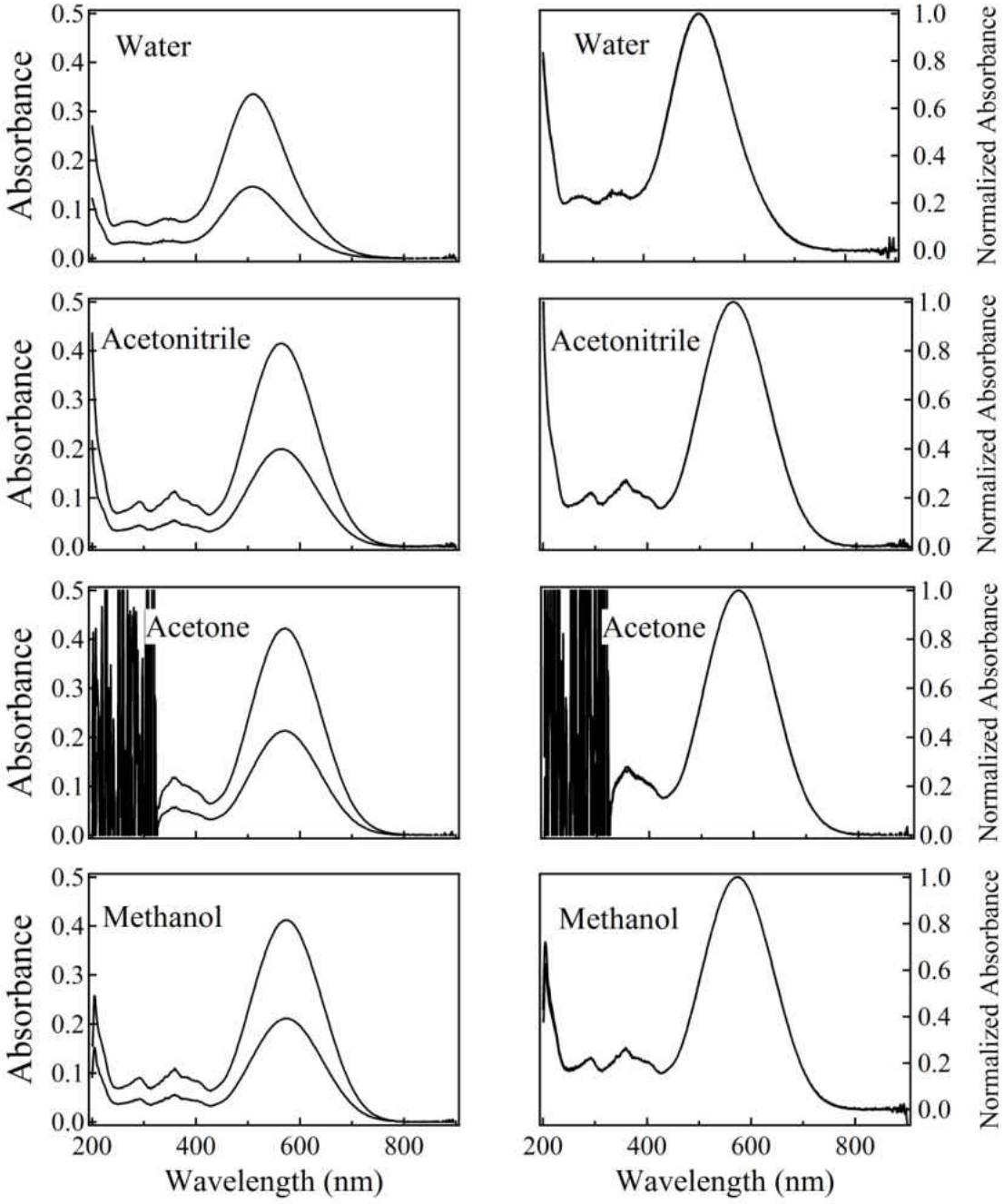

Appendix A, continuation.

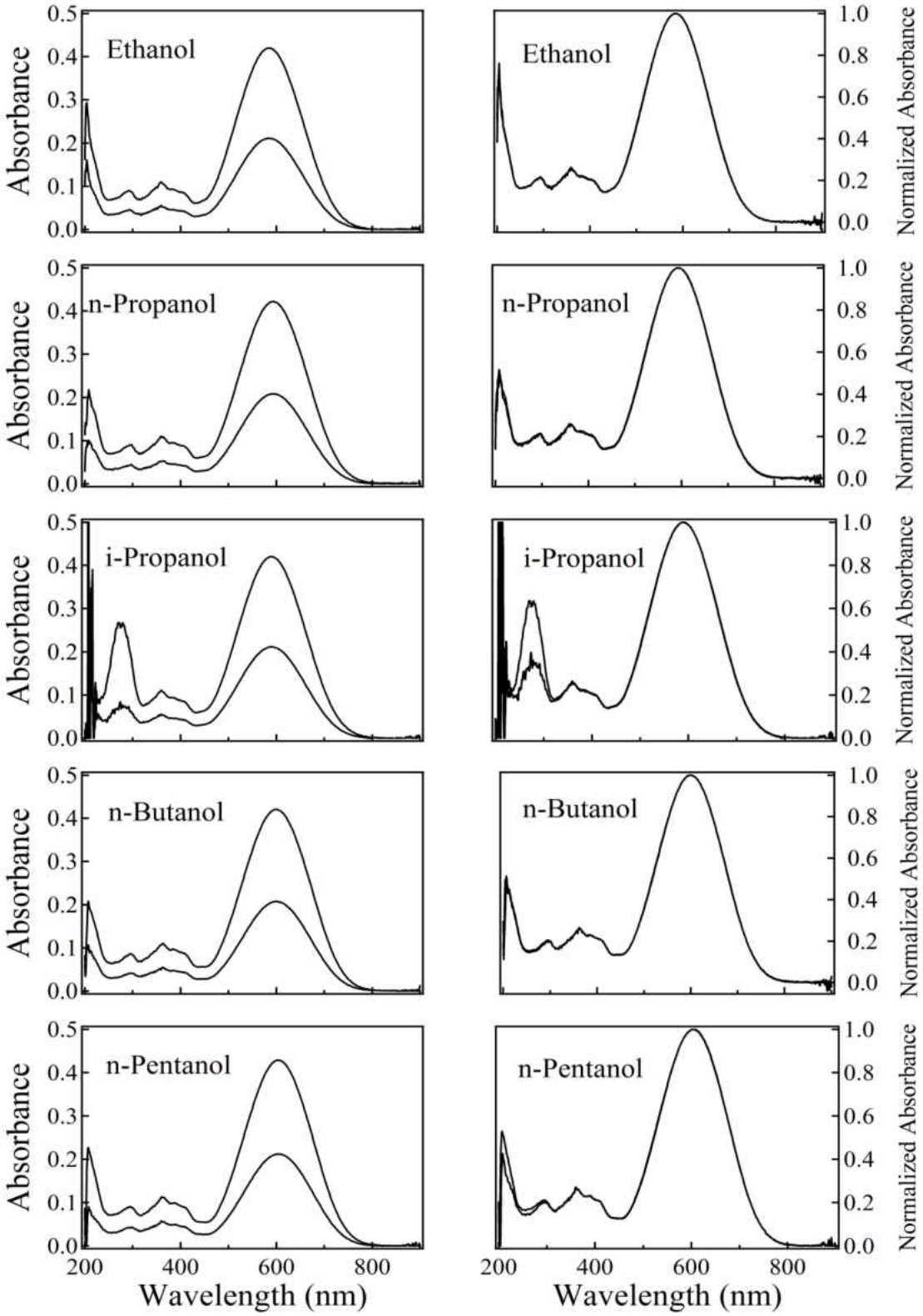

Appendix B: Absorption spectra of HITC in various solvents. Panels at left: top curve: 5μM, bottom curve: 1μM. Panels at right: respective normalized absorption spectra. The noise observed in acetone is due to the high absorption of this solvent below 280nm.

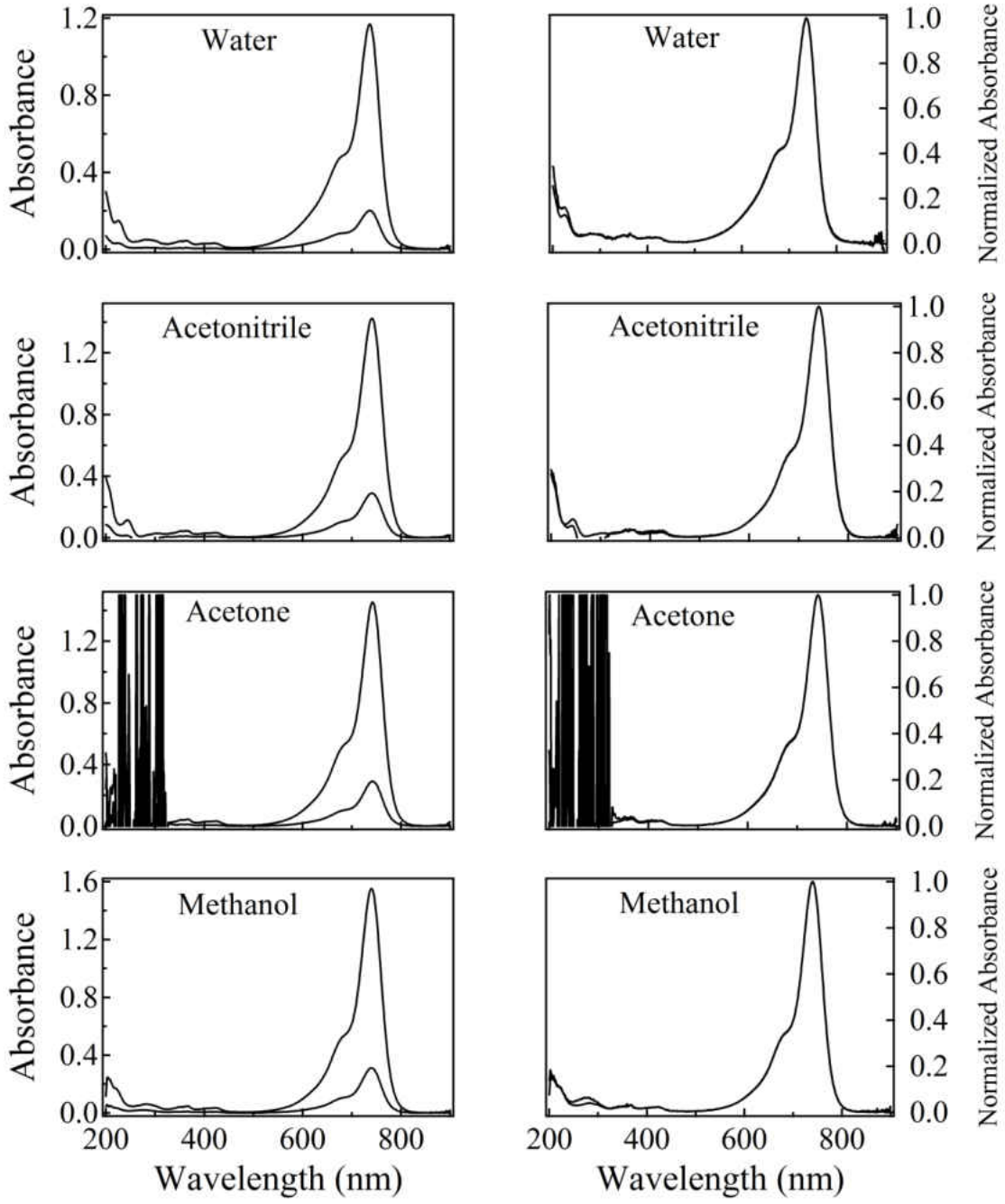

Appendix B, continuation

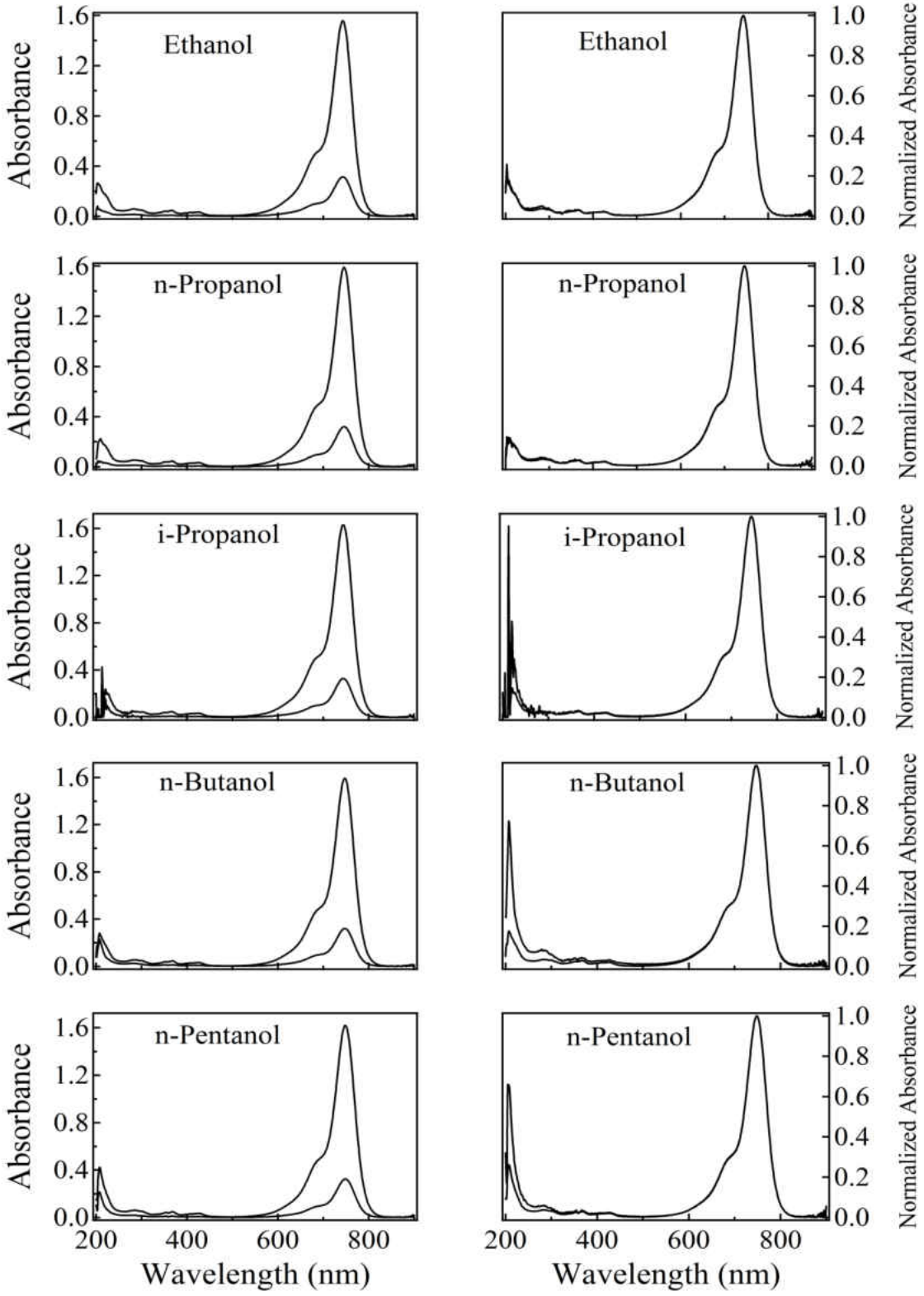

Appendix C: Absorption spectra of DiR in various solvents. Panels at left: top curve: 5μM, bottom curve: 1μM. Panels at right: respective normalized absorption spectra. The noise observed in acetone is due the high absorption of this solvent below 280nm.

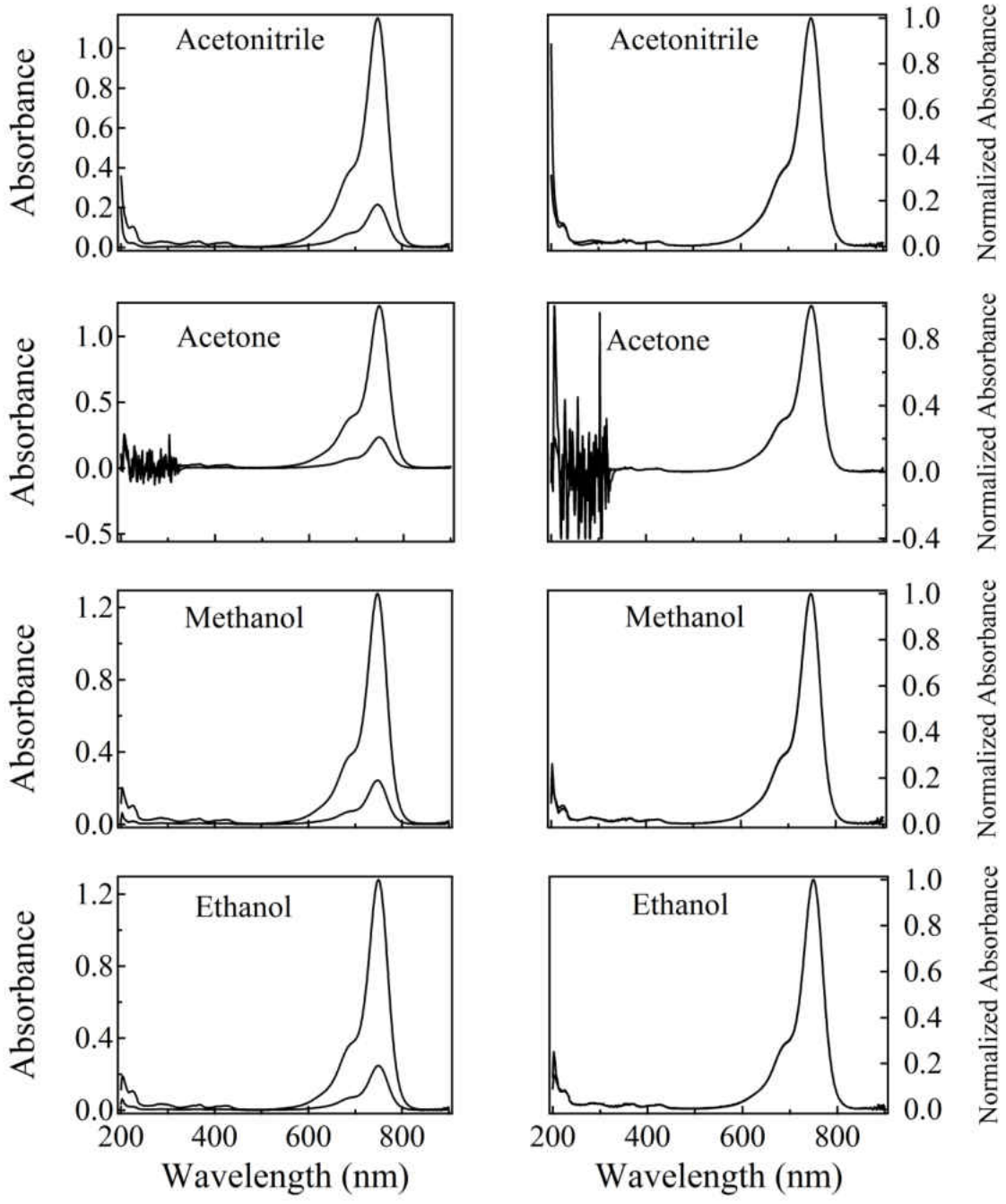

Appendix C, continuation

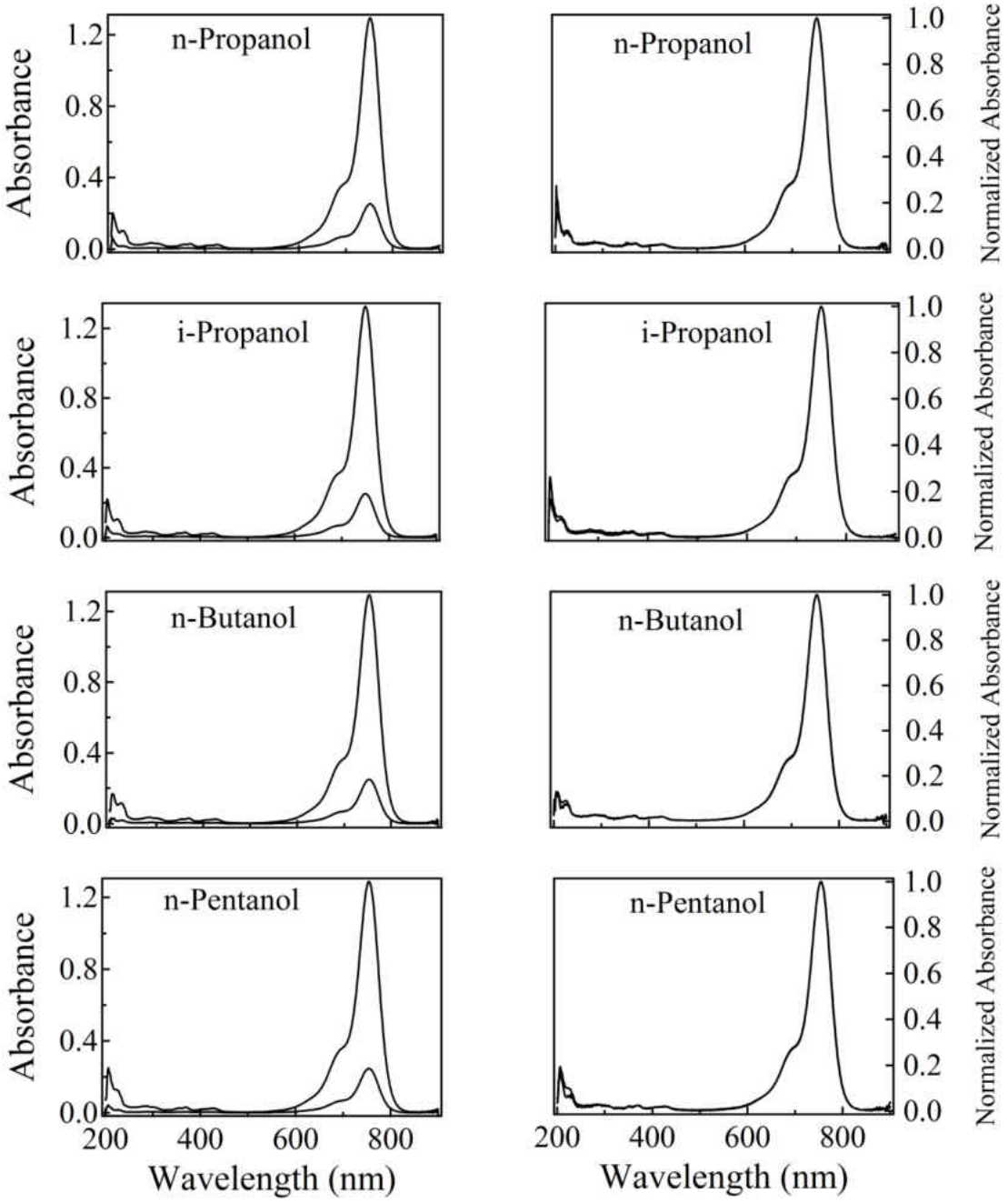

Appendix D: Absorption spectra of Cardiogreen in various solvents. Panels at left: top curve: 5μM, bottom curve: 1μM. Panels at right: respective normalized absorption spectra. Note exception for acetone: panel at left: top curve: 10μM, bottom curve: 5μM. The noise observed in acetone is due to the high absorption of this solvent below 280nm.

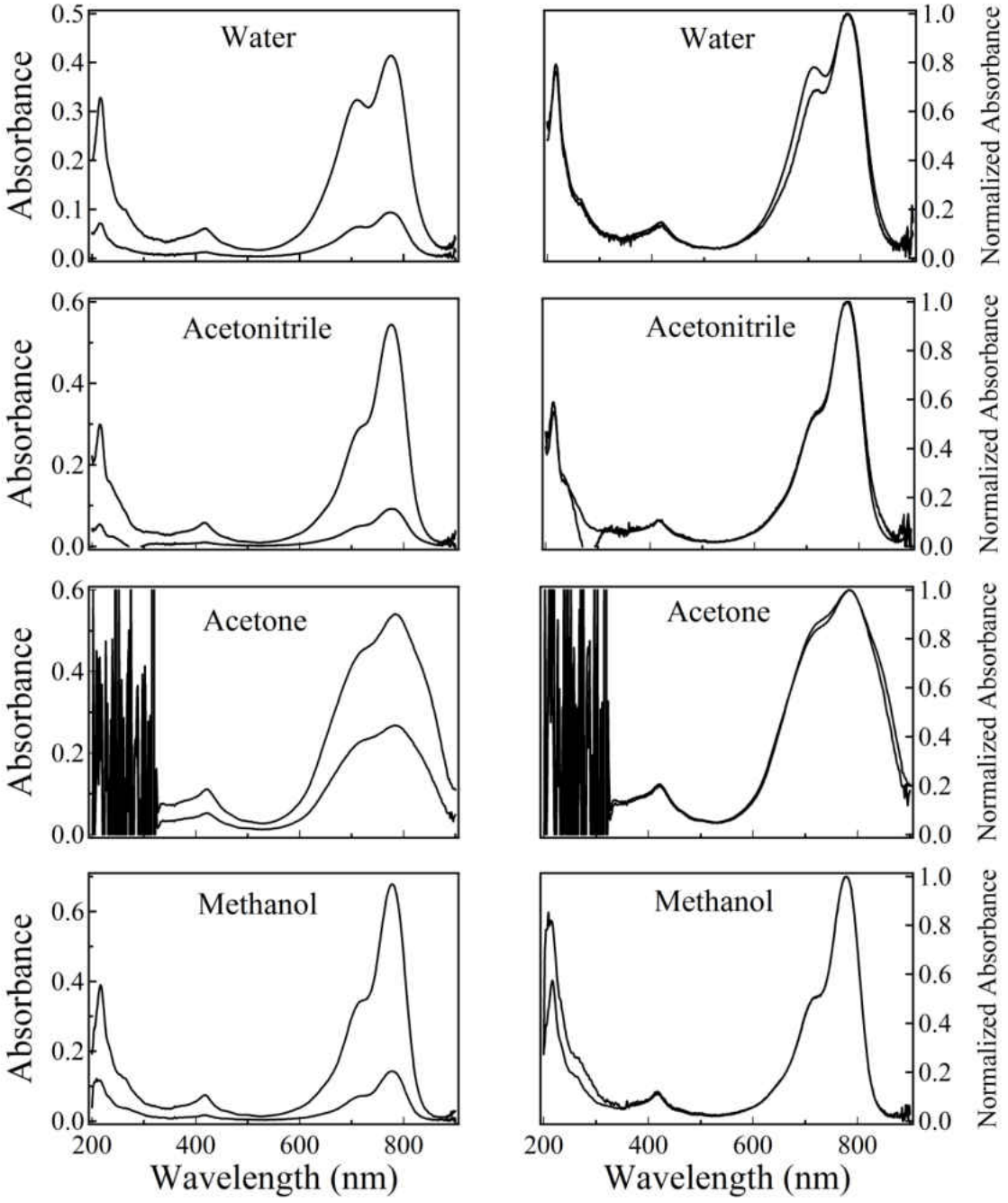

Appendix D, continuation.